

Aim and Scope

The objective of the *Journal of Residuals Science & Technology* (JRS&T) is to provide a forum for technical research on the management and disposal of residuals from pollution control activities. The Journal publishes papers that examine the characteristics, effects, and management principles of various residuals from such sources as wastewater treatment, water treatment, air pollution control, hazardous waste treatment, solid waste, industrial waste treatment, and other pollution control activities. Papers on health and the environmental effects of residuals production, management, and disposal are also welcome.

Editor-in-Chief

P. Brent Duncan
Department of Biology
University of North Texas
Denton, TX, USA
pduncan@unt.edu

Assistant Editor

James Lee
james.lee3918@gmail.com

Editorial Advisory Board

Muhammad Abu-Orf
AECOM, USA
mohammad.abu-orf@aecom.com

Nafissa M. Bizo
City of Philadelphia Water Department
nafissa.bizo@phila.gov

Richard Dick
Cornell University, USA
rid1@cornell.edu

Eliot Epstein
Epstein Environmental Consultants
epsteinee@comcast.net

Guor-Cheng Fang, Ph.D.
Hungkuang University, Taiwan
gcfang@sunrise.hk.edu.tw

Robert Hale
Virginia Institute of Marine Science, USA
hale@vims.edu

Paul F. Hudak
University of North Texas, USA
hudak@unt.edu

Blanca Jimenez Cisneros
Inst. de Ingenieria, UNAM, Mexico
bjc@mumas.iingen.unam.mx

Julia Kopp
Technische Universitat Braunschweig,
Germany
j.kopp@tu-bs.de

Uta Krogmann
RutgersUniversity, USA
krogmann@aesop.rutgers.edu

D. J. Lee
National Taiwan University, Taiwan
djlee@ntu.edu.tw

Giuseppe Mininni
Via Reno 1, Italy
mininni@irsa.rm.cnr.it

Lynne H. Moss
CDM Smith
mosslh@cdmsmith.com

John Novak
Virginia Tech, USA
jtnov@vt.edu

Nagaharu Okuno
The University of Shiga Prefecture,
Japan
okuno@ses.usp.ac.jp

Jan Oleszkiewicz
University of Manitoba, Canada
oleszkie@ms.umanitoba.ca

Banu Örmeci
Carleton University, Canada
banu_ormeci@carleton.ca

Ian L. Pepper
University of Arizona, USA
ipepper@ag.arizona.edu

Ioana G. Petrisor
Co-Editor-in-Chief
Environmental Forensics Journal, USA
Environmental.Forensics@gmail.com

Bob Reimers
Tulane University, USA
rreimers@tulane.edu

Dilek Sanin
Middle East Technical University,
Turkey
dsanin@metu.edu.tr

Heidi Snyman
Golder Associates Africa (Pty) Ltd.,
South Africa
hsnyman@golder.co.za

Ludovico Spinosa
Consultant at Commissariat
for Env. Energ. in Region,
Puglia, Italy
ludovico.spinosa@fastwebnet.it

P. Aarne Vesilind
Bucknell University, USA
aarne.vesilind@gmail.com


Doug Williams
California Polytechnic State
University, USA
wmsenr@thegrid.net

JOURNAL OF RESIDUALS SCIENCE & TECHNOLOGY—Published quarterly—January, April, July and October by DEStech Publications, Inc., 439 North Duke Street, Lancaster, PA 17602.

Indexed by Chemical Abstracts Service. Indexed/abstracted in Science Citation Index Expanded. Abstracted in Current Contents/Engineering, Computing & Technology. Listed in ISI Master Journal.

Subscriptions: Annual \$219 per year. Single copy price \$60. Foreign subscriptions add \$45 per year for postage.

(ISSN 1544-8053)

 DEStech Publications, Inc.

439 North Duke Street, Lancaster, PA 17602-4967, U.S.A.

©Copyright by DEStech Publications, Inc. 2015—All Rights Reserved

C O N T E N T S

Research

- Study on Migration and Pollution in Shallow Groundwater Near a Slag Field** 191
LIDE WEI
- Pollutant Removal by Gravel Contact Oxidation Treatment System in Taipei** 199
JIN XU, SHANG-LIEN LO, HOME-MING CHEN, KE-QIANG DING and RAN GONG
- Improvement of Industrial-scale Anaerobic Digestion by Enzymes Combined with Chemical Treatment** 205
MICHAEL RECKTENWALD, ESTERA SZWAJECER DEY and OLOF NORRLÖW
- Polycyclic Aromatic Hydrocarbon Accumulation in *Phragmites australis* Grown on Constructed Wetland for Sludge Stabilization** 215
YUBO CUI, WANJUN ZHANG, HONGJIE SUN, WEI-MIN WU and XUEJUN ZOU
- Traffic Environmental Capacity and MFD Based Traffic Emission Dynamic Control Model** 221
YIMAN DU, YUHAN JIA, JIANPING WU, MING XU and SENYAN YANG
- Health Risk Assessment of Heavy Metals and As in Vegetable and Soil System in Chongqing, Southwest of China** 231
CHENG ZHANG, YONGMIN WANG, ZHENGLING ZHANG, DINGYONG WANG, CHENGZHONG LUO and FENG XU
- Root Nitrogen Uptake in Wastewater-Irrigated Pepper Fields** 241
XIAOHUI LU, PEIFANG WANG, YANJIE ZHANG and DOU ZHI
- The Research of Corrected First Order Kinetics on Hydrolysis and Biogas Generation in Batch Anaerobic Digestion** 249
LEI FENG, HONGLI KOU, XUDONG ZHANG and RUNDONG LI

Study on Migration and Pollution in Shallow Groundwater Near a Slag Field

LIDE WEI*

*State Key Laboratory of Geomechanics and Geotechnical Engineering, Institute of Rock and Soil Mechanics,
Chinese Academy of Sciences, Wuhan 430071, China*

Department of Civil, Environmental and Natural Resources Engineering, Luleå University of Technology, Luleå 97187, Sweden

ABSTRACT: This paper investigates contaminant migration in groundwater near tail slag through large-scale three-dimensional numerical simulation, comparison of numerical simulation results and test results and prediction on the status and scope of groundwater pollution, to provide a scientific theory basis for management of the tailings. It supposes that a 2D simulation model should be used for inverse analysis to get key saturated permeability coefficients for large-scale, three-dimensional numerical simulation. The key parameters of the materials used in dispersion calculations should be identified based on unsaturated material dispersion test results and empirical values in geotechnical engineering. The comparison results show that the numerical simulation results basically agree well with the test results, so that numerical simulation can be used as the basis of groundwater environmental evaluation. As time goes on, the arsenic concentration in the slag field migrates outward slowly, but the concentration in the groundwater does not exceed 0.00001 kg/m^3 .

INTRODUCTION

Snear tail slags has recently been a hot topic in earth science. At present, relevant studies on groundwater pollution can be mainly categorized into 2 types [1~7]: one is to simulate and analyze indoor soil column experiment and field experiment, and the other is to predict the status and scope of groundwater pollution by establishing a mathematical model analysis. However, research including both processes of large-scale three-dimensional numerical simulation and comparison between numerical simulation results and test results for Arsenic in groundwater, is relatively rare.

Arsenic (As) is one of the most hazardous elements to human health that causes carcinogenic skin diseases, internal cancers, and non-carcinogenic diseases such as diabetes, peripheral neuropathy, and cardiovascular conditions. Previous research on groundwater As contamination has typically focused on water quality analyses and spatial modeling of As concentration in contaminated areas using geostatistics [8]. The main sources and paths of As in areas suffering from local groundwater contamination have been difficult to

identify for the contaminant migration in groundwater near a tail slag presented in this paper. Here, we combine geostatistical analyses of water-sample data with numerical simulations for As transport modeling. For As in groundwater, some recent modeling studies for 1D flow conditions [9~11], while some 2D reactive transport model study were reported [12,13]. A small, 3D transport model study was reported recently [14]. However, research including both processes of large-scale three-dimensional numerical simulation and comparison between numerical simulation results and test results for Arsenic in groundwater, is relatively rare.

In this paper, research of contaminant migration in groundwater near a tail slag is presented to provide scientific support for the management of the tailings [15], which predicts the scope of groundwater pollution. This paper offers the following innovative highlights: first, it considers that a 2D model should be used for inverse analysis to get key saturated permeability coefficients for large-scale, 3D numerical simulation; second, it supposes that the key parameters of the materials used in dispersion calculation should be identified based on unsaturated material dispersion test results and empirical value in geotechnical engineering; finally, the numerical simulations match the test data and can inform groundwater management decisions.

*Author to whom correspondence should be addressed. Tel: 008613995592605;
Fax: 027-87197386; E-mail: ldwei@whrsm.ac.cn

GOVERNING EQUATIONS FOR FLUID FLOW AND SOLUTE TRANSPORT

A COMSOL Multiphysics model was built for solute transport in porous media [16].

Fluid Flow

Richards' equation governs the saturated-unsaturated flow of water in the soil. The soil is open to the atmosphere, so atmospheric pressure changes do not affect the flow. Here, Richards' equation is used for single-phase flow:

$$(C + Se \times S) \frac{\partial H_p}{\partial t} + \nabla \cdot (-K \nabla (H_p + D)) = Q_s \quad (1)$$

where C denotes the specific moisture capacity (m^{-1}); Se is the effective saturation of the soil (dimensionless); S is a storage coefficient (m^{-1}); H_p represents the dependent variable pressure head (m); t is time (d); K is the hydraulic conductivity (m s^{-1}); D is the coordinate (for example, x , y , or z) that represents vertical elevation (m); and Q_s is a fluid source defined as volumetric flow rate per unit volume of soil (s^{-1}). In this equation, $S = (\theta_s - \theta_r)/(1 \text{ m})$ where θ_s and θ_r denote the volume fraction of fluid under saturation and after drainage, respectively.

For unsaturated flow, the fluid moves through the soil but may or may not completely fill the pores in the soil. Here, the parameter θ is used to denote the volume fraction of fluid within the soil. The coefficients C , Se , and K vary with pressure head, and H_p together with θ make Richards' equation nonlinear. The specific moisture capacity, C , relates to the variations in soil moisture to pressure head as $C = \partial\theta/\partial H_p$. In the governing equation, C decides the storage changes caused by varying fluid content since $C \partial H_p/\partial t = \partial\theta/\partial t$. Because C , the first term in the time coefficient, goes to zero at saturation, time change in storage depends on the compression of the aquifer and water under saturated conditions. The saturated storage varies with the effective saturation, as represented by the second term in the time-coefficient. Furthermore, K is a function that defines how readily the porous media transmits fluid. The relative permeability of the soil, kr , increases with increasing fluid content given by $K = Ks kr$, where Ks (m/s) is the constant hydraulic conductivity at saturation.

Groundwater flow and solute transport are linked by fluid velocities. To follow the form of the transport

equation, the fluid velocities are deduced from Darcy's law:

$$u = -k_r K_s \nabla (H_p + D) \quad (2)$$

Solute Transport

The equation that governs advection and dispersion is

$$\frac{\partial}{\partial x_i} \left[\theta D_{Lij} \frac{\partial c}{\partial x_j} \right] - \frac{\partial}{\partial x_i} (cu_i) + \theta \sum_{k=1}^n R_k = \frac{\partial(\theta c)}{\partial t} \quad (3)$$

where c denotes the dissolved concentration; D_L is the hydrodynamic dispersion tensor; Rk is the added solute per unit volume of water per unit time; X_i is the cartesian coordinate; and t is the time. θD_L in three-dimensional case can be expressed as (COMSOL 2008):

$$\left\{ \begin{array}{l} \theta D_{Lxx} = \alpha_1 \frac{u^2}{|u|} + \alpha_2 \frac{v^2}{|u|} + \alpha_3 \frac{w^2}{|u|} + \theta D_m \theta^{7/3} / \theta_s^2 \\ \theta D_{Lyy} = \alpha_2 \frac{u^2}{|u|} + \alpha_1 \frac{v^2}{|u|} + \alpha_3 \frac{w^2}{|u|} + \theta D_m \theta^{7/3} / \theta_s^2 \\ \theta D_{Lzz} = \alpha_1 \frac{u^2}{|u|} + \alpha_3 \frac{v^2}{|u|} + \alpha_3 \frac{w^2}{|u|} + \theta D_m \theta^{7/3} / \theta_s^2 \\ \theta D_{Lxy} = \theta D_{Lyx} = (\alpha_1 - \alpha_2) \frac{uv}{|u|} \\ \theta D_{Lxz} = \theta D_{Lzx} = (\alpha_1 - \alpha_3) \frac{uw}{|u|} \\ \theta D_{Lzy} = \theta D_{Lyz} = (\alpha_2 - \alpha_3) \frac{vw}{|u|} \end{array} \right. \quad (4)$$

GEOLOGICAL MODEL FOR HYDROGEOLOGY STUDY IN THE STUDY AREA

The ground layer in the study area is mainly composed of clay and carbonate rocks. The ground layer is divided into six materials mainly based on their permeability as follows: material 1 is tail slag; material 2 is clay; material 3 is unsaturated limestone with a certain distance away from groundwater; material 4 is saturated limestone within the scope of groundwater; material 5 is base rock with very low permeability; and material 6 is sandy gravel.

Two simulation models based on exploratory boring are shown in Figures 1 and 2. The simulation model in

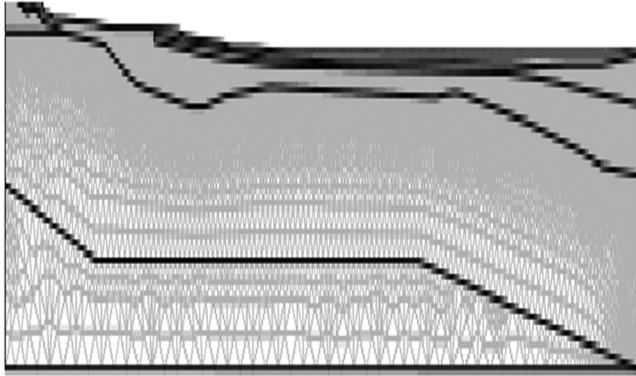


Figure 1. 2D FEM model.

Figure 1 is 10.462 km in length and 1.058 km in height, which is jointed by a lake; while the simulation model in Figure 2 is modeled by 8 profiles, which is 1.840 km in length along the y direction, 0.89 km in width along the x direction, and 0.439 km in height. The 2D model is divided into 42,236 elements with 21,648 nodes, while the 3D model is divided into 67,968 elements with 14,620 nodes.

MODEL PARAMETERS FOR FLOW SIMULATION

The seepage field must be simulated accurately to get reasonable simulation results of contaminant migration. Here, the seepage field is simulated as saturated—unsaturated stable seepage. For the model in Figure 1, the boundary conditions are as follows. The upper surface accepts rainfall infiltration and forms a flux boundary: the flux at the slag surface is 3.2×10^{-8} m/s, which is equal to the local average annual rainfall of 1012 mm; while the flux at the clay surface is 1.6×10^{-9} m/s, which is 5% of the rainfall. The flux of the slag surfaces is 3.2×10^{-8} m/s because of the following reasons. First, the saturated permeability coefficients of the slag (0.0001 m/s and 0.0001 m/s) are high so the rain water on the slag surface flows into the slag and can be stored in the lower slag. Second, the clay surface under the slag is sunken so it can keep the water from slag surface and some water from clay surface. Finally, the water stored in the lower slag is covered by thick slag, so evaporation of rain is little. The flux of the clay surfaces is 1.6×10^{-9} m/s because of the following reasons. The saturated permeability coefficients of the clay are very low, so most of the rain water on the clay surface runs off. And some of the water evaporates, so water penetration through clay surface is low. The two border surfaces vertical to the x-axis are set as constant hydraulic head: one of the constant

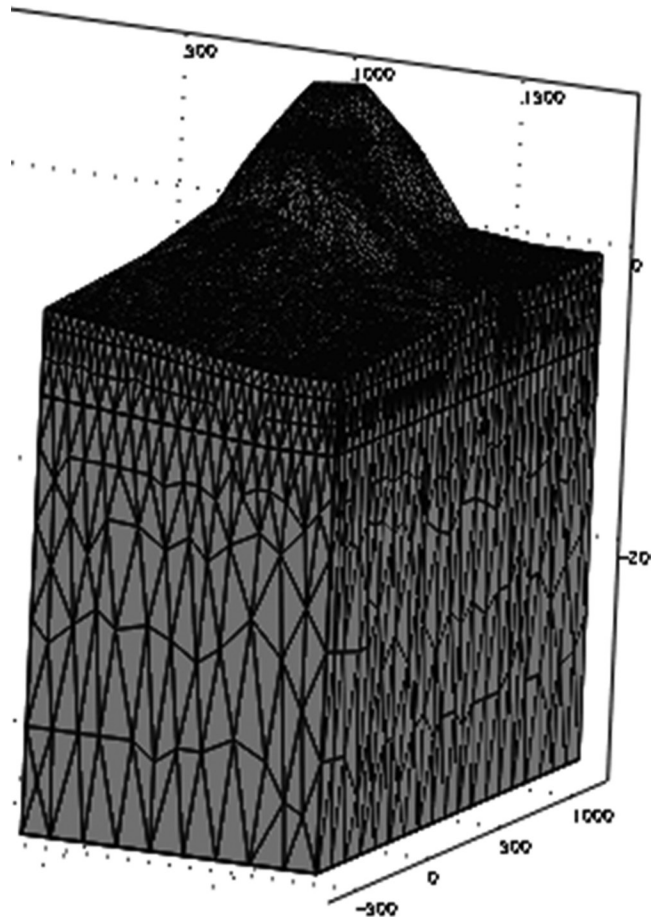


Figure 2. 3D FEM model.

hydraulic heads is the hydraulic head in an exploratory hole; while the other is the hydraulic head of the lake at the boundary. The bottom surface is set as a boundary with zero flux.

Soil-water characteristic curves for material 1 and material 2 are from volumetric pressure plate test, and the pore volume fractions are gotten from the corresponding soil-water characteristic curves. The residual water volume fractions for material 1 and material 2 are from a drying method. The saturated permeability coefficients for material 1 and material 3 are from a water injection test. Other parameters are determined accord-

Table 1. Model Parameters for Flow Simulation.

Material	mat.1	mat.2	mat.3	mat.4	mat.5	mat.6
k_s /m/s	0.0001	0.00001	0.001	10^{-6}	0.001	
k_p /m/s	0.0001	0.00001	0.001	10^{-6}	0.001	
Pore volume fraction	0.32	0.571	0.25	0.25	0.20	0.35
Residual water volume fraction	0.06	0.158	0.01	0.01	0.01	0.01

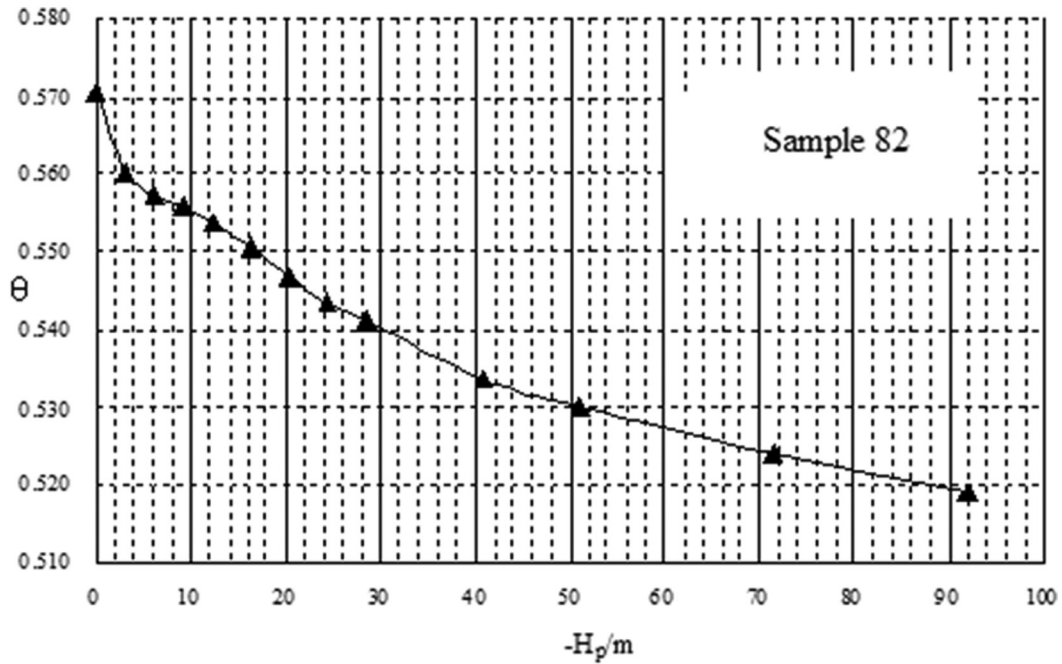


Figure 3. Soil-water characteristic curve for material 2.

ing to geotechnical engineering values. All saturated permeability coefficients of the materials but those of material 2 are shown in Table 1. The permeability coefficients of material 2 are important for determining the seepage field, so they are determined by inverse analysis according to the test results. Materials 1 and

2, whose soil-water characteristic curves are obtained from test results, are unsaturated materials. Figure 3 shows the soil-water characteristic curves of material 2. Test results indicate that the saturated permeability coefficient of material 2 in the vertical direction ranges from 5×10^{-9} m/s to 1×10^{-7} m/s. Simulation analysis

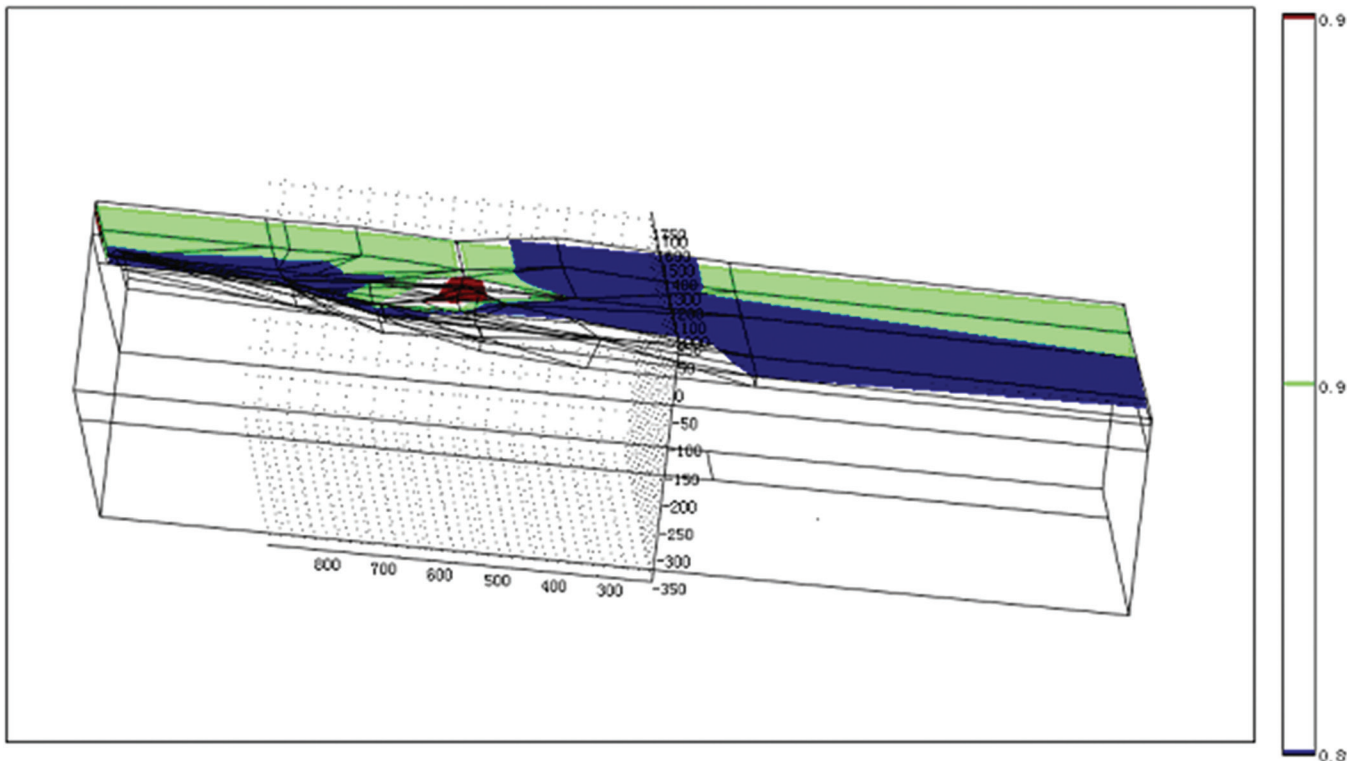


Figure 4. Saturation contour in clay.

Table 2. Model Parameters of Pollutant Migration.

Material	mat.1	mat.2	mat.3	mat.4	mat.5	mat.6
$dm, m^2 s^{-1}$	10^{-9}	$1.85e-6$	10^{-9}	10^{-9}	10^{-9}	10^{-9}
$\alpha_1 \cdot \alpha_2 \cdot m$	1	0.001	2	2	2	3
$\alpha_3 \cdot m$	2	0.002	2	2	2	3

shows that the simulation of the seepage field can fit the actual seepage field better if the saturated permeability coefficient in vertical is 8×10^{-8} m/s and that in horizontal is 3×10^{-8} m/s.

Model Parameters for Flow Simulation

The seepage field of the 3D model in Figure 2 is simulated as saturated—unsaturated stable seepage, and the following boundary conditions for the seepage simulation are used. The upper surface accepts rainfall infiltration and the border belongs to flux boundary: the flux of the slag surfaces is $3.2e-8$ m/s while that of the clay surfaces is 1.6×10^{-9} m/s. The two border surfaces vertical to the x -axis are set as symmetric boundaries because they belong to watersheds. We consider lateral migration of the pollutant by convection and ignore lateral migration of the pollutant by diffusion at the two border surfaces. The two border surfaces vertical to the y -axis are set as boundaries with constant hydraulic head: one is the hydraulic head in the exploratory hole on the boundary; while the other is -61 m based on the simulation results of 2D COMSOL model. The bottom surface is set as a boundary with a zero flux.

The solute component identification test shows that the concentrations of As in slag solute is 0.051 mg L^{-1} while that of the solute on the clay surface is 0.002 mg L^{-1} .

Table 3. The Clay Saturation of Survey Results.

Soil Sample No.	Depth	Saturation
	m	%
1754	7.50–7.70	100
1755	17.90–18.10	99
1756	14.30–14.50	98
1757	12.90–13.10	100
1758	12.00–12.20	95
1759	8.60–8.80	86
1760	18.20–18.50	97
1761	18.20–18.40	99
1762	15.70–15.90	95
1763	20.70–20.90	95
1764	21.60–21.80	98
1765	25.40–25.60	93

The following conditions are set for migration simulation. The initial value of slag solute is set to 0.051 mg L^{-1} while that of other solutes are set to zero. Boundary conditions are as follows. A flux boundary is set to the upper surface of the model. The flux of the tailings surfaces is $(3.2 \times 10^{-8}) \times 51 \text{ mg m}^{-2} \text{ s}^{-1}$ while that of the clay surfaces is $(1.6 \times 10^{-9}) \times 2 \text{ mg m}^{-2} \text{ s}^{-1}$. The flux of the border surface with the higher constant hydraulic heads is zero. An advective flux model is set to the border surface with the lower constant hydraulic heads. The fluxes of the two border surfaces vertical to the x -axis are set to zero. The flux of the bottom surface is zero.

The parameters of the materials used in dispersion calculation are shown in Table 2. The molecular diffusion coefficient of material 2 is $dm = 1.8521 \times 10^{-6} \text{ m}^2 \text{ s}^{-1}$ based on unsaturated dispersion test results. Other parameters in Table 2 are determined according to geotechnical engineering.

Simulation Results and Discussion

Survey results show that clay has a high saturation of about 0.9 as in Table 3. Simulation results show that the saturation of clay near the slag in Figure 4 is also about 0.9 too. Simulation results are consistent with survey results.

Groundwater quality near the slag field is tested and analyzed to evaluate the slag field effects on surrounding groundwater. Table 4 gives the groundwater sampling sites, as well as the test results and corresponding numerical simulation results. It can be seen that the numerical simulation results and test results are basically identical. Hence, the numerical simulation results can be used as the basis of groundwater environmental evaluation.

Figure 5 provides some solute migration simulation

Table 4. Comparison between Test Results and Corresponding Numerical Simulation Results.

Sample	Plane Site	Depth	Test Result	Simulation Result
			$\rho(B)/(mg L^{-1})$	$\rho(B)/(mg L^{-1})$
ZKJ-1	Distance away from the tails along y -direction is 1457 m.	20 m	0.003	0.001
ZKJ-2	Distance away from the tails along x -direction is 105.67 m.	148 m	< 0.001	0.0003

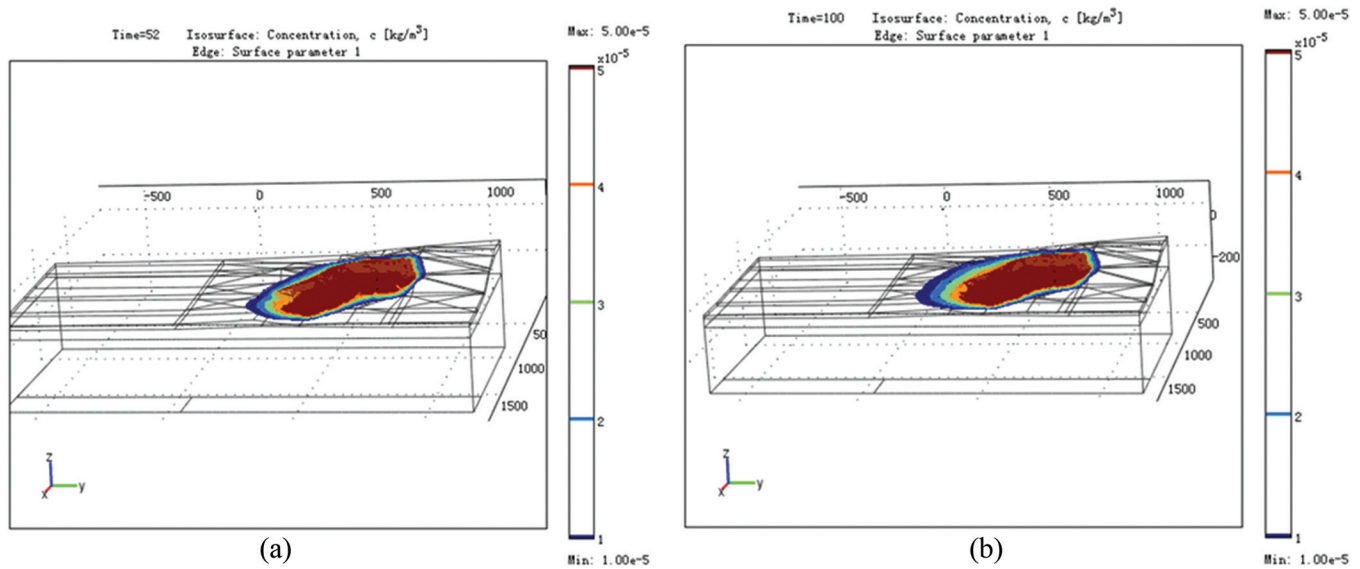


Figure 5. Simulated concentration contour of As in groundwater. (a) 52 years after disposal started (b) 100 years after disposal started.

results. As time goes on, the As concentration in the slag field migrates outward slowly. The dispersion velocity near groundwater is so large that the As concentration in the groundwater does not increase with time. The final As concentration in the groundwater does not exceed $0.00001 \text{ kg m}^{-3}$.

CONCLUSIONS

1. Simulation results show that the clay near the tails has a high saturation of about 0.9, which is consistent with survey results.
2. Comparison shows that the numerical results and test results are basically identical so that the numerical simulation results can be used as the basis of groundwater environmental evaluation.
3. Over 100 years of simulation, the pollution plume from the slag field migrates outward slowly. The dispersion velocity near groundwater is so large that the As concentration in the groundwater does not increase with time. The final As concentration in the groundwater does not exceed $0.00001 \text{ kg m}^{-3}$, which is the legislative upper limit of second grade water.

ACKNOWLEDGMENT

The author would like to thank for the help from Project (51074152) supported by the National Natural Science Foundation of China.

REFERENCES

1. Xue Q., Liang B., Liu J., et al., Numerical simulation of petroleum components transport in unsaturated zone and its' application, *Chinese Journal of System Simulation*, Vol. 17, No. 11, 2005, pp. 2589–2592 (in Chinese).
2. Lv J., Zhang Y., Su P., et al. 1999, Study on phosphorus transport in soil, *Chinese Journal of Soil science* 36(1):75–82 (in Chinese).
3. Yang J., Yi Z., Jia W., et al, Field experimenton solute transport in an unsaturated soil, *Chinese Journal of Advances in Water Science*, Vol. 4, No. 4, 1993, pp. 245–252 (in Chinese).
4. An D., Jiang Y., Xi B., et al., Analysis for remedial alternatives of unregulated municipal solid waste landfills leachate-contaminated groundwater, *Frontiers of Earth Science*, Vol. 7, No. 3, 2013, pp. 310–319.
5. Berlina M., Kumarb G. S., Nambia I. M., Numerical modelling on transport of nitrogen from wastewater and fertilizer applied on paddy-fields, *Ecological Modelling*, Vol. 278, 2014, pp. 85–99. <http://dx.doi.org/10.1016/j.ecolmodel.2014.02.008>
6. Cheng J., Hu J., Reviews on numerical method for solving solute transport problems in the saturated porous media, *China Journal of Hydrogeology and Engineering Geology*, No. 2, 2003, pp. 99–106 (in Chinese).
7. Glinskii M. L., Pozdniakov S. P., Chertkov L. G., Regional flow and transport simulation of liquid radioactive waste disposal at the Siberian Chemical Combine for long- and super-long-term postinjection periods, *Radiochemistry*, Vol. 56, No. 6, 2014, pp. 649–656.
8. Gaus I., Kinniburgh D.G., Talbot J. C., Webster R., Geostatistical analysis of arsenic concentration in groundwater in Bangladesh using disjunctive kriging. *Environmental Geology*, Vol. 44, 2003, pp. 939–948. <http://dx.doi.org/10.1007/s00254-003-0837-7>
9. Moldovan B. J., Hendry M. J., Characterizing and quantifying controls on arsenic solubility over a pH range of 1–11 in a uranium mill-scale experiment. *Environmental Science and Technology*, Vol. 39, No. 13, 2005, pp. 4913–4920. <http://dx.doi.org/10.1021/es0482785>
10. Postma D., Larsen F., Minh Hue, N. T., Duc M. T., Viet P. H., Nhan P. Q., Jessen S., Arsenic in groundwater of the Red River floodplain, Vietnam: Controlling geochemical processes and reactive transport modeling. *Geochimica et Cosmochimica Acta*, Vol. 71, No. 21, 2007, pp. 5054–5071. <http://dx.doi.org/10.1016/j.gca.2007.08.020>
11. Abdur R., Kenji J., Yoshinari H., et al., Mathematical modeling of biologically mediated redox processes of iron and arsenic release in groundwater, *Environmental Geology*, Vol. 58, 2009, pp. 459–469. <http://dx.doi.org/10.1007/s00254-008-1517-4>

12. Jung H. B., Charette M. A., Zheng Y., Field, laboratory, and modeling study of reactive transport of groundwater arsenic in a coastal aquifer. *Environmental Science and Technology*, Vol. 43, No. 14, 2009, pp. 5333–5338.
13. Irwan I., Katsuaki K., Distinguishing potential sources of arsenic released to groundwater around a fault zone containing a mine site, *Environmental Earth Sciences*, Vol. 63, No. 3, 2011, pp. 595–608. <http://dx.doi.org/10.1007/s12665-010-0727-8>
14. Ilka W., Henning P., Craig T. S., *et al.* Evaluation of conceptual and numerical models for arsenic mobilization and attenuation during managed aquifer recharge, *Environmental Science and Technology*, Vol. 44, 2010, pp. 5035–5041. <http://dx.doi.org/10.1021/es100463q>
15. Wei L.. 2011. Study report of experiment of soil and numerical simulation on pollution the groundwater environment of copper slag disposal pit in Puji. Study Report of Institute of Rock and Soil Mechanics of Chinese Academy of Sciences (in Chinese).
16. COMSOL, A. B. 2008. The COMSOL Multiphysics Reference Guide, COMSOL Office, Sweden. doi:10.12783/issn.1544-8053/12/4/1

Pollutant Removal by Gravel Contact Oxidation Treatment System in Taipei

JIN XU^{1,*}, SHANG-LIEN LO², HOME-MING CHEN³, KE-QIANG DING¹ and RAN GONG¹

¹*School of Environmental Engineering, Nanjing Institute of Technology, Nanjing, P.R.China*

²*Graduate Institute of Environmental Engineering, Taiwan University, Taipei*

³*Sewage Systems Office, Public Work Department, Taipei City Government, Taipei*

ABSTRACT: The Guiyang gravel contact oxidation treatment system was constructed to purify the combined sewage and rainwater in Taipei. In this study, influent and effluent were sampled monthly for the analyses of dissolved oxygen (DO), suspended solids (SS), biochemical oxygen demand (BOD), chemical oxygen demand (COD), ammonia nitrogen and nitrate. Results showed that removal rates of BOD, SS and NH₃-N ranged 85–95% (averaged 90%), 70–95% (averaged 85%), and 70–90% (averaged 80%), respectively. Therefore, the gravel contact oxidation system is quite effective in pollution control for combined sewage and rainwater. However, microbial denitrification was not effective due to high concentrations of dissolved oxygen in non-aeration zones of the gravel contact oxidation treatment system. Although the concentration of NH₃-N decreased quickly, nitrogen was not removed by microbial degradation. It was only a migration process among different forms of nitrogen. It is, therefore, important to effectively control aeration in the front zone of the gravel contact oxidation treatment system to improve the removal efficiency of total nitrogen.

INTRODUCTION

THE gravel contact oxidation system, among many other kinds of ecological engineering technologies, is a conventional method to strengthen the natural water purification process. The gravel contact oxidation with the packed medium of gravel acts as a biofilm carrier [1,2]. Pollutants are removed by biofilm attached to the filter surface through adsorption, absorption, sedimentation and metabolic effects, etc [3]. The purification process of gravel contact oxidation system includes physiochemical process and biological process. When the sewage flows through the gravel bed for a long time, biofilm forms on the surface of gravel and pollutants are degraded by biofilm absorption and used for the metabolism of the biofilm. In short, biofilm plays a key role on sewage purification in the gravel contact oxidation system. As a subsurface flow system, a gravel contact oxidation system provides a large contact surface area between the sewage and the biofilm. Purification effect is, therefore, better than that of surface flow system [4]. To treat sewage more effectively, a gravel contact oxidation system is

often filled with gravels of varying tightness and different sizes. It can be generally divided into two layers. The upper layer of gravel is often arranged loosely, where sewage flows fast to maintain aerobic condition. The lower layer of gravel is, however, packed tightly. Sewage passes through slowly and aeration pipes are laid on the bottom of the gravel bed to keep aerobic condition. In addition, sewage with high concentration of suspended solids flows directly into the gravel bed, easily blocking the pores and reducing the hydraulic loading and decreasing the removal efficiency. Thus, a grit chamber unit was added to remove suspended solids in sewage to reduce clog before the sewage passing through the gravel bed.

MATERIAL AND METHODS

Site Description

The Guiyang gravel contact oxidation treatment system is located in the high beaches of the upstream of Zhongxing Bridge, Taipei. It covers an area of 3,850 m², of which the area of the gravel contact oxidation unit is about 1,930 m² (excluding road area). The influent, which is combined sewage and rainwater, is collected from Guiyang pumping station. The catchment area of

*Author to whom correspondence should be addressed. Tel: 13770321434, Fax: 025-86118974, E-mail: xujin100408@163.com

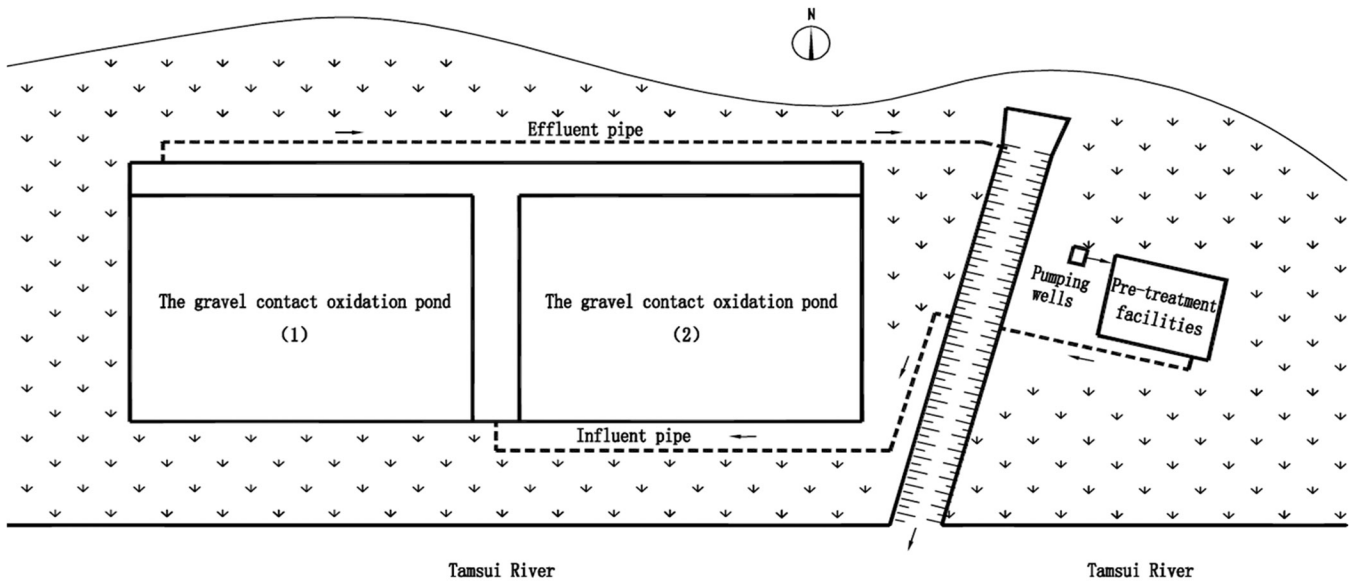


Figure 1. Map of the gravel contact oxidation treatment system site.

the pumping station is about 69,100 m², ranging from the north of Guangzhou Street to the south of Neijiang Street, Chongqing South Road to the west of Roosevelt Road, till the riverside of Tamsui River. Treatment capacity of the treatment system is about 10,000 m³d⁻¹, including all sewage collected from Guiyang pumping station. In the collected catchment area, the discharge pipe line is in network distribution, connected to Guiyang Pump Station. Sewage is then sent to the gravel contact oxidation system (Figure 1).

Primary water quality parameters of the designed sewage quality are listed in the following: BOD 40 mgL⁻¹, NH₃-N 18 mgL⁻¹ and SS 40 mgL⁻¹. The designed removal rate is 75% for BOD, SS and NH₃-N; or BOD < 10 mgL⁻¹, SS < 10 mgL⁻¹ and NH₃-N < 5 mgL⁻¹.

The system includes the following four parts, the

influent unit, the pre-treatment unit, the gravel contact aeration oxidation unit, and the effluent unit (Figure 2). The combined sewage flows into the pre-treatment unit under gravity. The rectangular grid at the front of the pre-treatment unit with grid space of 20 mm is used to remove coarse suspended solids. A set of automatic water quality analyzer is placed at inlet to monitor SS and other water quality parameters. When SS concentration is too high, the influent is stopped automatically to avoid high concentrations of SS entering into gravel processing unit, which could decrease porosity and reduce the service life of the gravel contract oxidation system. The sewage then flows into the grit chamber, the purpose of which is to remove sand with particle size larger than 0.2 mm. The design capacity of the grit chamber is 1800 m³m⁻²d⁻¹.

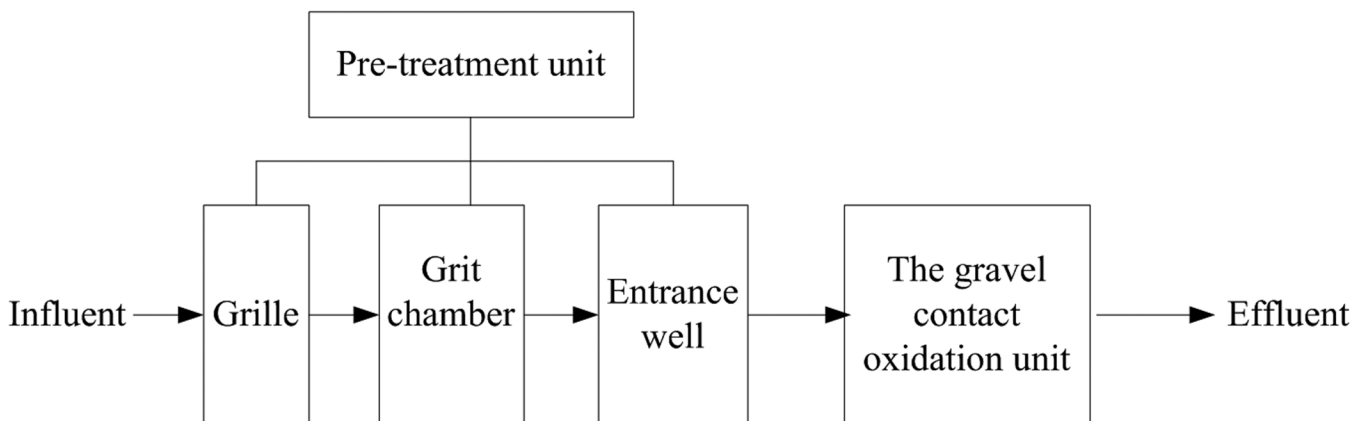


Figure 2. The flow chart of the gravel contact oxidation treatment system.

Gravel Contact Aeration Oxidation Treatment Unit

The Guiyang gravel contact oxidation treatment system was divided into two identical parallel treatment parts considering the space limit. The two units were filled with gravel, the particle size of which is 10–25 mm. The gravel contact aeration oxidation treatment units also consist of two separate parts to deal with high concentrations of ammonia nitrogen in the influent. The front part is an aeration zone, with an effective area of 2,346 m². The latter is non-aeration zone, with an effective area of 782 m². The hydraulic retention time of the aeration zone is 4.5 h, and it is 1h for the non-aeration zone. Therefore, the total hydraulic retention time of the gravel contact aeration oxidation units is 5.5 h. Treatment processes such as organic matter degradation and ammonia nitrogen nitrification occurred in the aeration zone. In the non-aeration zone, processes such as settling of total suspended solid and nitrogen removal by denitrification were also expected.

Water Sampling

From June 2012 to January 2014, influent and effluent were sampled monthly for analyses of DO, NH₃-N, NO₃-N, BOD, COD, and SS. All water quality parameters were analyzed using standard methods described in APHA-AWWAPCF [5].

RESULTS AND DISCUSSION

SS Removal

SS was removed mainly by precipitation and filtration in the gravel contact oxidation treatment process. According to Figure 3, after pre-treatment of the grit chamber, SS concentration of the effluent entering into the gravel contact oxidation unit ranged 10–30 mgL⁻¹, which was not too high. The effluent SS concentration ranged 2–4 mgL⁻¹ and the removal efficiency was 70–95%.

BOD, COD Removal

Some organic matter could be removed quickly through sedimentation and filtration in the gravel contact oxidation system. Soluble organic materials could also be removed by microorganism adsorption and degradation in aerobic conditions. Figure 4 demonstrates the variation of COD and BOD concentration in the influent and effluent: COD concentrations of ranged 30–95 mgL⁻¹ of the influent and 10–20 mgL⁻¹ of the effluent. BOD concentrations of the influent were 13–22 mgL⁻¹ and 1.0–4.2 mgL⁻¹ in the effluent. The removal rate was as high as 85–95%. The concentrations of COD in both influent and effluent were much higher than BOD. In Figure 5, DO concentrations of influent and especially effluent were high, indicating

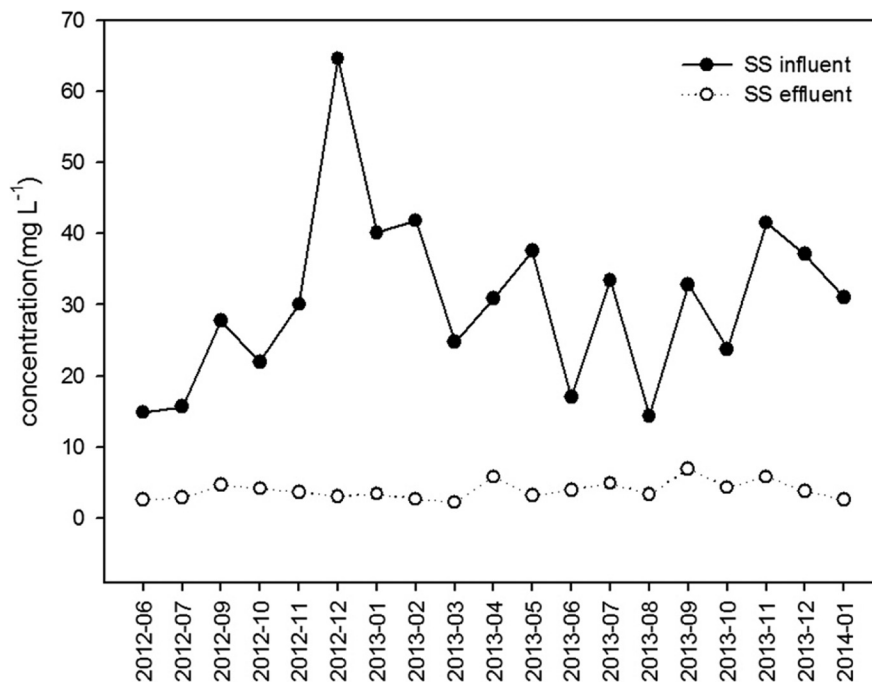


Figure 3. Influent and effluent SS concentrations of the treatment system.

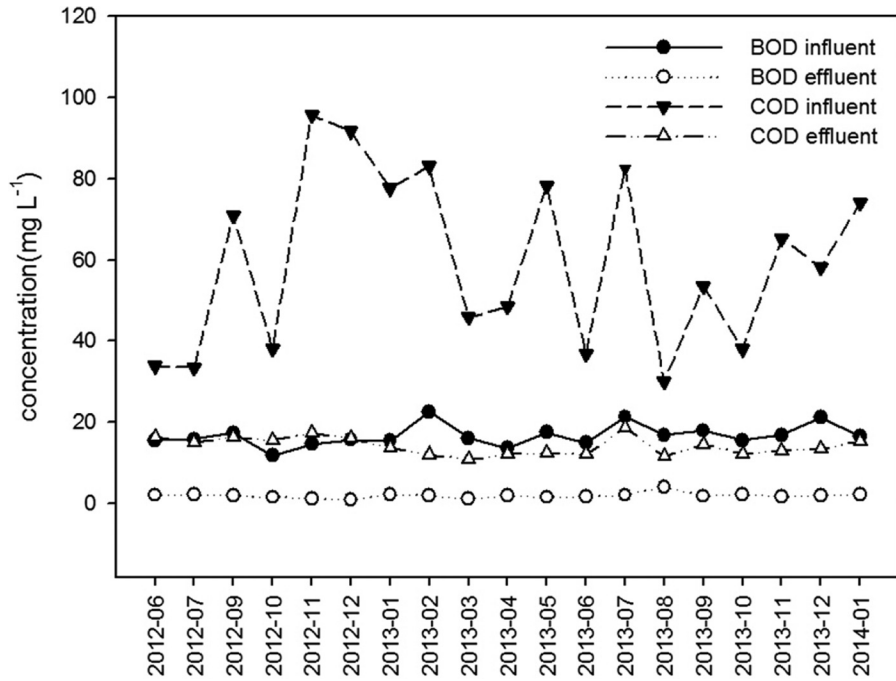


Figure 4. Influent and effluent BOD and COD concentrations of the treatment system.

that biodegradable organic matter was removed sufficiently with adequate dissolved oxygen. BOD concentrations in the effluent were very low. The large difference in BOD and COD concentrations showed that the combined sewage contained much non-biodegradable organic compound. It was difficult to remove such organic compounds just by the gravel contact oxidation system, although COD removal efficiency was high.

Ammonia Nitrogen Removal

The removal mechanisms for ammonia nitrogen by the gravel contact oxidation system include adsorption, filtration and sedimentation, microbial nitrification and denitrification, and ammonia nitrogen volatilization. Among these, microbial nitrification and denitrification play an important role in nitrogen removal process

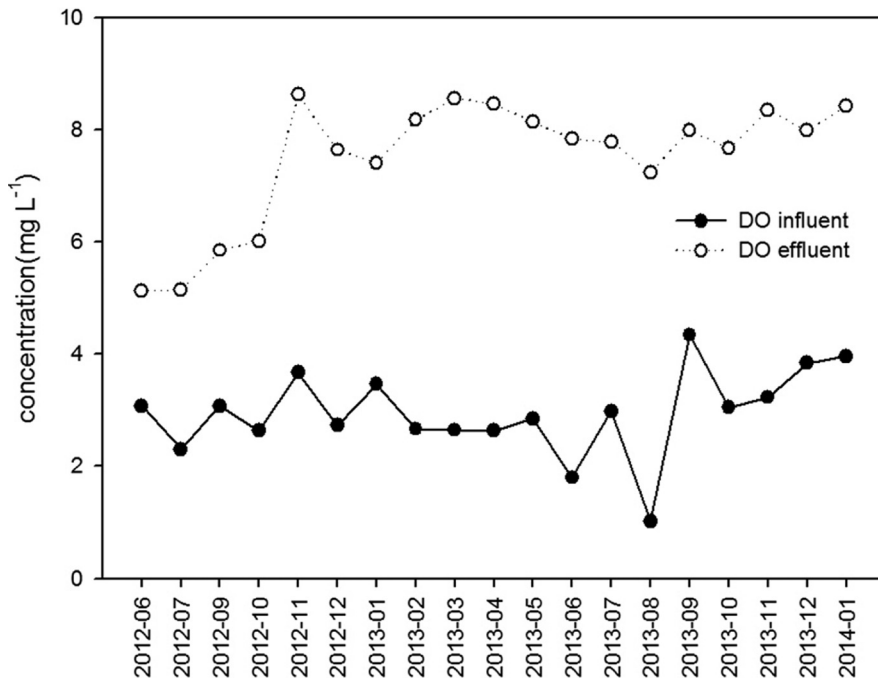


Figure 5. Influent and effluent DO concentrations of the treatment system.

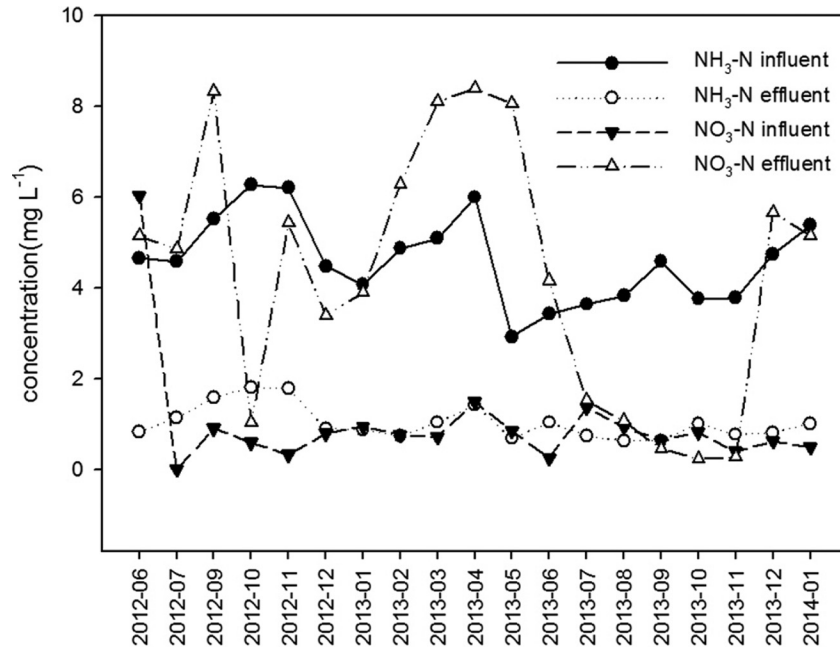


Figure 6. Influent and effluent NH₃-N and NO₃-N concentrations of the treatment system.

[6,7,8]. Figure 6 demonstrates the ammonia nitrogen purification effect of the gravel contact oxidation system. Results show that, the ammonia nitrogen concentration decreased quickly. The concentrations of ammonia nitrogen in the influent were 3–7 mgL⁻¹, while the concentrations of ammonia nitrogen in the effluent decreased to 1 mgL⁻¹. The removal rate reached 70–90%. The average nitrate concentration of influent was 1.0 mgL⁻¹, while the average effluent concentration was 4.28 mgL⁻¹. In the first half of the gravel contact oxidation treatment system (aeration zone), microbial nitrification was accomplished completely. Then the combined sewage flowed into the non-aeration zone with a large amount of dissolved oxygen (Figure 5), although the system was not aerated. The denitrification process could not complete successfully. Ammonia nitrogen has converted into nitrate and nitrite under aerobic conditions. Therefore, ammonia nitrogen concentrations in the effluent were very low, while nitrate concentrations increased considerably. Nitrogen in the system was not removed through nitrification and denitrification processes.

CONCLUSIONS

1. The gravel contact oxidation system is quite effective for combined sewage and rainwater system. The removal efficiency of BOD and SS ranged 75–80%, 70–95% respectively. There was no

seasonal variation for contaminants removal in the system due to the small temperature difference in Taipei throughout the year.

2. The gravel contact oxidation system was divided into two zones, aeration and non-aeration. For excessive aeration in the first half part, the sewage still contained large amounts of oxygen when it flowed through the non-aerated area. The microbial denitrification was relatively poor. Although ammonia nitrogen concentration decreased, nitrate concentration increased simultaneously. Nitrogen was not removed by the system. It was just a migration process among different forms of nitrogen. Therefore, aeration in the front zone of the gravel contact oxidation treatment system should be controlled in order to improve the removal efficiency of nitrogen.

ACKNOWLEDGEMENTS

This research was supported by National Science Foundation of China with the No. 41101465, 41371121 and 41271329, Jiangsu Overseas Research & Training Program for University Prominent Young & Middle-aged Teachers and Presidents, Special Projects for Alliance Construction by Chinese Academy of Sciences, and Science and Technology Support Project of Jiangxi Province (20122BBG70160).

REFERENCES

1. Juang D. F., Tsai W. P., Liu W. K., and Lin J. H. 2008. "Treatment of polluted river water by a gravel contact oxidation system constructed under riverbed," *International Journal of Environmental Science & Technology*, 5(3): 305–314. <http://dx.doi.org/10.1007/BF03326025>
2. Fan C., and Wang W. S. 2006. "Evaluation of efficiency of the pebble-based contact chamber technique applied to the treatment of domestic sewage," *Journal of Environmental Protection (in Chinese)*, 29(2):91–102.
3. Lin J. W. 2011. "The cost-benefit analysis of gravel contact oxidation treatment, Master's Thesis (in Chinese)," National Taiwan Ocean University, Taiwan.
4. Tsai W. P. 2007. "Benefit Evaluation for improvement of water quality of rivers using a gravel-packed reactor, Master's Thesis (in Chinese)," National Central University, Taiwan.
5. APHA-AWWA-WPCF, 1995. "Standard Methods for the Examination of Water and Wastewater, nineteenth ed.," American Public Health Association, Washington, DC.
6. Kemp, M. C., and George, D. B. 1997. "Subsurface flow constructed wetlands treating municipal wastewater for nitrogen transformation and removal," *Water Environment Research*, 69(7), 1254–1262. <http://dx.doi.org/10.2175/106143097X126019>
7. Wang L., and Li T. 2011. "Anaerobic ammonium oxidation in constructed wetlands with bio-contact oxidation as pretreatment," *Ecological Engineering*, 37(8): 1225–1230. <http://dx.doi.org/10.1016/j.ecoleng.2011.03.008>
8. Fu L. L. 2009. "Experimental research and mechanism analysis on sewage treatment with gravel Contact oxidation reactor," *Science & Technology Review*, 13:92–95.

Improvement of Industrial-scale Anaerobic Digestion by Enzymes Combined with Chemical Treatment

MICHAEL RECKTENWALD^{1,*}, ESTERA SZWAJECER DEY² and OLOF NORRLÖW³

¹*Kemira Oyj, P.O. Box 44, FI-02271 Espoo, Finland*

²*Pure and Applied Biochemistry, Lund University, P.O. Box 124, SE-22100 Lund, Sweden*

³*BION KB, Kung Kristoffersgata 3a, SE-25234 Helsingborg, Sweden*

ABSTRACT: The effect of a new developed process for biogas boosting was studied at a municipal wastewater treatment plant in industrial scale over the period of three years. After pre-selection studies in the lab and short industrial setups, four hydrolytic enzymes and sodium citrate were combined and tested for a two-year period. The year 2007 was picked as reference year. In February 2008, the dosage was started. Some immediate changes in the digestion system could be observed like gas production increase and sludge volume reduction. Yet the adaption to the chemical dosage took several months. A stable production was achieved about 6 months after the start of the dosage. In 2009 it was assumed that the system had adapted to the chemical dosages and that stable running parameters were achieved. Mainly the results from the years 2007 as reference and 2009 as resulting year are compared, showing clearly positive effects on process stability, increased gas production by 16% and minimized sludge volumes by 13%.

INTRODUCTION

ANAEROBIC digestion of wastewater sludge is an effective and low-cost method to reduce sludge volumes for disposal [1]. Sludge handling and disposal represent a considerable cost factor for wastewater treatment plants. Therefore novel methods are investigated to make sludge methanization more effective. Dry wastewater sludge consists in general of 60–70% of organic matter, the remaining 30–40% being mostly sand and other inert inorganic matter. The organic matter in the sludge binds large parts of the water, resisting to dewatering and increasing the sludge volumes. At many wastewater treatment plants (WWTPs) in Europe, anaerobic digestion is a commonly used treatment for the stabilization of especially the organic part of the sludge. The organic matter is degraded and the resulting sludge volumes for disposal are minimized. The first step of the anaerobic degradation, the hydrolysis, is considered to be the rate-limiting step [2]. Different chemical and physical sludge disintegration methods have shown to enhance the performance of the digesters [3,4,5,6,7]. A different approach is the enzymatic pre-treatment [8,9,10]. Following a pre-selection in lab

scale, hydrolytic enzymes act on a specific biopolymer present in the sludge substrate, release products with lower molecular weight to the solution and submit it to more effective degradation. The mechanistic approach is the disruption of the floc structure and the release of elevated amounts of proteins, peptides and carbohydrates to solution [11,12]. The low-molecular organic matter becomes more available for the subsequent metabolic steps of the anaerobic digestion. The released organic matter induces a higher metabolic turnover to the acidogenic bacteria and hence an increased performance to the digestion chamber.

Initial laboratory and pilot-scale experiments based on only enzymatic solubilization of organic matter [13,14] showed that the enzymatically pre-treated municipal sludge solubilized the particulate organic matter more effectively. The anaerobic digestion of the pre-treated sludge resulted in a significant increase of methane production compared to untreated sludge. The use of complexing agents like sodium citrate improved the performance of enzymes in lab scale considerably [15,16]. In the pre-studies, the addition of complexing agents like citric acid, sodium tripolyphosphate and EDTA removed cations such as Ca^{2+} , Mg^{2+} , Fe^{2+} and Fe^{3+} from the floc structure. The addition of complexing agents like EDTA or sodium tripolyphosphate (STPP) is a method to extract extracellular polymeric

*Author to whom correspondence should be addressed.
E-mail: michael.recktenwald@kemira.com; Tel.: +358(50)4099379

substances (EPS) from sludge, and was known to release increased amounts of proteins, carbohydrates and humates. The treatment resulted in the degradation of the floc network and in the enhanced release of organic matter. The effect of de-bridging and deflocculation of sludge particles improved the accessibility of added enzymes to the substrate and increased their lifetime by prohibiting the deactivation by being entrapped in the floc structure. The degradation of larger aggregates resulted also in an increase of the specific surface area available for enzymatic hydrolysis. The application of complexing agents enabled the reduction of the enzyme dosage to an economically interesting level. Sodium citrate was picked for the industrial trials because it is completely biodegradable, cheap and has no negative impact on e.g. the pH-levels in the digestion chamber. By that way the application of a combination of sodium citrate and enzymes became economically feasible for testing in industrial scale [17].

The large size set-up was chosen to get a realistic view on the increase of the gas production, on the reduction of sludge volumes and on the improvement of the dewatering properties, as well as on the quality of the achieved solid phase and the possible feedback effects on the treatment plant. The observation period of three years allowed the collection of a sufficiently stable database for a safe statistic evaluation.

MATERIALS AND METHODS

Digestion System of WWTP Kristianstad

The digestion system of WWTP Kristianstad consists of three digestion chambers that are connected in series. The feed flow to the digestion system is thickened sludge from the biological treatment. The average residence time in 2006, before the experimental period, was given as 25 d, and the total size was 200 000 PE (communication by the operators of the WWTP). The sludge to the digestion system is generated in a com-

bined primary and secondary treatment. The sludge to the digestion chambers is thickened by pre-dewatering on a filter drum to about 3% (Figure 1). The temperature in the mesophilic digestion system is 36°C.

Scaling Up Experimental Size, Scaling Down Dosage

Economic feasibility forced the minimization of the dosages along with the scaling-up steps from lab to industrial size application (Table 1). In earlier publications, higher chemical dosages were used in order to push the system into the desired effects and to understand the involved chemical mechanisms focused on the lab scale effects [14,15,16,17]. In industrial size, the long-term effects prevail, the industrial system reacts with a certain delay that is difficult to simulate in lab and pilot scale.

Chemical Dosage Point and Mixing

The dosage point of the chemicals was chosen to be the feeding pipe system to the digestion chambers (Figure 1). The chemical dosage pumps were connected to the sludge feed pumps that gave some mixing effect between added chemicals and feed sludge, but the main mixing was done inside the digestion chambers. It was expected that also under thorough mixing it would take several residence times to achieve the final enzyme concentration.

Chemical Dosage in the Startup and Safe-run Phase

Before the startup, it was discussed how to reach good mixing and fast adaption of the digestion system to the chemical dosage. It was decided to start with an increased dosage, and to cut the dosage to half later when significant effects appear as e.g. gas increase and sludge reduction. In the beginning, it

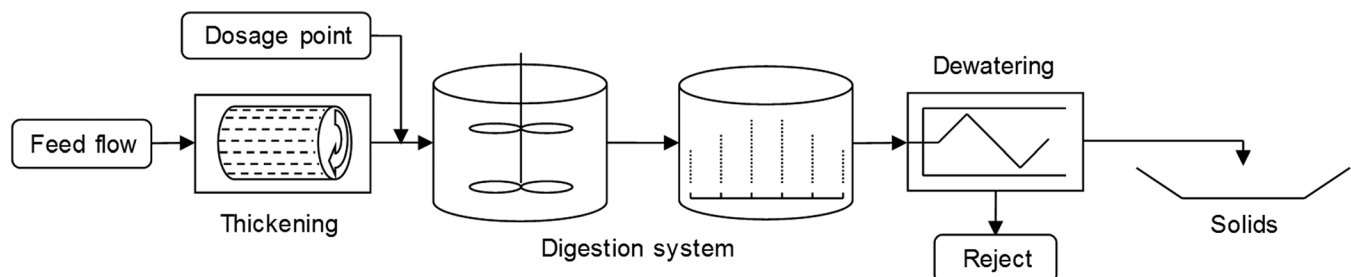


Figure 1. Enzyme dosage point at the digestion system of the WWTP Kristianstad.

Table 1. Chemical Dosages from Lab to Advanced Industrial Trials.

	Lab Tests	Initial Ind.* Trials	Advanced Ind.* Trials	Unit
Enzyme	100–200	< 2.5	< 0.25	[kg/t DS]
Cpx**	200–500	< 5	< 1	[mol/m ³]
Duration	0.1–1	10–100	> 1000	[d]
Publication	[15,16]	[17]	present article	

*Ind.: industrial scale.

**Cpx: Complexing agent.

was not clear how long this startup phase would take, and when the system was stable enough to go to a lower dosage.

The dosage comprised four types of hydrolytic enzymes (cellulase, lipase, alpha-amylase and a protease, supplied by Kemira Kemi AB, Sweden) and sodium citrate (supplied by Kemira Kemi AB, Sweden) as 50% solution (Table 2). The three enzymes cellulase, lipase and alpha-amylase were dosed as a mixture from one storage tank (enzyme mix). The protease was dosed from a separate storage tank to prohibit the hydrolysis of the other enzymes. Also the sodium citrate had its own storage tank. The three components (enzyme mix, protease and sodium citrate solution) were dosed separately in a timed sequence to prohibit their degradation by mixing and dwelling in the feed pipes. The dosage in [g/m³] refers to the ready enzyme liquid [g] and the feed volume to the digesters in [m³]. In the startup phase, the dosage for each of the enzymes was 12.5 g/m³, and for the sodium citrate 1 mol/m³. Later after the indication of clear effects, the dosage was reduced to half for each component, and then kept constant throughout the whole experimental period to the end of 2009 and further for commercial application.

Daily Parameters: Gas, Feed and Exit Flows

The parameters for gas, feed and exit flows were

Table 2. Chemical Dosages and Periods.

Parameters	Trade Name	Startup	Long-term Run
Protease	Kemira BDP-100	12.5 g/m ³	6.25 g/m ³
Cellulase	Kemira BDP-200	12.5 g/m ³	6.25 g/m ³
Lipase	Kemira BDP-300	12.5 g/m ³	6.25 g/m ³
alpha-Amylase	Kemira BDP-400	12.5 g/m ³	6.25 g/m ³
Na-citrate	Kemira BDP-035	1 mol/m ³	0.5 mol/m ³
Start		7 February 2008	15 July 2008
Period		158 d	>900 d*

*Exceeding the experimental period of this article.

Table 3. Parameters Determined Daily and Monthly.

Parameters	Determination	Unit	Amount of Single Data
Gas flow from digestion	Daily	[m ³ /d]	> 355
Feed flow to digestion	Daily	[m ³ /d]	> 355
Exit flow from digestion	Daily	[m ³ /d]	> 355
Dry solids* (DS)	Monthly	[%]	12
Volatile suspended solids* (VSS)	Monthly	[%]	12
Wet sludge for disposal (WSD)	Monthly	[t]**	12

*Dry and volatile suspended solids of the feed and exit flows [20].

**[t]: Metric tons.

logged by daily routine measurements of the WWTP, and later used for statistical evaluation on a daily basis as single data and as monthly averages (Table 3). The gas production was measured by the internal gas gauge system of the WWTP. The feed and exit flows of the digestion chamber are routine parameters for the control of the digestion process. The daily parameters (gas flow, feed and exit flow) were processed to monthly averages for the reason of better comparability to the other parameters determined monthly.

Monthly Parameters: Solids in Feed and Exit Flows

Due to better practicability, monthly averages were measured of the wet sludge for disposal volumes (WSD), dry solids (DS) and volatile suspended solids (VSS) in the feed and exit flows (Table 3). The above mentioned parameters (gas, feed and exit flows) were comprised to monthly averages and used for the calculation of additional monthly averages of the parameters that are later presented in the results part.

Derived Parameters

For the evaluation of the experimental period, the derived parameters (Table 4) were obtained from the daily and monthly logged parameters (Table 3).

Table 4. Derived Parameters.

Parameters	Determination	Unit
Residence time	Daily	[d]
Feed and exit DS***	Monthly	[t]
Feed and exit VSS****	Monthly	[t]
Gas yield per feed VSS	Monthly	[m ³ /t feed VS]
Gas yield per degraded VSS	Monthly	[m ³ /t deg VS]

***DS: Dry solids.

****VSS: Volatile suspended solids (550°C).

Table 5. Sporadically Measured Parameters.

Parameters	Determination	Unit
Gas quality (methane)	Few times per year	[%]
Temperatures	Automatic	[°C]

Sporadically Measured Parameters

The gas composition was constant during the whole experimental period at approx. 65% methane. Samples were only sporadically taken every few months because no bigger impact on the gas composition was expected. The temperature was automatically measured for process surveillance, but not logged (Table 5).

Completeness of the Datasets

The daily datasets about the gas flows, the feed and exit flows of the digestion chamber are composed of 365 single data every year (366 data in 2008) logged by the WWTP. Due to failure in the measurement devices, a maximum of 7 data were discarded from the yearly datasets, so that the monthly averages could be derived from yearly datasets with over 358 single values.

RESULTS AND DISCUSSION

Stability of the Periods

The running mode of an industrial scale WWTP is dynamic and subjected to continuous changes depending on e.g. the weather and inflow volumes from the municipal sources. In Kristianstad the wastewater mainly originates from households and from fruit and vegetable processing industries.

Comparison of Data on Daily and Monthly Basis

Due to practical reasons, the values that were not automatically logged by the WWTP had to be measured on monthly basis. In order to check the reliability of the daily logged data against the monthly averages, the two daily datasets are compared against their monthly averages in a cumulative norm distribution (Figures 2 and 3, Table 6).

Statistical Treatment of the Daily Logged Data

The daily measured data for daily gas production (Figure 2) and residence time (Figure 3) of 2007 and 2009 were sorted from the lowest to the highest, ac-

ording to their size in order to get a statistical distribution along the x -axis. For the y -axis, a counter was calculated where 1 is divided by the whole count of the values (here 1/358), see Table 3.

Statistical Treatment of the Monthly Averages

Based on the 12 points of monthly measurements in the years 2007 and 2009, a cumulative logarithmic norm distribution was calculated. The 12 single points were transformed to natural logarithms. The average μ and the standard deviation σ were calculated over the 12 logarithms and put into the cumulative distribution function Φ , resulting in a logarithmic normal distribution.

Cumulative Distribution Function

$$F(x, \mu, \sigma) = \Phi\left(\frac{\ln x - \mu}{\sigma}\right)$$

μ = Average

σ = Standard deviation

The use of only 12 points for the calculation of a logarithmic normal distribution effects that the standard deviation is considerably smaller than the one based on 358 single points (Table 6, Figures 2 and 3).

The availability of daily data gives us the possibility to compare the daily logged data against their monthly averages. This was done with the daily gas production and feed sludge to the digester expressed as residence time. In Figures 2 and 3, the daily logged gas produc-

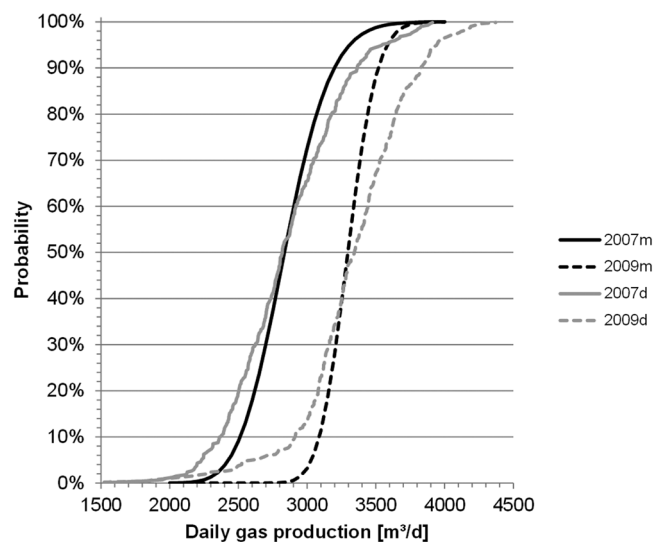


Figure 2. Cumulative norm distribution of the daily gas production as single values (grey, 2007d, 2009d) and monthly averages (black, 2007m, 2009m) in 2007 (ref) and 2009.

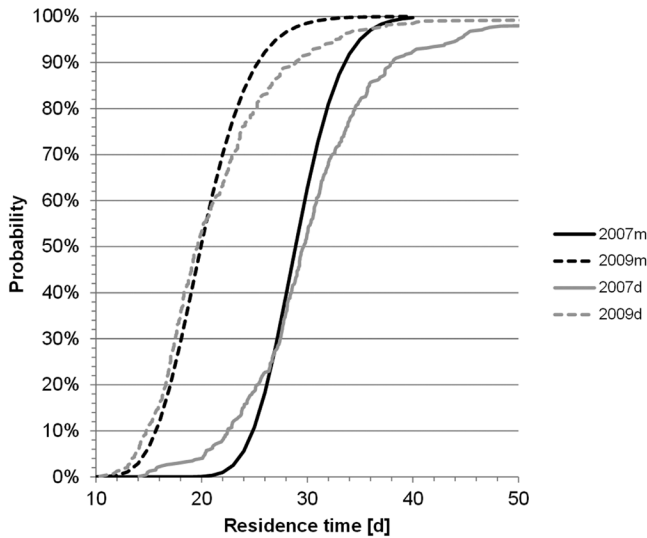


Figure 3. Cumulative norm distribution of the daily residence time derived from the daily feed flows as single values (grey, 2007d, 2009d) and monthly averages (black, 2007m, 2009m) in 2007 (ref) and 2009.

tion and residence times are compared to their monthly averages in 2007 (reference year) and 2009 (year with chemical treatment) in a cumulative norm distribution. The grey lines (2007d and 2009d) are based on the daily logged 355 values, the black lines (2007m and 2009m) are based on the 12 monthly averages of the same dataset.

Comparison of Daily Logged Data and Monthly Averages

Both the results from the daily-based and monthly-based values show similar values. The steeper slope of the log-norm distributions based on the monthly averages (2007m and 2009m) compared to the daily values (2007d and 2009d) is due to the smaller standard deviation (Table 6) of the monthly-based dataset. In Table 6 can be seen that the daily logged data show a higher standard deviation than the monthly averages due to a higher range of deviations caused by daily measurements. In the further discussion, the conclusions are referred to the monthly datasets.

The Figures 2 and 3 show an average increase in the monthly averages of the daily gas production from 2846 (2007m) to 3300 (2009m) m^3/d , a relative increase by 16%. At the same time, the residence time decreased from an average 29.1 (2007m) to 20.3 (2009m) days. The shorter residence time was due to changes in the pre-dewatering device to the digesters. With a shorter residence time, also a lower gas production should be expected. But due to the chemical addi-

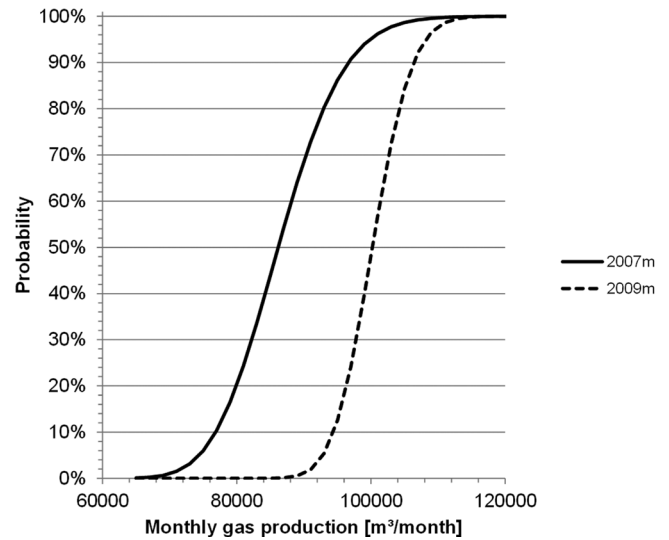


Figure 4. Cumulative norm distribution of the monthly gas production as monthly averages in 2007 (ref) and 2009.

tion the gas production increased instead. The further evaluation below will give a more detailed picture of the factors contributing to the higher gas production.

The average monthly gas production increased from 86,504 to 100,301 m^3/month (Figure 4, Table 6). This is an increase of 16%. It can be compared to the increased daily gas production (Figure 2). The methane content was only sporadically measured. It ranged between 63% and 67% during the experimental period. However, there is a yearly period of lower methane content during late autumn in October and November, where the methane percentage decreases to below 60% due to seasonal substrate changes caused by waste

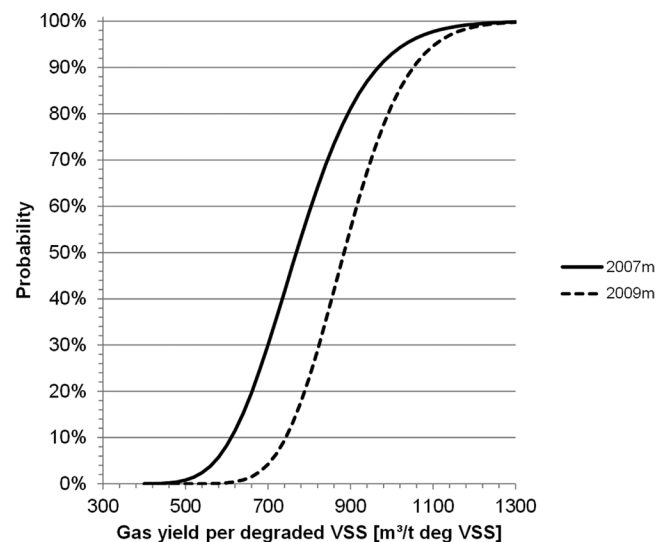


Figure 5. Cumulative norm distribution of the monthly produced gas per tonne degraded volatile suspended solids [$\text{m}^3/\text{t deg VSS}$] in 2007 (ref) and 2009.

streams from the surrounding food industry. The methane content recovers after this period.

The VSS was measured once or a few times per month [20], the monthly average was taken, and the quotient of produced gas versus degraded VSS was calculated. Figure 5 shows a 14% increase of the gas yield per degraded ton VSS from 780–892 m³/t deg VSS, indicating a better turnover and transformation of organic matter to biogas. At the same time, Figure 6 indicates a decreased gas yield per feed VSS by –15% from 485 to 414 m³/t feed VSS. The decrease can be caused by three effects: (1) the DS load increased during the experimental time (Figure 6), (2) due to the increased flows, the residence time went down from 29.1 (2007m)–20.3 (2009m) days (Figure 3), (3) the periodically high feed flows caused a temperature decrease by temporarily 2°C from 36–34°C. The temperatures were not continuously logged (Table 5).

The amount of monthly disposed wet sludge (Figure 7) decreased from 970–841 t/month. This decline by 13% was achieved although the measured monthly feed dry solids to the digester system increased considerably by 41% from 226–319 t/month (Figure 8). At the same time, the dry solids of the wet sludge for disposal that was produced from the decanters increased from average 18 to over 20%. The data for the dry solids of the wet sludge for disposal were not consequently logged month by month especially for the reference period 2007, so that only a rough average of 18% based on a few measurements in 2007 can be given for the whole reference period of 2007, and 20% for the period of 2009. Anyway the sludge dryness was improved

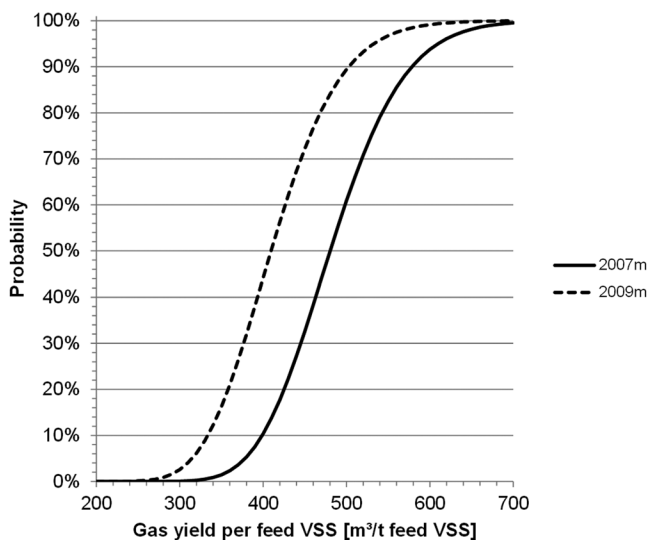


Figure 6. Cumulative norm distribution of the monthly produced gas per ton feed volatile suspended solids [m³/t feed VSS] in 2007 (ref) and 2009.

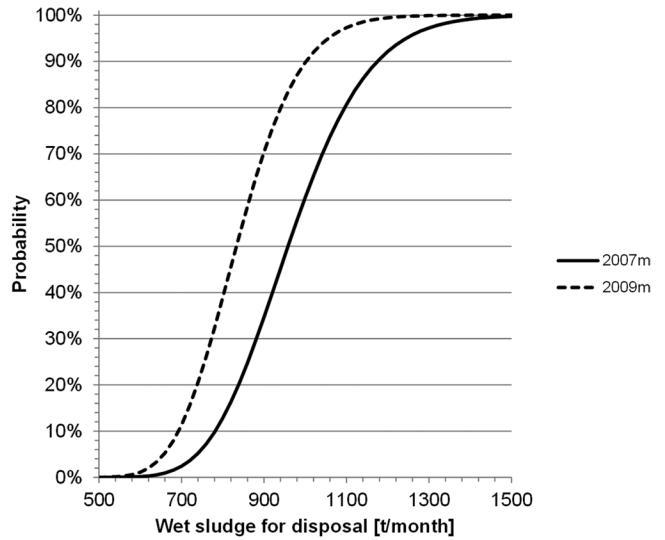


Figure 7. Cumulative norm distribution of the monthly disposed wet sludge [t/month] from the decanters in 2007 (ref) and 2009.

in 2009, and periodically considerably better dry solids of more than 20% could be produced on the decanters. It is hypothesized that due to the better solubilization and degradation of water-rich organic matter, such as EPS [17,18] that typically resists effective dewatering, the sludge was dewatered more effectively [19].

Also the quotient of the dry solids exit flow from the digester versus the dry solids feed flow into the digester indicates an increased degradation of organic matter. The quote decreased by 31 % from 0.777–0.536 t/t (Figure 9). It can be considered as a sort of mass balance over the flows in and out of the digestion system. The decrease of the quote indicates an increased turnover and improved degradation of organic matter.

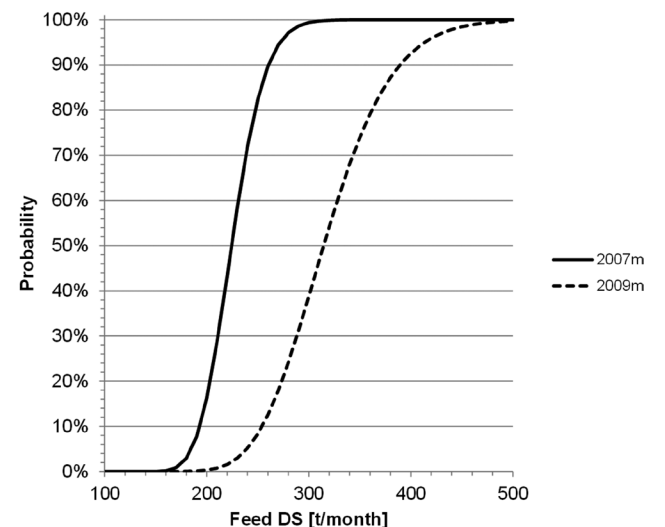


Figure 8. Cumulative norm distribution of the monthly feed dry solids [t/month] to digestion in 2007 (ref) and 2009.

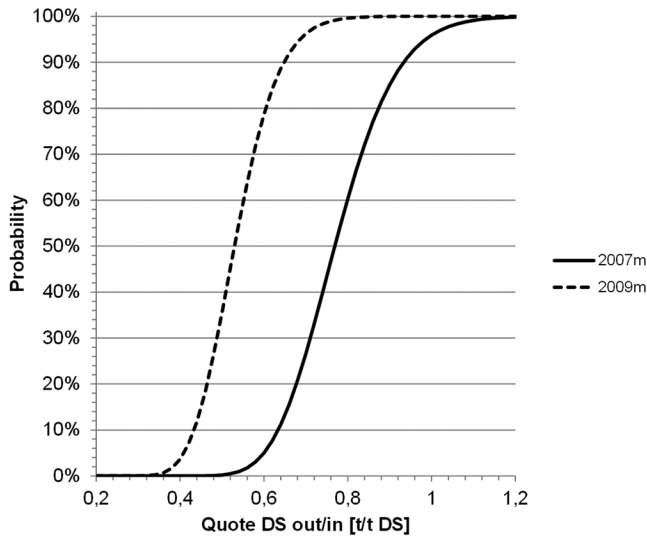


Figure 9. Cumulative norm distribution of the quote of monthly dry solids exit flow from the digester versus the dry solids feed flow into the digester [t/t] in 2007 (ref) and 2009.

Startup Phase in 2008 Showing the Adaption of the System

In Figure 10, the absolute cumulative gas production based on the daily logs can be seen in the years 2007 (reference phase), 2008 (startup phase) and 2009 (result phase). The graph for 2007 is stable at lower

values delivering the reference, the graph for 2009 is stable at higher values. Soon after the startup of the chemical addition in the beginning of February 2008, an increase in gas production can be registered in the graph of 2008 already in March. Also Figure 11, showing the relative changes in gas production of 2008 in relation to the reference year 2007, confirms a clear boosting effect already in March, about one month or one residence time after the startup. In the further run of 2008 (Figures 10 and 11), a clear decrease in September can be seen, possibly as an answer of the system to the dosage changes in mid-August. But the system adapted and recovered already in October.

Compared to the clear increase in gas production after the startup in February 2008, the decrease in wet sludge production from the decanter is delayed. The decrease of the wet sludge volumes starts to get visible after 4 to 5 months from the start of dosage, and becomes really obvious in the end of the year 2008 (Figure 12). This result indicates that the microbial consortium in the industrial digestion system needs 4 to 5 months, approximately 4 to 5 residence times, to adapt to the chemical addition. Possibly during this time, changes can be seen in the microbial composition, favouring the microbes that degrade the solubilized and easier accessible organic matter.

Table 6. Summary of Daily Data and Monthly Averages, Standard Deviations.

Parameters	Unit	Year	Database	Median	Average	Std Dev	Std Dev [%]	Diff. to Ref 2007	Figure Reference
Daily gas production	[m ³ /d]	2007d	daily	2819	2848	399	14		Figure 2, grey solid line
	[m ³ /d]	2009d	daily	3343	3334	405	12	+17%	Figure 2, grey dotted line
	[m ³ /d]	2007m	monthly	2845	2846	264	9		Figure 2, black solid line
	[m ³ /d]	2009m	monthly	3273	3300	168	5	+16%	Figure 2, black dotted line
Residence time	[d]	2007d	daily	29.6	31	11.5	37		Figure 3, grey solid line
	[d]	2009d	daily	19.6	21.2	6.8	32	-32%	Figure 3, grey dotted line
	[d]	2007m	monthly	28.5	29.1	3.29	11		Figure 3, black solid line
	[d]	2009m	monthly	20	20.3	3.77	19	-30%	Figure 3, black dotted line
Monthly gas production	[m ³ /month]	2007	monthly	85791	86504	7764	9		solid line
	[m ³ /month]	2009	monthly	100199	100301	4655	5	+16%	dotted line
Degraded VSS gas yield	[m ³ /t deg VSS]	2007	monthly	740	780	140	18		solid line
	[m ³ /t deg VSS]	2009	monthly	888	892	120	13	+14%	dotted line
Feed VSS gas yield	[m ³ /t feed VSS]	2007	monthly	481	485	71.2	15		solid line
	[m ³ /t feed VSS]	2009	monthly	432	414	63.9	15	-15%	dotted line
Wet sludge for disposal	[t/month]	2007	monthly	957	970	156	16		solid line
	[t/month]	2009	monthly	829	841	122	15	-13%	dotted line
Feed DS	[t/month]	2007	monthly	227	226	27.3	12		solid line
	[t/month]	2009	monthly	310	319	53.6	17	+41%	dotted line
Quote DS out/in	[t/t]	2007	monthly	0.798	0.777	0.116	15		solid line
	[t/t]	2009	monthly	0.538	0.536	0.084	16	-31%	dotted line

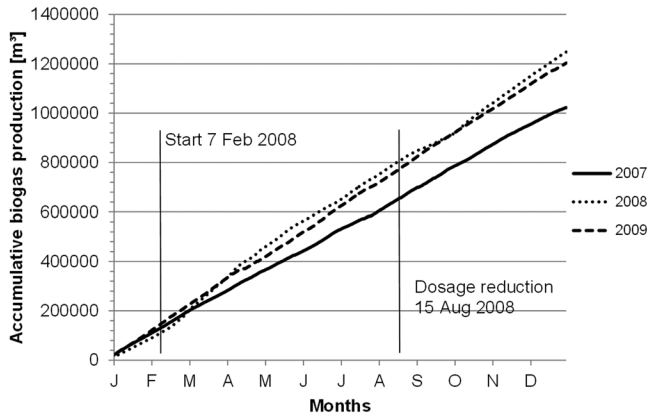


Figure 10. Cumulative absolute gas production in 2007, 2008 and 2009.

Increased Dry Solids After the Centrifuge

As a positive side effect, the sludge dewatering in the decanter centrifuge was easier and the resulting DS for disposal increased from 18% to over 21% in the beginning. Due to technical reasons and in order to keep the decanter in a steady running mode, the final DS amount was later set to be 20%.

Economy

With a price for the produced gas of 1 SEK/m³ and a price for the disposal of wet sludge of 300 SEK/t, the yearly benefit of the chemical addition was calculated to be SEK 622,000 (approx. EUR 70,000), based on an additional income of SEK 160,000 from gas sales and expense savings of SEK 462,000 due to minimized sludge volumes. The numbers are taken from the an-

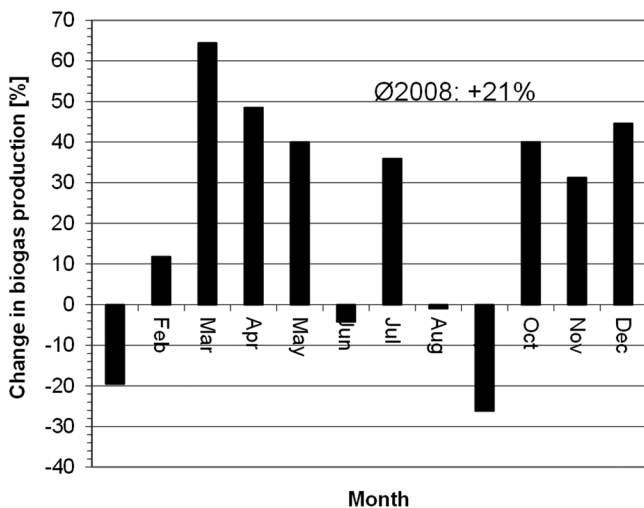


Figure 11. Changes in biogas production in 2008 after the startup compared to the reference year 2007.

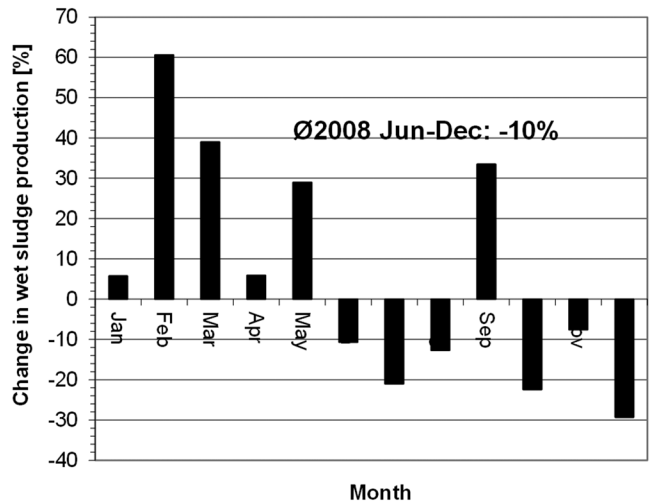


Figure 12. Changes in wet sludge for disposal production 2008 after the startup compared to the reference year 2007. Sludge minimization starts clearly in June.

nual reports of WWTP Kristianstad. It can be clearly seen that the main benefit comes from sludge volume savings.

The chemical (enzyme and complexing agent) cost can be assumed to be between 300,000 and 400,000 SEK for the whole year. The profitability depends strongly on the local circumstances, such as the cost for sludge disposal or the income per produced cubic meter of gas. The market price for the produced biogas was given as 1 SEK/m³ at the lower end of the possible scale, and defined by the local contracts. The energy content of 1 m³ purified methane is comparable to 1 kg of car petrol. As the market price for purified biogas is considerably higher, an own biogas purification plant could increase the benefit.

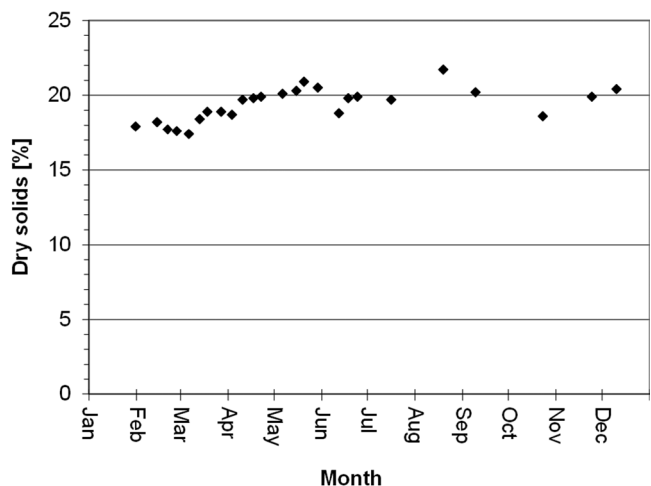


Figure 13. Produced dry solids of digested sludge after decanter dewatering in 2008.

Table 7. Economy from Increased Gas and Minimized Sludge Production.

	2007 (ref)	2009	Change	Benefit
Gas production	1,040,000 m ³	1,200,000 m ³	+15%	160,000 SEK
Disposed sludge	11,635 t	10,095 t	-15%	462,000 SEK
			Total:	622,000 SEK

SUMMARY

Over a period of three years, the WWTP of Kristianstad was the object of investigations concerning the improvement of the biogas production by the addition of a complexing agent as chemical activator (sodium citrate) and a set of four enzymes. The whole year 2007 was used as reference period. The logged data from the WWTP were used as basis for the calculations of the expected changes in the gas, liquid and solid feed and exit flows, resulting in a sort of a surely incomplete, but still representative mass balance over an industrial digester system. A few data were logged daily as e.g. the gas flow, the liquid feed and exit flows of the digestion system. The comparison of the statistically evaluated data shows that the data on daily basis are as reliable as the averages on monthly basis. Due to practical reasons, some datasets as e.g. dry solids and volatile suspended solids in feed and exit flows were logged on monthly basis and used in order to get a rough overview over the changes in the digester system that were initiated by the chemical addition. The statistical evaluation refers mainly to the reference period 2007 and the result period 2009. The evaluation of whole-year periods can be considered to be more practicable because periodical events like e.g. seasonal weather changes will play a minor effect in the evaluation. In addition, the yearly based dataset is bigger and gives a safer basis for statistical evaluation.

The year 2008 is considered separately because of the observation of some interesting startup effects. The startup of the chemical dosage in the beginning of 2008 triggered almost immediately the increase of the gas production one month later, whereas the response by decreased sludge volumes was delayed by 4 to 5 months, corresponding to approximately 4 to 5 residence times. The digester system also responded slightly by less gas production and increased wet sludge production when, due to economic reasons, the dosage was cut to half in August 2008.

Indications for improved gas production

- Higher absolute gas production in [m³/d] and [m³/month] (Figures 2 and 4)

- Higher gas yield per degraded VSS in [m³/t deg VSS] (Figure 5)

Indications for process disturbances

- Higher feed flow in 2009 in [t DS] (Figure 8)
- Shorter residence time in [d] (Figure 3) due to increased feed flow
- Lower gas yield per feed VSS in [m³/t feed VSS] (Figure 6) due to increased feed flow and shorter residence time

Indication for a more stable process

- Lower quote of exit DS vs. feed DS in [t/t] (Figure 9)
 - Indicating a better turnover of organic matter in the digester system
 - Despite the fact of higher feed flows, shorter residence times and lower temperatures in the digester system
- Less wet sludge for disposal in [t/month] (Figure 7)

CONCLUSIONS

The model about improved methanization of wastewater sludge by improved enzymatic sludge solubilization that was elaborated in lab scale was successfully tested in industrial scale. The treatment gave a clear increase in gas production and gas yields (+16%, Table 6), and a clear decrease of sludge volumes for disposal (-13%, Table 6). Even higher feed flows to the digestion system, causing reduced residence times (Table 6) and temporarily decreased temperatures in the digestion, gave only minor process disturbances. It can be hypothesized that the chemical addition stabilized the digestion system. In addition, it can be assumed that at least the sludge volumes for disposal would even show higher reduction rates in comparison to the reference year. The additional feed flow in 2009 could as well be a reason for the increased gas production, but in this case the considerably shortened residence time from 29 to 20 days would basically have led to decreased gas volumes.

The application of this approach required no additional treatment step in form of e.g. a separate enzyme

hydrolysis, and therefore needed minimum investments for a set of chemical pumps. The technical setup was very simple and basically only consisted of adding the chemicals to the feed flow of the digestion system.

A further target should be a minimization of the dosage. Also the reduction of the number of different enzymes should be considered as it can be assumed that some of the applied enzymes contributed more to the sludge solubilization than others. It can also be hypothesized that there is no direct correlation between the dosage and the response of the digestion system. The system was started by increased dosages during an initial period that was indicated by increased gas production after a few weeks and by decreased sludge production after 4 to 5 months. After this period, the system seemed to have achieved a new state of balance by a possible shift in the microbial community [21,22] that needed only a little stimulation by continued chemical additions to remain stable.

ACKNOWLEDGEMENTS

The authors wish to thank the WWTP Kristianstad for their support.

REFERENCES

- Madsen, M., Holm-Nielsen, J.B., Esbensen, K.H., "Monitoring of anaerobic digestion processes: A review perspective", *Renewable and Sustainable Energy Reviews* 15, 2011, pp. 3141–3155. <http://dx.doi.org/10.1016/j.rser.2011.04.026>
- Luo, K., Yang, Q., Li, X.M., Yang, G., Liu, Y., Wang, D.B., Zheng, W., Zeng, G.M., "Hydrolysis kinetics in anaerobic digestion of waste activated sludge enhanced by a amylase", *J. Biochem. Eng.* 62, 2012, pp. 17–21. <http://dx.doi.org/10.1016/j.bej.2011.12.009>
- Ødegaard, H., "Sludge Minimization technologies—An overview", *Water Science and Technology*, 49 (10), 2001, pp. 31–40.
- Vera, M.A., Nickel, K., and Neis, U., "Disintegration of sewage sludge for improved anaerobic biodegradation", Proceedings of the 57th Annual Conference of the Western Canada Water and Wastewater Association, Saskatoon, Saskatchewan, Canada, October 16–19, 2005; Putz G., Ed.; Western Canada Water and Wastewater Association: Calgary, Alberta, Canada, 2005, pp. 05/1-05/9.
- Neyens E., J. Baeyens J., "A review of thermal sludge pre-treatment processes to improve dewaterability", *Journal of Hazardous Materials B98*, 2003, pp. 51–67. [http://dx.doi.org/10.1016/S0304-3894\(02\)00320-5](http://dx.doi.org/10.1016/S0304-3894(02)00320-5)
- Fang, W., Zhang, P., Zhang, G., Jin, S., Li, D., Zhang, M., Xu, X., "Effect of alkaline addition on anaerobic sludge digestion with combined pretreatment of alkaline and high pressure homogenization", *Biore-source Technology* 168, 2014, pp. 167–172. <http://dx.doi.org/10.1016/j.biortech.2014.03.050>
- Carlsson, M., Lagerkvist, A., Morgan-Sagastume, F., "The effects of substrate pre-treatment on anaerobic digestion systems: A review", *Waste Management* 32, 2012, pp. 1634–1650. <http://dx.doi.org/10.1016/j.wasman.2012.04.016>
- Ayol A., "Enzymatic treatment effects on dewaterability of anaerobically digested biosolids-I: performance evaluations", *Process Biochemistry*, 40, 2005, pp. 2427–2434. <http://dx.doi.org/10.1016/j.procbio.2004.09.023>
- Roman, H. J., Burgess, J. E., and Pletschke, B. I., "Enzyme treatment to decrease solids and improve digestion of primary sewage sludge", *African Journal of Biotechnology*, 5(10), 2006, pp. 963–967.
- Yang, Q., Luo, K., Li, X., Wang, D., Zheng, W., Zeng, G., Liu, J., "Enhanced efficiency of biological excess sludge hydrolysis under anaerobic digestion by additional enzymes", *Biore-source Technology*, 101, 2010, pp. 2924–2930. <http://dx.doi.org/10.1016/j.biortech.2009.11.012>
- Dey, E.S., Szewczyk, E., Wawrzynczyk, J., Norrlöw, O., "A novel approach for characterization of exopolymeric material in sewage sludge", *Journal of Residuals Science and Technology*, 3(2), 2006, pp. 97–103.
- Watson, S.D., Akhurst, T., Whiteley, C.G., Rose, P.D., Pletschke, B.I., "Primary sludge floc degradation is accelerated under biosulphidogenic conditions: Enzymological aspects", *Enzyme and Microbial Technology*, 34(6), 2004, pp. 595–602. <http://dx.doi.org/10.1016/j.enzmictec.2004.01.004>
- la Cour Jansen, J., Davidsson, Å., Dey, E.S., Norrlöw, O., "Enzyme assisted sludge minimization", In Chemical Water and Wastewater Treatment VIII, Proceedings of the 11th Gothenburg Symposium, Orlando, Florida, United States of America, November 8–10, 2004; Hahn, H. H., Hoffmann, E., Ødegaard, H., Eds.; IWA Publishing: London, 2004; pp. 345–353.
- Wawrzynczyk, J., Dey, E.S., Norrlöw, O., Jansen, J.I.C., "Alternative method for sludge reduction using commercial enzymes", Proceedings of the 8th CIWEM/Aqua Enviro European Biosolids and Organic Residuals Conference, Wakefield, West Yorkshire, UK, 2003; Lowe P., Hudson J.A., Eds.; Aqua Enviro Technology Transfer, 2003; pp. 1–5.
- Wawrzynczyk, J., Recktenwald, M., Norrlöw, O., Dey, E.S., "The function of cation-binding agents in the enzymatic treatment of municipal sludge", *Water Research*, Volume 42, Issues 6-7, 2008, pp. 1555–1562. <http://dx.doi.org/10.1016/j.watres.2007.11.004>
- Wawrzynczyk, J., Recktenwald, M., Norrlöw, O., Dey, E.S., "Solubilisation of sludge by combined chemical and enzymatic treatment", *African Journal of Biotechnology*, Vol. 6 (17), 2007, pp. 1994–1999.
- Yu, G.H., He, P.J., Shao, L.M., Zhu, Y.S., "Extracellular proteins, polysaccharides and enzymes impact on sludge aerobic digestion after ultrasonic pretreatment", *Water Research*, 42, 2008, pp. 1925–1934. <http://dx.doi.org/10.1016/j.watres.2007.11.022>
- Subramanian, S.B., Yan, S., Tyagi, R.D., Surampalli, R.Y., "Extracellular polymeric substances (EPS) producing bacterial strains of municipal wastewater sludge: Isolation, molecular identification, EPS characterization and performance for sludge settling and dewatering", *Water Research*, 44, 2010, pp. 2253–2266. <http://dx.doi.org/10.1016/j.watres.2009.12.046>
- Recktenwald, M., Wawrzynczyk, J., Norrlöw, O., Dey, E.S., "Significant improvement of industrial scale anaerobic digestion by the addition of glycosidic enzymes", *Journal of Environmental Science and Health, Part A*, Volume 43, Issue 13, 2008, pp. 1536–1540. <http://dx.doi.org/10.1080/10934520802293693>
- APHA, Standard Methods for the Examination of Water and Wastewater, 21st ed., American Public Health Association, Washington, DC, USA, 2005.
- Demirel, B., Scherer, P., "The roles of acetotrophic and hydrogenotrophic methanogens during anaerobic conversion of biomass to methane: a review", *Rev. Environ. Sci. Biotechnol.*, 7, 2008, pp. 173–190. <http://dx.doi.org/10.1007/s11157-008-9131-1>
- Xin, X.D., He, J.G., Qiu, W., Tang, J., Liu, T.T., "Microbial community related to lysozyme digestion process for boosting waste activated sludge biodegradability", *Biore-source Technology*, 175, 2015, pp. 112–119. <http://dx.doi.org/10.1016/j.biortech.2014.10.042>

Polycyclic Aromatic Hydrocarbon Accumulation in *Phragmites australis* Grown on Constructed Wetland for Sludge Stabilization

YUBO CUI¹, WANJUN ZHANG¹, HONGJIE SUN^{1,*}, WEI-MIN WU² and XUEJUN ZOU¹

¹College of Environment & Resources, Dalian Nationalities University, Dalian 116600, China

²Department of Civil & Environmental Engineering, William & Cloy Codiga Resource Recovery Research Center, Center for Sustainable Development & Global Competitiveness, Stanford University, Stanford, CA 94305-4020, USA

ABSTRACT: A pilot-scale constructed wetland was tested for the disposal and stabilization of sludge from a municipal wastewater treatment plant. The accumulation and distribution of sixteen polycyclic aromatic hydrocarbons (PAHs) in the plants of *Phragmites australis* grown on the wetland receiving the sludge was investigated in comparison with native plants without the sludge to examine the effectiveness using *P. australis* as PAHs bioaccumulator. The experiment lasted for three years and divided into three phases: year 1 was adjustment phase; year 2 was operational phase; year 3 was natural stabilization phase. Analysis of the distribution of PAHs in native *P. australis* showed that the sequence of PAHs content in the plants was leaves > stems > roots at 2583, 2198 and 899 µg/kg (DW), respectively. After two year load and one year natural stabilization, the PAHs content in the loaded sludge declined by 63%; the tested plants in the constructed wetland accumulated much more PAHs than native plants. The bioconcentration factor (BCF) of leaves was slightly higher than that of roots and stem i.e. 3.759, 3.518 and 3.368, respectively. The respective PAHs contents in the roots, stems and leaves of the tested *P. australis* were 7313, 7002 and 7814 µg/kg (DW), being 8.13, 3.19 and 3.02 times of that in the native one, respectively. The BCF of roots and stems of the low molecular weight (MW) PAHs (2–3 ring PAHs) predominated as 5.02 and 4.93 in all samples from the constructed wetland, while the BCF of middle-MW PAHs (4 ring PAHs) was 3.15 and 2.1, and that of high-MW PAHs (5–6 ring PAHs) was 2.29 and 2.63, respectively. In the leaves, the BCF of low-MW and middle-MW PAHs was 4.03 and 4.17, which was higher than 2.81 of high-MW PAHs. The results demonstrated that this plant can effectively remove PAHs from the sludge discharged to the wetland.

INTRODUCTION

THE wide application of aerobic activated sludge process for municipal wastewater and industrial treatment has resulted in a great amount of waste sludge, which causes urgent problems of sludge treatment and disposal, especially in China. The sludge could be used as a resource of fertilizer or soil conditioner because it contains nitrogen, phosphorus, potassium, organic matter, and other microelements. However, the contents of various pollutants in the sludge limit the application. Polycyclic aromatic hydrocarbons (PAHs) have been found in the sludge [1] and tend to accumulate in sediments and soils due to their hydrophobicity and high lipophilicity. These compounds have persistence, low biodegradability and carcinogenic properties.

The sludge produced in industrial wastewater treatment may have high PAHs contents up to 2000 mg/kg [1]. According to Chinese standards of PAHs for agricultural application, benzo(a) pyrene (BaP) content should be less than 3 mg/kg dry weight (DW). Other countries require higher standards. For instance, Denmark set up the total quantity of PAHs of 3 mg/kg DW on July 1, 2007. The Netherlands regulates the PAHs content in uncontaminated soil ranging from 0.02 to 0.05 mg/kg DW [2].

Previous studies suggested that some plants can be used for remediation of soils contaminated with PAHs [3–5]. Constructed wetland receiving wastewater sludge has been proposed a new approach for degradation and transformation of PAHs in wastewater sludge [6–7]. The constructed wetland for sludge treatment is also known as sludge drying reed bed, and its relevant research and application are increasingly extensive, especially in the aspects of sludge dewatering, organic

*Author to whom correspondence should be addressed.
E-mail: city-water@163.com

matter stabilization, removal of nitrogen and phosphorus, etc. [6, 8, 9]. Sludge produced from the wastewater treatment process contains some organic micro-pollutants as a consequence of the human activities. Hazardous organic compounds such as linear alkylbenzene sulfonates (LASs) and nonylphenoethoxylates (NPEs) have been reported to degrade in a reed bed with a mineralization of 98% of LAS and 93% of NPE [10]. Also the concentrations of personal care products (fragrances) and various pharmaceuticals have been reported to be reduced effectively [11]. However, to date, no detailed research on PAHs degradation and transformation from sludge by the plants in the wetland has been published. We have conducted experiments to investigate PAHs transformation from the stabilized sludge in the constructed wetland for three years. The results demonstrated that a typical plant *Phragmites australis* can serve effectively as PAHs bioaccumulator for the removal of PAHs

MATERIALS AND METHODS

Pilot-scale Constructed Wetland

A pilot-scale constructed wetland system, which was built inside the Dalian Development Zone Wastewater Treatment Plant, Liaoning Province, China, was composed of sludge pump, sludge feed tank and reed bed. The size of reed bed was 3.0 m × 1.0 m × 1.3 m in height (0.65 m of filled media layer and 0.65 m height of holding space). The media in the reed bed unit comprised a 0.2 m slag layer, a 0.2 m gravel layer, a 0.05 m coarse sand layer, and a 0.2 m fine sand layer from the bottom to the top. The holding space of 0.65 m in height was available for the storage of de-watered sludge. The drainage system was made of 3 m perforated PVC pipe with 0.2 m in diameter and located on the bottom of the bed. Sludge leachate was collected and pumped back to the wastewater treatment system for treatment.

Operation and Maintenance

The experiment lasted for three years and divided into three phases: (1) year 1: was adjustment phase; (2) year 2 was operational phase; and (3) year 3 was natural stabilization phase.

The system started in mid-May of year 1. After plants of *Phragmites australis* were transplanted and cultivated in the pilot test area for 25 days, the sludge was loaded on the bed periodically. Sludge (600 L)

was loaded into the holding space within 30 min every week. The load of sludge in the bed was performed for a total of 18 times in year 1 and ended at the end of October. The system was then operated in the same way for 24 times in year 2. At the end of year 2, the calculated thickness of sludge loaded reached a height of 8.4 m based on water content in sludge of average 99.1%. Total suspended solid (TSS) and volatile suspended solid (VSS) concentrations of raw sludge (before dried in the wetland) were 8.6 g/L and 7.04 g/L, respectively. Sludge loading rate on the reed bed was averaged 43.6 kg/m² per year. At the end of year 2, the measured sludge thickness was approximately 0.29 m. The PAHs removal performance was estimated based on PAHs content at the end of the test period.

PAHs Analyses

Samples were pretreated via the following procedures. After air-dry at ambient condition and, grinded through 100 mesh sieve, sample (1.0 g) was added in a 100 ml Erlenmeyer flask together with 2.0 g of anhydrous sodium sulfate and 1.0 g of copper powder. Subsequently, the sample was mixed with 60 ml of n-hexane-dichloromethane (1:1) mixed solvent, ultrasonically extracted for 90 min, centrifuged for 30 min at 3000 r/min. After rotary evaporation, the supernant was concentrated to a constant volume of 4.0 ml prior to further use.

Sample purification was performed using column chromatography method. Firstly, chromatography media were made of 2.0 g silica gel and 3.0 g anhydrous sodium sulfate (dried at 600°C for 6h) which were mixed homogeneously in the beaker with a small amount of n-hexane. Then the media were filled with a mixture of cotton wool and 0.3 g quartz (60–80 mesh, activated at 130°C for 16 h) at the bottom into a glass column and the column was infiltrated with 10 ml hexane. The column was filled with the sample, and was eluted with 40 ml of n-hexane-dichloromethane (1:1) mixture solvent. The eluted solution was collected, and rotary evaporated and adjusted to a constant volume of 2.0 ml by using highly pure nitrogen gas. The PAHs content was determined by GC/MS according to external standard method.

PAHs determination was conducted using a GC-2010 gas chromatography/mass spectrometry instrument (Shimadzu, Japan) with a capillary column of SE-54 high-resolution paddy quartz. (length of 30.00 m, internal diameter of 0.25 mm, film thickness of 0.25 μm). The temperature program was set from ini-

tial column temperature of 100–280°C at 5°C/min, then the temperature was maintained for 30 min. The injection volume was 1.0 µL. The carrier gas was high purity nitrogen. The column flow rate, makeup gas flow rate and pre-column pressure were 0.88 mL/min, 20 mL/min and 85.6 kPa, respectively. A split injection method was processed with a split ratio of 10:1. The inlet temperature and detector temperature were 280°C. EI ionization mode was adopted with the ionization energy of 70 eV. The scanning slope of full-scan mode ranged from 100 to 400 amu.

According to the retention time and Total Ion Chromatography (TIC) of 16 PAHs, and SIM and characteristic ions, the standard curves of 16 PAHs were obtained. The recovery rates of standard additions were 61.45–114.44%, the correlative coefficients were 99.1–99.99%.

RESULTS AND DISCUSSION

PHA Removal Performance of the Pilot Test System

The average PAHs content of the raw sludge measured was 5.69 mg/kg. The low-molecular-weight PAHs (2–3 rings Nap, Acy, Ace, Fle, Phe, Ant and Fla) predominated up to 48.0%; the middle-molecular-weight PAHs (4 rings Pyr, BaA, Chr, BaF and BkF) and high-molecular-weight PAHs (5–6 rings BaP, IcP, DaA and DaP) accounted for 33.1% and 18.9%, respectively. At the end of year 3, the average PAHs content in stabilized sludge was 2.08 mg/kg, and the low-MW, middle-MW and high-MW PAHs accounted for 39.2%, 38.6% and 22.2%, respectively. This indicated that the total PAH removal efficiency was about 63% with reduction of low-, middle-, and high-MW PAHs by 70.1, 56.2, and 57.1%, respectively. This suggested that lower MW corresponds to higher PAH removal efficiency while more than 42% of middle- and high-MW fractions remained in the sludge.

PAHs Distribution in Native *Phragmites australis*

The samples of native *Phragmites australis* (i.e. control which did not exposed to sludge) were taken at the end of the plant growth season. The PAHs contents in the three major plant portions are presented in Table 1. The percentages of low-, middle-, and high-MW PAHs in total PAHs were listed in Table 2.

Based on the results in Tables 1 and 2, The PAHs in the native *P. australis* were mainly low-MW frac-

Table 1. Distribution of PAHs in native *Phragmites australis* (µg/kg).

No.	PAHs	Roots	Stems	Leaves
1	NaP	2.1	37.5	19.5
2	Acy	30.7	133.4	46.4
3	Ace	62.8	203.8	149.1
4	Fle	176.0	417.7	155.2
5	Phe	220.3	415.6	157.0
6	Ant	129.4	368.9	435.2
7	Fla	11.6	109.2	84.5
8	Pyr	22.5	109.0	168.1
9	BaA	32.9	44.5	108.2
10	Chr	14.6	93.2	595.9
11	BbF	23.6	64.6	1.685
12	BkF	22.6	26.8	175.0
13	BaP	5.9	5.9	65.6
14	IcP	38.6	40.0	105.9
15	DaA	80.7	70.5	65.2
16	BgP	24.7	52.0	84.1

tions which were 70.4% and 76.9% in roots and stems, respectively, indicating that the light fraction predominantly accumulated in the plants. The middle-MW and high-MW PAHs contents were relatively low, being 12.9%, 16.7% (in roots) and 15.4%, 7.7% (in stems), respectively. However, the middle-MW and low-MW PAHs predominated in the native *Phragmites australis* leaves with the contents of 47.1% and 40.5%, but high-molecular-weight PAHs only contented 12.4%.

Further detailed analysis indicated that the stems of native *P. australis* had relatively higher content of low-MW PAHs (including Phe, NaP, Acy, Ace, Fle, Phe) than that in roots and leaves. However, the middle-MW and high-MW PAHs (including Pyr, BaA, Chr, BbF, BkF, BaP, IcP, BgP) contents in leaves were much higher than that in roots and stems. Moreover, Chr was the most effectively adsorbed by *Phragmites australis*.

The source of PAHs in the native *P. australis* may result from the absorption of PAHs from atmosphere. Previous research indicated that about $44 \pm 18\%$ of PAHs in atmosphere was adsorbed by plants [12]. The results in this study indicated that stems and leaves exposed in atmosphere and, therefore, played a ma-

Table 2. Percentages of Low-, Middle-, and High-Molecular Weight PAHs in Total PAHs (% w/w).

PAHs	Roots	Stems	Leaves
Low-molecular-weight	70.4	76.9	40.5
Middle-molecular-weight	12.9	15.4	47.1
High-molecular-weight	16.7	7.7	12.4

Table 3. Distribution of PAHs in Tested *Phragmites australis* in Year 2 ($\mu\text{g}/\text{kg}$).

No.	PAHs	Roots			Stems			Leaves		
		Sep	Oct	Nov	Sep	Oct	Nov	Sep	Oct	Nov
1	NaP	11.1	11.1	48.2	77.3	80.7	71.5	52.3	48.5	72.4
2	Acy	38.7	38.7	59.7	229.1	169.2	161.4	52.5	95.0	110.4
3	Ace	125.5	125.5	211.8	239.5	319.3	283.2	220.9	174.6	124.6
4	Fle	213.1	213.1	309.2	428.9	532.9	503.4	339.7	386.5	391.6
5	Phe	281.2	281.2	355.9	498.8	504.0	587.5	231.6	235.8	128.3
6	Ant	291.2	291.2	476.0	396.9	484.2	451.2	515.1	523.0	523.4
7	Fla	79.5	79.5	117.3	127.1	315.3	239.2	128.9	110.3	207.9
8	Pyr	90.0	90.0	107.3	126.8	135.3	147.4	178.1	243.7	282.3
9	BaA	90.9	90.9	188.5	104.8	95.4	75.2	118.1	249.8	136.2
10	Chr	25.6	25.6	99.5	168.0	186.2	168.1	601.0	606.4	651.6
11	BbF	106.9	106.9	214.3	184.8	311.2	111.9	194.0	182.3	272.7
12	BkF	69.1	69.1	170.2	77.2	76.5	119.6	239.2	428.9	229.1
13	BaP	19.2	19.2	33.9	58.0	47.0	54.5	71.4	79.4	147.3
14	IcP	119.8	119.8	104.4	111.8	164.9	155.5	176.1	163.3	157.0
15	DaA	105.1	105.1	105.1	87.7	184.0	147.8	77.8	187.4	95.1
16	BgP	53.4	53.4	81.5	65.2	150.8	76.6	153.3	161.9	152.2

major role in absorption of PAHs from atmosphere directly, mainly including low-MW PAHs such as Ace, Fle, Phe, Ant and Chr. The high PAHs content found in the leaves suggested that the heavy PAHs fraction was derived from atmospheric deposition in gaseous or particulate forms on the leaves, and that atmospheric fall-out might be the main input pathway for PAHs into the plants. While low contents in the roots might result from uptaking the relative low PAHs content in the soil or sediments at the site of the native *P. australis* grew [13].

Table 4. Distribution of PAHs in *Phragmites australis* in Year 3 ($\mu\text{g}/\text{kg}$).

No.	PAHs	Roots	Stems	Leaves
1	NaP	90	95	82
2	Acy	226	437	122
3	Ace	330	380	360
4	Fle	480	438	400
5	Phe	1090	1246	1375
6	Ant	1184	1205	755
7	Fla	570	246	62
8	Pyr	278	249	257
9	BaA	126	324	1395
10	Chr	1524	382	690
11	BbF	96	176	544
12	BkF	315	423	348
13	BaP	370	860	780
14	IcP	239	234	357
15	DaA	222	168	172
16	BgP	173	139	115

Distribution of PAHs in Plants of *Phragmites australis* from the Test Site

Distribution of PAHs in plants of *P. australis* grown on the pilot constructed wetland site at the end of year 2 and year 3 is summarized in Tables 3 and 4. The comparison of total contents of PAHs in different *P. australis* parts are presented in Table 5.

The results in this study indicated that low-MW PAHs predominated in *P. australis* roots and stems with relatively high content of BbF. However, the leaves of the tested plants had higher content of middle-MW and high-MW PAHs, especially Chr.

The distribution of PAHs in the tested plants in year 2 indicated that the PAHs content in roots increased as time elapsed, and reached the peak value in November, while PAHs contents in stems and leaves increased to the peak values in October. The increase in the contents demonstrated the ability of *P. australis* for PAHs bioaccumulation.

Table 5. Total Contents of PAHs in Tested *Phragmites australis* ($\mu\text{g}/\text{kg}$).

Part	Tested <i>P. australis</i>				Native <i>P. australis</i>
	Year 2			Year 3	
	Sep	Oct	Nov	Nov	
Roots	1720	2683	3645	7313	899
Stems	2982	3757	3354	7002	2193
Leaves	3350	3877	3682	7814	2583

The PAHs concentration in plants is influenced by plant species and PAHs content in environment. PAHs content differentiate in different parts of a plant. It was reported that the plant near industrial zone had a high total PAHs content of 12,300 $\mu\text{g}/\text{kg}$ in roots [14]. In this study, the tested *P. australis* had bioaccumulation ratio of 813% in roots, 319% in stems and 302% in leaves compared to the native plants. Apparently, PAHs were taken up by roots and translated to the stems and then leaves within plant body. Chr was detected the highest content of 1,524 $\mu\text{g}/\text{kg}$ in roots while Nap was the lowest (90 $\mu\text{g}/\text{kg}$). Ant content was the highest (1,246 $\mu\text{g}/\text{kg}$) in stems, while Nap was the lowest (95 $\mu\text{g}/\text{kg}$). Phe content was the highest (1395 $\mu\text{g}/\text{kg}$) and Fla was the lowest (62 $\mu\text{g}/\text{kg}$) in leaves. BaP as a compound normally used as a guideline value in China, its contents in the root, stem and leaf in the year 3 were 370, 860 and 780 $\mu\text{g}/\text{kg}$, generating obvious bioaccumulation.

Gao *et al.* (2009) investigated PAHs absorption by different plant roots and observed that PAHs content in composition in soils and size of plant affected the bioaccumulation ability [15]. A taller plant showed slightly poor absorption capability than a shorter plant. PAHs with 2-rings and 3-rings were more easily translated within plants. High-MW PAHs were mainly derived from atmospheric deposition [13]. The results of this study supports above hypotheses.

Bioaccumulation Factor (BCF) of *Phragmites australis*

PAHs can be taken up by roots and leaves and translated within plants. The PAHs bioaccumulation ability can be described using bioaccumulation factor (BCF) as

$$BCF = \frac{C_p}{C_s}$$

where C_p and C_s represent the PAHs content in plant part (roots, stems, or leaves) and sediment or sludge in this study, respectively.

BCF in the roots, stems and leaves of *P. australis* at the end of year 3 are listed in the Table 6.

The calculated BCF values of roots ranged from 0.403 (BaA) to 11.991 (Phe), those of stems ranged from 0.74 (BbF) to 13.71 (Phe), and those of the leaves ranged from 0.78 (Fla) to 15.13 (Phe). Based on the results in Table 6, 87.5% of PAHs species accumulated in the tested *P. australis*. The BCF of low-MW PAH in the tested *P. australis* roots, stems and leaves are 5.02, 4.93 and 4.03, respectively. The high BCF values

Table 6. BCF of PAHs in Roots, Stems and Leaves of *Phragmites australis*.

No.	PAHs	Roots	Stems	Leaves
1	NaP	1.125	1.188	1.025
2	Acy	1.642	3.175	0.886
3	Ace	2.562	2.950	2.795
4	Fle	4.111	3.751	3.426
5	Phe	11.991	13.707	15.127
6	Ant	6.507	6.622	4.149
7	Fla	7.194	3.105	0.782
8	Pyr	3.067	2.747	2.836
9	BaA	0.837	2.152	9.267
10	Chr	9.513	2.385	4.307
11	BbF	0.403	0.739	2.286
12	BkF	1.929	2.591	2.131
13	BaP	1.840	4.276	3.878
14	IcP	2.724	2.667	4.069
15	DaA	2.290	1.733	1.774
16	BgP	2.308	1.854	1.534
Total		3.518	3.368	3.759

may be due to relatively high hydrophobicity and bio-availability of these PAHs. The BCF of middle-MW in *P. australis* roots, stems and leaves were 3.15, 2.12 and 4.17, respectively. The values of high-MW PAHs were 2.29, 2.63 and 2.81, respectively. Although PAHs are easily taken up by roots and leaves, the translation mechanism within *P. australis* was not clear yet [16]. Based on the results of this study, the tested *P. australis* accumulated PAHs effectively compare with native plants. The higher PAH contents in soil corresponded higher PAH contents in *P. australis*. Especially the increased PAH contents in the stems and leaves of the tested *P. australis* could result from root absorption and translation in plant.

The increase in BCF values of the tested plants demonstrated that the PAHs removal of 60% can be contributed to the adsorption and accumulation by the plants. However, the contribution of the evaporation of light fraction and microbial biodegradation of PAHs cannot be ruled out. Further study is needed to characterize these two factors.

CONCLUSIONS

PAHs in soils and sludge can be effectively adsorbed, transferred and accumulated in plants of *Phragmites australis*. Based on the results of the pilot scale constructed wetland test, after two years of sludge loading and one year of natural stabilization, more than 60% of PAHs in the sludge was removed. The reduction of

PAHs content was likely significantly contributed by the adsorption, transportation and accumulation via the plants. The PAHs contents in the roots, stems and leaves of the tested *P. australis* increased significantly, and reached 7.313, 7.002 and 7.814 mg/kg (DW), which were 8.13, 3.19 and 3.02 times of the contents in the roots, stems and leaves of the native *P. australis*, respectively. Low-MW PAHs accumulated more easily than middle-MW and high-MW PAHs in the plants. The results indicated that PAHs can be substantially removed by wetland plants via uptaking into plant tissues, depends on molecular weight of the PAH species. The distribution of the PAHs components in the plant was species-dependent and most of them accumulated in the leaves.

ACKNOWLEDGEMENTS

This work was supported by The National Natural Science Foundation of China (No. 51278088), the Scientific Research Foundation of Public Welfare Undertakings, Liaoning Province (2014004006) and the Fundamental Research Funds for the Central Universities in China (DC201502070203). Dr. Wei-Min Wu was a visiting professor at Dalian Nationalities University during the project period.

REFERENCES

- Cooper P., Willoughby N. and Cooper D. (2004). The use of reed-systems for sludge drying. *Water and Environment Journal*, 18(2), 85–89. <http://dx.doi.org/10.1111/j.1747-6593.2004.tb00502.x>
- Cui Y. B., Guo Z. Q., Liu Y. H., and Yang M. L. (2011). Ecological Stabilization for Sewage Sludge. *Journal of Civil, Architectural & Environmental Engineering*, 33(4), 151–156.
- Cui Y. B., Sun H. J., Yang M. L., and Liu Y. H. (2012). Plant Growth for Sewage Sludge Ecological Stabilization. *Journal of Residuals Science & Technology*, 9(1), 47–53.
- Dettenmaier E. M., Doucette W. J. and Bugbee B. (2009). *Chemical Hydrophobicity and Uptake by Plant Roots*. *Environmental Science & Technology*, 43(2), 324–329. <http://dx.doi.org/10.1021/es801751x>
- Gao, Y. Z., Cao X. Z., Kang F. X., and Cheng Z. X. (2011). PAHs pass through the cell wall and partition into organelles of arbuscular mycorrhizal roots of ryegrass. *Journal of Environmental Quality*, 40(2), 653–656. <http://dx.doi.org/10.2134/jeq2010.0320>
- Guo W., Pei Y. S., and Yang Z. F. (2011). Assessment on the distribution and partitioning characteristics of polycyclic aromatic hydrocarbons (PAHs) in Lake Baiyangdian, a shallow freshwater lake in China. *Journal of Environmental Monitoring*, 13(3), 681–688. <http://dx.doi.org/10.1039/c0em00583e>
- Gao Y. Z. and Zhu L. Z. (2004). Plant uptake, accumulation and translocation of phenanthrene and pyrene in soils. *Chemosphere*, 55(9), 1169–1178. <http://dx.doi.org/10.1016/j.chemosphere.2004.01.037>
- Lee H. K., Wright G. J. and Swallows W. H. (1990). The identification of sources of PAH by using concentration ratios of total PAH and Pb. *International Journal of Environmental Studies*, 36(4), 273–277. <http://dx.doi.org/10.1080/00207239008710605>
- Mo C. H., Cai Q. Y., Wu Q. T. (2001). A study of polycyclic aromatic hydrocarbons (PAHs) in municipal sludge of China. *Environmental Science*, 21(5), 613–618.
- Nielsen, S. (2005). Mineralisation of hazardous organic compounds in a sludge reed bed and sludge storage. *Water Science and Technology* 51: 109–117.
- Matamoros, V., Nguyen, L. X., Arias, C. A., Nielsen, S., Laugen, M. M., Brix, H. (2012). Musk fragrances, DEHP and heavy metals in a 20 years old sludge treatment reed bed system. *Water Research*, 46: 3889–3896. <http://dx.doi.org/10.1016/j.watres.2012.04.027>
- Simon R. W., Kevin C. J. (1994). The significance of polynuclear aromatic hydrocarbons applied to agricultural soils in sewage sludges in the U.K. *Waste Management & Research*, 12(1), 49–59.
- Simonich S. L. and Hites R. A. (1994). Vegetation-atmosphere Partitioning of polycyclic aromatic hydrocarbons. *Environmental Science and Technology*, 28(2), 939–943. <http://dx.doi.org/10.1021/es00054a028>
- Song X. Y., Sun L. N., Yang X. B. (2008). Contamination Status of Polycyclic Aromatic Hydrocarbon in Topsoils of Liao River Basin. *Journal of agro-environment science*, 27(1), 216–220.
- Tao Y. Q., Zhang S. Z., Zhu Y. G., and Christie P. (2009). Uptake and acropetal translocation of polycyclic aromatic hydrocarbons by wheat (*Triticum aestivum* L.) grown in field-contaminated soil. *Environmental Science & Technology*, 43(10), 3556–3560. <http://dx.doi.org/10.1021/es803368y>
- Uggetti E., Ferrer I., Llorens E., and García J. (2010). Sludge treatment wetlands: A review on the state of the art. *Bioresource Technology*, 101(9), 2905–2912. <http://dx.doi.org/10.1016/j.biortech.2009.11.102>

Traffic Environmental Capacity and MFD Based Traffic Emission Dynamic Control Model

YIMAN DU^{1,2,*}, YUHAN JIA^{1,2}, JIANPING WU^{1,2}, MING XU³ and SENYAN YANG¹

¹Department of Civil Engineering, Tsinghua University, Beijing 100084

²Jiangsu Province Collaborative Innovation Center of Modern Urban Traffic Technologies, Nanjing 210096

³Beijing University of Posts and Telecommunication, Beijing 100876

ABSTRACT: In recent years, the transportation system has become a major source of air pollution. Consequently, it is vital to improve traffic efficiency to preserve urban air quality. Based on the environmental traffic capacity and the macroscopic fundamental diagram theory, the multi-objective programming model is adopted to describe the relationship between traffic emissions and traffic capacity. Then a dynamic traffic volume control method is developed for regional traffic management, which is the feedback gating control method based on the traffic conditions in controlled urban areas. As a case study, the proposed methodology is applied to a road network located in central area of Nanjing. The traffic flow going in and out the study area is controlled by gates via signals to make sure the vehicle amounts and emissions in study area are under the threshold obtained by multi-objective model. The results show that traffic efficiency has improved significantly and that the urban air quality is ensured. This paper can offer some recommendations regarding urban traffic management and air pollution control.

1. INTRODUCTION

In the process of urbanisation, urban social and economic development has been restricted by failure to satisfy the increasing traffic demand, and has polluted the urban ecological environment. Evidence shows that the urban transport system has become a major source of air pollution, and, in some cities, vehicle emissions account for 90% of the air pollution [1]. There are six categories of harmful automobile emissions; carbon monoxide, hydrocarbons, nitrogen oxides, odour, particulate and photochemical smog, and more than 140 kinds of material composition. Some studies show that traffic emissions are a major component or source of secondary atmospheric particulate matter. The severity of the negative impact on public health caused by traffic emissions is comparable to that of a traffic accident [2]. The corresponding studies relevant to Beijing traffic junctions show that the particulate matter of traffic emissions is the primary factor affecting the air pollution levels of traffic junctions [3]. In April 2014 the Beijing municipal environmental protection bureau stated that motor vehicle emissions made up 31.1% of Beijing's local pollutant sources [4].

To accomplish the objective of sustainable transportation, it's necessary for urban transport to meet the needs of the urban system, and the criteria concerning the objective constraints of the environment [5]. This can be achieved by controlling points and reducing traffic regional air pollution with effective road and vehicle control measures. The "Traffic Environmental Capacity" was first proposed by Colin Buchanan with the definition of "The maximum traffic flows per unit time on the condition that traffic flow won't lead to environmental deterioration" [6]. He defined the health and safety of pedestrians as constraint conditions and quantified environmental traffic capacity by pedestrian delay. Following his report, traffic environmental capacity has been widely researched. Shiran proposed that the atmospheric diffusion of pollutants from motor vehicle exhaust can cause variation of traffic volume in other parts of the network, and that environmental capacity should be calculated at area-wide [7]. Traffic environmental capacity expressions of qualitative analysis considering diffusion and self-purification of traffic pollution were developed by Li by using the box-diffusion model of vehicle exhaust [8]. Wei *et al.* [9] built a calculating and controlling model of traffic environmental capacity based on system analysis, which provides a scientific basis for the control of vehicle ownership with constraints on environmental ca-

*Author to whom correspondence should be addressed.
E-mail: ymducp@gmail.com

capacity [10]. Chen discussed and analysed the causes of environmental pollution and the relationship between them and the amount of automobiles in the form of graphs [11]. Yang predicted the maximum capacity of passenger cars in cities with the constraint conditions of environment capacity and built bi-level optimization prediction models [12]. Wang analysed section traffic capacity under the standard of air quality, then built the traffic environment capacity model and motor vehicle pollutants emission factor planning target calculating model [13]. Lu built a bi-level and multi-objective programming model based on expressway pollution and ramp control, which is limited to an expressway without considering the problem of network Origin/Destination (OD) balance [14].

In conclusion, the following problems can be summarized:

1. The majority of studies on traffic environmental capacity to date are purely theoretical with limited practical applications.
2. The total traffic environment capacity is only estimated quantitatively in the urban planning stage, which is usually used to control vehicle ownership. There is minimal research focused on real-time traffic dynamic control. The majority of this research is restricted to one or two roads and cannot be applied to a wider area.
3. The issue of traffic dynamic control based on traffic congestion has been discussed frequently. However, there is no research which takes both entire pollutant emissions and traffic efficiency into account.

Based on above issues, the objective of this paper is:

1. Establishing a macroscopic fundamental diagram for the study area based on measured data and model simulations.
2. Taking the traffic environmental capacity as a constraint condition, this paper will develop a multi-objective programming model to describe the relationship between the traffic volume and environmental condition.
3. Establishing a dynamic controlling model by means of traffic optimization and feedback control to reduce the amount of exhaust emissions.

2. FEEDBACK GATING CONTROL MODEL

The strategy of feedback gating control was adopted to control the traffic flow via the gates, which are se-

lected around the boundary of the controlled area. The setting of the traffic signals at each gate can be modified accordingly.

The goal of the controller is to maintain the traffic volume of the controlled area at the threshold, which is the upper limit of vehicles that maximises traffic efficiency and also minimises the vehicle emissions. The threshold is decided in the following sections by optimisation calculation. According to the strategy, the inflow should be restricted to maximize the throughput of the controlled area and keep the emission of CO under the limit. Once the emissions exceed the threshold, the gating control will be triggered where the gates represent the signalised intersections selected around the boundary of the controlled area. The setting of the traffic signals at each gate can be modified accordingly. The gating control contains two steps of judging criteria. The first is to judge whether the Net Volume (NV in veh/h, means the net vehicle amount that exists in the study area) reaches the threshold at λ . If the NV is larger than the threshold, then the second judging criterion starts, which is to estimate the traffic situation for each gate (signalised intersection) by analysing the traffic detector data. By calculating the average speed and delay, the system can determine which signals at which gates need to be adjusted.

The logic of feedback control is illustrated in Figure

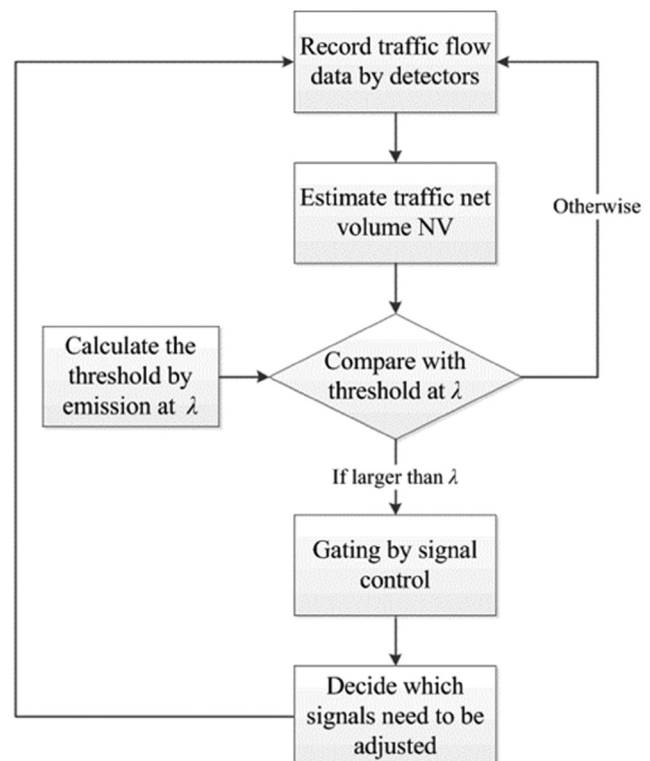


Figure 1. The logic of feedback control.

1, where the λ means the weighting coefficient of optimization which will be illustrated in Section 3. In this case, it was assumed that the detectors were deployed in each lane of controlled area. It is easy to obtain the appropriate information for each link by simulation. However, it is unrealistic to distribute the detectors on every link of road network due to the budgetary restrictions and complexity of maintenance. Therefore, the Selected Travel Distance (STD in veh·km/h) is utilised in this study to reflect the Vehicle Mile Travelled (VMT). The STD has the same trend as the VMT, and facilitates the use of a detailed control method with fewer detectors than the previous research (Du *et al.*, 2014).

3. RELATION MODEL BETWEEN TRAFFIC FLOW AND EMISSIONS

Based on the logic of feedback control, the determination of the threshold is essential to traffic environmental capacity control. Therefore, a multi-objective programming model was used to describe the relationship between the volume of vehicles and the exhaust emissions and to determine the threshold.

3.1. Decision Objective 1: Traffic Environmental Capacity

The traffic environmental capacity is the maximum load of the pollutant emissions from the transportation system that the traffic environment can accommodate.

Since the late 1960s, Europe, the United States, Japan and other countries have conducted various studies on the diffusion model of vehicle exhaust pollutants. These models are typically applied to diffusion on highways and urban roads. The vehicle exhaust diffusion models that are commonly used include the box-model, Gaussian model, empirical model, and the turbulent diffusion (numerical) models. The Gaussian model can simulate the diffusion of vehicle exhaust pollutants on open and flat highways, however, it does not work when there are high-rise buildings on both sides of the road [15,16]. The Numerical simulation model can handle the street atmospheric diffusion with complex structures, but the process and the boundary conditions are too complex for wider application [17]. The empirical model is simple, however, it lacks a solid theoretical foundation and is not yet suitable for practical applications [18]. Though the box-model is not a perfect model and is unable to perfectly reflect reality, this model is relatively easy to calculate and is

applicable to the study area due to the ease with which the parameters can be observed [19]. Therefore, the box-model can be adopted by using the dimensional analysis method to calculate the concentration diffusion of vehicle pollutants emissions.

$$C_m = \frac{Q_m [K_1 \sin^2 \theta + (K_2 L/W) \cos^2 \theta]}{\mu (\sqrt{x^2 + z^2} + l_0)} \quad (1)$$

$$F_m = \frac{[K_1 \sin^2 \theta + (K_2 L/W) \cos^2 \theta]}{\mu (\sqrt{x^2 + z^2} + l_0)} \quad (2)$$

C_m = Concentration of vehicle pollutant dispersion, mg/m³

m = Vehicle pollutant emission type

Q_m = The source strength of gaseous pollutant emission m , mg/(s·m)

μ = The wind speed near the calculation points

x, z = The horizontal and vertical distances from the pollution central to the monitoring point, m

l_0 = The initial diffusion scale, m

K_1, K_2 = Reflect the impact of the street structure on pollutant concentration distribution when blowing a vertical and parallel wind respectively, and vary depending on cities and road types, determined by the experimental or measured data

L, W = The length and width of the road, m

θ = The angle between the wind and the road, degree

The emissions of moving vehicles are calculated by the continuous pollution line source, and the line source centreline is the route centreline. For a certain type of vehicle (e.g. private car), the source strength is calculated by gaseous pollutants' emission sources:

$$Q_m = \frac{\sum_{i,j \in E} (A_{ij} \times E_m)}{3600} \quad (3)$$

i, j = Section ID

A_{ij} = Hour volume of traffic of vehicle k

E_m = Emission factor of pollutant emission, g/(pcu·km)

$$C_m = \kappa_m \times C_m^s \quad (4)$$

κ_m = Contribution rate of vehicle pollutant concentration for pollutant m

C_m^s = The standard concentration for environmental quality of pollutant m , mg/m³

Therefore, the objective function is:

$$\begin{aligned} \min C &= \min \sum_m C_m = \min \sum_m (Q_m \times F_m) \\ &= \min \sum_m \left(\frac{\sum_{i,j \in E} (A_{ij} \times E_m)}{3600} \times F_m \right) \end{aligned} \quad (5)$$

3.2. Decision Objective 2: Throughput of Road Network

Godfrey first proposed the Macroscopic Fundamental Diagram (MFD) in 1969 [20]. The fundamental diagram of traffic flow is a diagram that gives the correlation between traffic flow and traffic density. The exit flow is maintained when the inflow exceeds the limits dictated by the simulation results [21]. Geroliminis and Daganzo derived the MFD of traffic flow and density based on real data from Japan and simulated data from San Francisco [22,23], and found that the shape of the MFD was influenced by the characteristics of the road network not the locations of the detectors. The curve of the MFD may depend on the traffic demand, however, it can be quite stable from day to day [24,25]. Therefore, the MFD is essential to deriving the threshold that maximizes the throughput of the controlled area.

The following equations were utilised to obtain the MFD. The NV can reflect the horizontal axis of the MFD, while the Selected Travelled Distance reflects the vertical axis of the MFD.

$$NV(k) = \sum_{i \in m} V_i(k) \quad (6)$$

$$STD(k) = \sum_{i \in n} q_i(k) \cdot L_i \quad (7)$$

where i is the link where the detectors are distributed; m is the set of links; $k = 0, 1, 2, \dots$ is the time interval; $V_i(k)$ is the estimated traffic volumes in each link during the i cycle k ; n is the set of links where the detectors are distributed; $q_i(k)$ is the measured traffic flow in link i during cycle k ; and L_i is the length of link i . The NV and STD are derived from the link measurements.

Figure 2 indicates that a macroscopic fundamental diagram shape (inverse U shape) appears during the simulation period with a moderate scatter effect via different replications [26]. Figure 2 illustrates that that the STD value increased with increase of the NV during the free-flow period, and the STD reached the maximum value. After the threshold was exceeded the STD

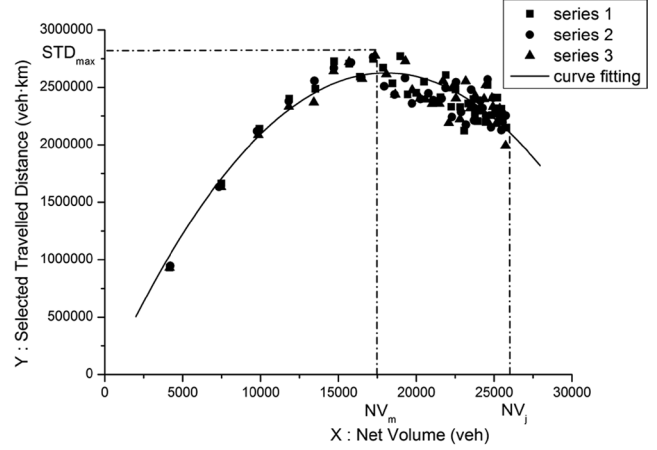


Figure 2. The macroscopic fundamental diagram of the road network.

value decreased as the NV value increase. The throughput and efficiency of the controlled area increases with the increase of the NV before the NV reaches NV_m , and then, the throughput degrades when the traffic flow reaches the threshold. To maximize the throughput and efficiency, the NV should be maintained in the optimal range. Therefore, the objective function is:

$$\max STD = \max \sum_{i,j \in E} (A_{ij} * L_{ij}) \quad (8)$$

3.3. Multi-objective Programming Model Development

The multi-objective programming model is developed as follows:

$$\begin{aligned} \min C &= \min \sum_m C_m = \min \sum_m (Q_m \times F_m) \\ &= \min \sum_m \left(\frac{\sum_{i,j \in E} (A_{ij} \times E_m)}{3600} \times F_m \right) \end{aligned} \quad (9)$$

$$\max STD = \max \sum_{i,j \in E} (A_{ij} \times L_{ij}) \quad (10)$$

Constraint conditions:

$$\begin{cases} \frac{\sum_{i,j \in E} (A_{ij} \times E_m)}{3600} \times F_m \leq \kappa_m \times C_m^s \\ \sum_{i,j \in E} A_{ij} \leq NV_m \\ A_{ij} \leq S_{ij} \end{cases} \quad (11)$$

S_{ij} = Capacity between section i and section j

3.4. The Solution of the Model

The linear weighting method is used to convert the model into a single objective model by introducing the weighting parameter λ to solve the objective programming model. Then the multi-objective programming model can be rewritten as a single objective function.

$$\min C' = \min(C - \lambda \times STD) \quad (12)$$

A modified ant colony algorithm was developed to solve this problem. The ant colony algorithm (ACO) was developed in recent years to solve a series of assignment problems, like the travelling salesman problem (TSP) and vehicle routing problem (VRP) [27,28].

Each OD pair is represented by an ant colony, and each ant represents 10 vehicles. The origin, O, is the colony's nest and the destination D is the food source. For each colony, the ants distribute a distinct type of pheromone that only the ants in the same colony will recognize. The pheromone trail on each link is initialised for each colony.

During each iteration for each colony, the probability an ant chooses the next node j from node I is given by

$$j = \begin{cases} \arg \max_{s \in allowed_k} \{(\tau_{is})^\alpha (\eta_{is})^\beta (\varepsilon_s)^\gamma\} & q \leq q_0 \\ J & \text{otherwise} \end{cases} \quad (13)$$

where $allowed_k$ is the set of all nodes of the forwarding star of node i that have not yet been visited; $q \in (0,1)$ is a user defined variable, which is 0.8 in this paper; q_0 , α , β , and γ are pre-set parameters; τ_{is} is the intensity of pheromone trail on arc (i, j) ; $\eta_{is} = 1/c'_{ij}$ a heuristic variable representing the reciprocal of the objective function value on the arc (i, j) and ε_s is another heuristic variable representing the reciprocal of the shortest distance from node s to the ant's D. J is the classic transition probability as follows

$$p_{ij}^{k+1} = \begin{cases} \frac{(\tau_{ij})^\alpha (\eta_{ij})^\beta (\varepsilon_j)^\gamma}{\sum (\tau_{ij})^\alpha (\eta_{ij})^\beta (\varepsilon_j)^\gamma} & \text{if } j \in allowed_k \\ 0 & \text{otherwise} \end{cases} \quad (14)$$

The updating of the pheromone consists of two stages; partial updating and global updating. After each ant completes its search in a colony, the arcs it passed will update by evaporation coefficient ρ_1

$$\tau_{ij} = (1 - \rho_1)\tau_{ij} + \rho_1\tau_0. \quad (15)$$

After the whole colony finishes the search, the road network will operate a global update:

$$\tau_{ij} = (1 - \rho_2)\tau_{ij} + \rho_2\Delta\tau_{ij} \quad (16)$$

$$\Delta\tau_{ij} = \sum \Delta\tau_{ij}^k \quad (17)$$

$$\Delta\tau_{ij}^k = \begin{cases} \frac{Q}{c'_{ij}} & \text{if } (i, j) \in \text{the best path} \\ 0 & \text{otherwise} \end{cases} \quad (18)$$

Where Q is constant and c'_{ij} is the objective function value of arc (i, j) .

The modified ant colony algorithm is:

1. Set initial values for the ant colony and pheromone. Set the maximum iteration number NC .
2. Place ants at each colony's O node. For each ant, repeat the next node by the transition probability rule. When an ant finishes the trip, implement the partial updating. Repeat until each ant in each colony reaches D.
3. Record the best solution for each iteration. Do the global updating.
4. If $NC < NC_{max}$, go to step 2. If the maximum iteration time is reached, then output the best solution for the objective function.

4. CASE STUDY

In this study, the area around the Nanjing Centre is regarded as the controlled region to simulate and demonstrate the Regional Traffic Environmental Dynamic Control technology. The study area features 22 intersections and a further 13 intersections are selected as the controlled "gates" at the boundary of controlled region. The traffic volume can be restricted at these "gates" and the controlled region can be protected during the peak period. The locations of the study area and the gates are indicated in Figure 3. The microscopic simulation software FLOWSIM is introduced in this study to objectively reflect the traffic situation in China [29,30,31]. In FLOWSIM each intersection and link is developed separately according to real situation including road capacity, maximum speed, lane width, and so on. When simulating, the OD data is assigned to the road network as traffic flow.

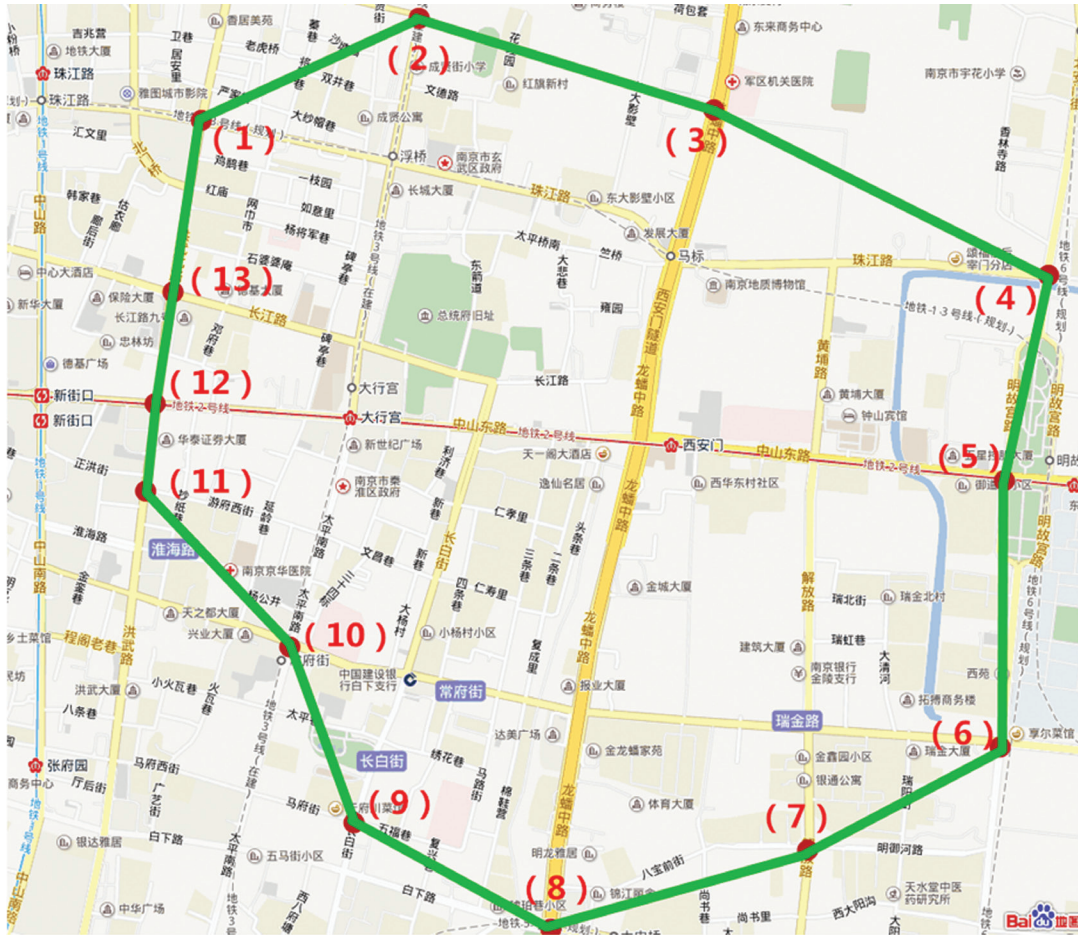


Figure 3. Layout of study area and Location of feedback gate.

The emission of CO is selected as the measure and only private cars are considered. According to the national grade II air quality standard defined in “Ambient Air Quality Standard (GB3095—2012)”, the CO value is set to be 10.0 mg/m³. The contribution rate of vehicle pollutant concentration for CO is set to be 74.1% [32]. According to Nanjing’s meteorological statistics, the average wind speed ranges from 1.7 m/s to 3.3 m/s, and it predominantly an east wind, therefore, the hourly average wind speed $\mu = 2$ m/s is adopted. The traffic environmental capacity is the largest when the wind direction is perpendicular to the road direction, and when the angle θ decreases, the traffic environmental capacity reduces. In this case study, the angle between wind and road is considered as 90 degrees to make comparisons [33]. x is set to be 30 m, and z is set to be 1.5 m. $K_1 = 1.81$, and $l_0 = 2$ m. Considering the low speed in peak period, the emission factor of CO is set to be $E_{km} = 62.28g / (pcu \cdot km)$, which is the standard emission factor at an average speed of 30 km/h in Nanjing city [34]. Simulation is used to develop the MFD and calculate the NV_m .

The weighting coefficient, λ , influences the model’s solution. Therefore, λ is set as different values to balance the weight of the environment and the traffic. The result is calculated according to the algorithm shown in Table 1.

It is shown in Table 1 that if λ is smaller then the environmental factors account for a larger weight. With the increase in the value of λ , the impact on the model

Table 1. Comparison of Computing Results Under Different λ .

λ	Emission of CO (mg/m ³)	Traffic Throughput (veh/h)
0.1	1.207	5880
0.2	2.204	9270
0.3	3.216	12230
0.4	3.780	13690
0.5	4.657	15720
0.6	5.626	17840
0.7	6.438	19510
0.8	7.280	21160
0.9	7.410	21410
1	7.410	21410

caused by the total traffic volume increases gradually. When λ is 0.9, the total CO emissions reach the limitation, with a constant total traffic flow of 21410. If the total traffic volume continues to increase, then the emissions will exceed the limitation. Therefore, the control criteria is set as $\lambda = 0.9$ in the study.

Two simulation scenarios were designed to compare the traffic conditions and CO between without- and with- the implementation of control logic. The simulation scenarios are based on the traffic data collected at peak hour (8:00 am–9:00 am) on 23 July 2014 in Nanjing. Multiple replications with different random seeds were carried out. The comparison of CO and the traffic between without- and with- control are shown below.

It is clear in Figure 4(a) that the inflows are con-

trolled to maintain the NV around NV_m when NV reaches the threshold and the gating control is switched on at $t = 20$ min. The STD stays at a high level after the gating control is switched on, compared to scenario 1 without gating control [Figure 4(b)]. Figure 4(c) shows a significant decrease in CO emissions, in contrast to the case without gating control. The difference in Figure 4(c) occurs approximately 10 minutes later than in Figure 4(a) and Figure 4(b). This is because, when the gating control begins, the vehicle speed in controlled area is still low and the emissions are high. However, 10 minutes later, the vehicle emissions decrease as the vehicles are operating smoothly and the difference between the two scenarios in Figure 4(c) begins to increase.

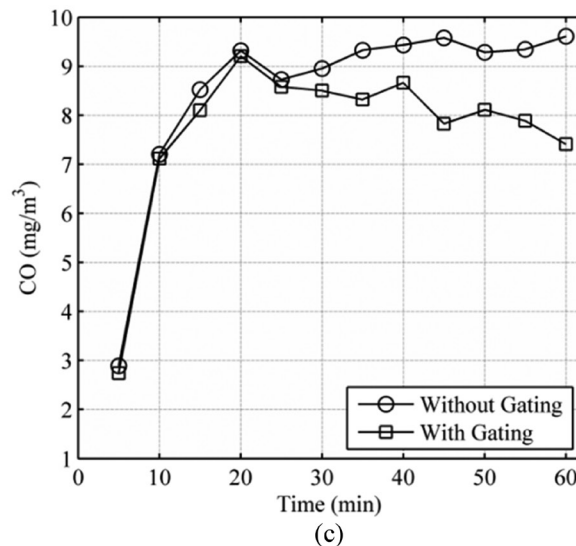
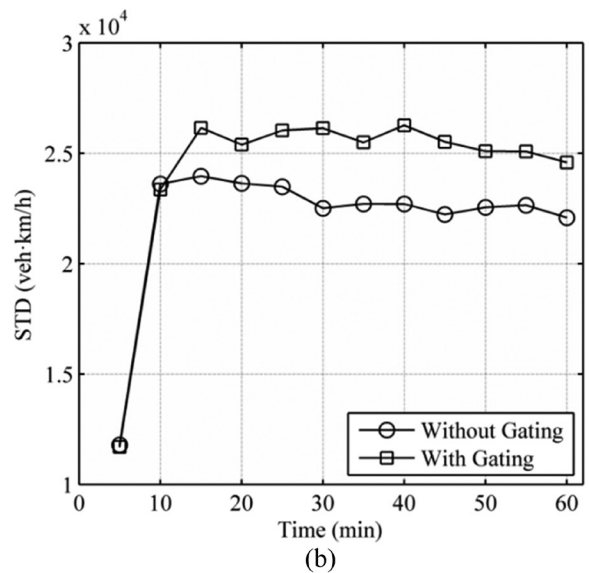
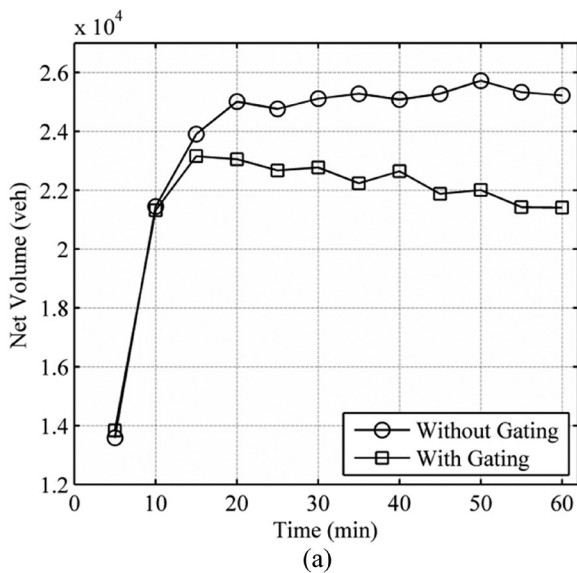


Figure 4. (a) The comparison of NV between with- and without- gating control; (b) The comparison of STD between with- and without- gating control; (c) The comparison of CO between with- and without- gating control.

5. CONCLUSION

Based on the environmental traffic capacity and the macroscopic fundamental diagram theory, the multi-objective programming model was adopted to describe the relationship between traffic emissions and traffic capacity. An improved dynamic regional traffic volume control strategy was proposed. The proposed methodology was applied to the area around the Nanjing Centre. The key nodes were identified based on the OD distribution of trips and the connectivity of the nodes. The microscopic traffic simulation model was employed as the test platform. The results show that the application of the feedback control strategy can significantly improve the efficiency and throughput and reduce the vehicle pollution emissions compared to the case without gating control.

Since this study was based on an hourly simulation, the wind speed and direction were assumed to be constant in the corresponding hour. However, future research should utilise more detailed information in the simulation to account for variations in the wind speed and direction.

6. ACKNOWLEDGEMENTS

The research reported in this paper was conducted as part of the project “The research and application of urban air environment regulation and control technology based on the Internet of Things”, as part of the State High-Tech Development Plan (The 863 program) funded by The Ministry of Science and Technology of the People’s Republic of China with the grant number 2012AA063303. The “Research on the Traffic Environment Carrying Capacity and Feedback Gating based Dynamic Traffic Control in Urban Network” project, funded by the China Postdoctoral Science Foundation with grant number 2013M540102, also supported this project.

7. REFERENCES

1. Yang, T., Wu, L., Xu, W. G. (2001) Evaluation about city traffic environment impact for sustainable development. *China Environmental Science [J]*. 21(3): 270–274. (in Chinese).
2. Jiang, Y. L. (2011) The source and formation mechanism of typical atmospheric pollutants in cities over China and their impact on air quality and coastal Primary Productivity [D]. Fudan University. (in Chinese).
3. Chen, Jh., Wang, W., Liu, H. J., Yue, X., Li, H., Tang, D. G. (2005) Pollution Property of Particulate s in the Air at the Traffic Crossing in Beijing Part I: Pollution Property of Particulates in the Air and It’s Affecting Factors [J]. *Research of Environmental Sciences*. 18(2):34–38. (in Chinese).
4. Yu R H. (2014) [N]. About 30% Beijing local pollutant sources are from Motor vehicles emissions. *People’s Daily*. 2014-04-16 (09).
5. Shen, J. S., Xu, Y. F., Lei, L. (1997) Thoughts on several issues of urban transport sustainable development [J]. *China Soft Science*, (7): 113–119. (in Chinese).
6. Colin Buchanan. (1963) *Traffic in Towns*.
7. Shiran, G. R. (1997) Area-wide environmental capacity based on air pollution criteria [D]. Sydney: The University of New South Wales?
8. Li, T. Z., Lin, J. S., Wu, M. T., *et al.* (2009) Concept and spatial analysis method of urban environmental traffic Capacity [J]. *Journal of Transportation Engineering*. 135(11): 873–879. [http://dx.doi.org/10.1061/\(ASCE\)TE.1943-5436.0000061](http://dx.doi.org/10.1061/(ASCE)TE.1943-5436.0000061)
9. Wei, Z. L., Shen, J. S., Xu, Y. F. (1997) Discuss about Traffic Environment Capacity and Traffic Environment Bearing Capacity [J]. *Economy Geography*. 17(1): 97–99.
10. Wei, Z. L., Shen, J. S., Xu, Y. F. (1997) Discuss about Traffic Environment Capacity and Traffic Environment Bearing Capacity [J]. *Economy Geography*. 17(1): 97–99.
11. Chen, J. X., Dong, Z. (2006) Environmental Factors in Urban Environment and Traffic Capacity [J]. *Journal of Chang’an University (Natural Science Edition)*. 26(6):77–80. (in Chinese)
12. Yang, Z. Z., Miao, G. Q., Feng, T. (2006) Forecast on Maximum Car Ownership with Constraint of Environmental Capacity in Urban [J]. *China Journal of Highway and Transport*. 19(6):92–101. (in Chinese)
13. Wang, Z. B., Qu, F., Chen, Y. Y. (2005) The Analysis of Microcosmic Environmental Traffic Capacity [J]. *Journal of Transportation Systems Engineering and Information Technology*. 5(4):53–56. (in Chinese)
14. Lu, Z. L., Fan, B. Q., Liu, J. J., Zhou, Y. H. (2006) Bi-level Multi-objective Programming Model for the Ramp Control and Pollution Control on Urban Expressway Networks [J]. *Control and Decision*. 21(1): 64–67.
15. Xie, S. D., Zhang, Y. H., Tang, X. Y. (1999) Dispersion Models for Vehicle Exhaust Pollutant [J]. *Environmental Science*. (1): 104–109. (in Chinese)
16. Liu, D., Lu, Z. L. (2012) A Survey of Vehicle Exhaust Pollutant Dispersion Models of Urban Roads [J]. *Environmental Science Survey*. 31(1): 10–12. (in Chinese)
17. Xie, S. D., Zhang, Y. H., Tang, X. Y. (1999) Dispersion Models for Vehicle Exhaust Pollutant [J]. *Environmental Science*. (1): 104–109. (in Chinese)
18. Jiang, Bo. (2003) Diffusion model of vehicles pollutant emissions on Wuhan City streets [D]. Wuhan: Wuhan University of Technology Master Thesis. (in Chinese)
19. Zhu, G. C., Wen, D. S. (2001) On diffusion box model of vehicle exhaust gas for urban road [J]. *Journal of Southeast University (Natural Science Edition)*. (4): 88–91. (in Chinese)
20. Godfrey, J. W. (1969) The mechanism of a road network. *Traffic Engineering and Control*, Vol. 11, pp. 323–327.
21. Ma, Y. Y. (2010) Research on the traffic signal control systems based on the sub-network coordination [D]. Tongji University. (in Chinese)
22. Geroliminis, N., Daganzo, C.F. (2007) Macroscopic modeling of traffic in cities. TRB 86th Annual Meeting (Paper # 07-0413), Washington, DC.
23. Geroliminis, N., and Daganzo, C. F. (2008) Existence of urban-scale macroscopic fundamental diagrams: some experimental findings. *Transportation Research Part B*, Vol. 42, pp. 756–770. <http://dx.doi.org/10.1016/j.trb.2008.02.002>
24. Ji, Y., Daamen, W., Hoogendoorn, S., Hoogendoorn-Laser, S., and Qian, X. (2010) Investigating the shape of the macroscopic fundamental diagram using simulation data. *Transportation Research Record*, 2161, pp. 40–48. <http://dx.doi.org/10.3141/2161-05>
25. Geroliminis, N., and Sun, J. (2011) Properties of a well-defined macroscopic fundamental diagram for urban traffic. *Transportation Research Part B*, Vol. 45, pp. 605–617. <http://dx.doi.org/10.1016/j.trb.2010.11.004>
26. Du, Y. M., Wu, J.P., Jia, Y.H. and Xu, M. (2014) MFD based Regional Traffic Volume Dynamic Control [J]. *Journal of Transportation System Engineering and Information Technology*. 14(3): 162–167. (in Chinese)
27. Dorigo M, Maniezzo V, Colomi A. (1996) Ant system: optimization by a colony of cooperating agents [J]. *Systems, Man, and Cybernetics, Part B: Cybernetics, IEEE Transactions*, 26(1): 29–41. <http://dx.doi.org/10.1109/3477.484436>
28. Dorigo, M., Gambardella, L. M. (1997) Ant colony system: A coop-

- erative learning approach to the traveling salesman problem [J]. *Evolutionary Computation, IEEE Transactions on*, 1(1): 53–66. <http://dx.doi.org/10.1109/4235.585892>
29. Jia, Y. H., Wu, J. P., Du, Y. M., and Qi, G. Q. (2014) Study on FLOWSIM and its Application for Isolated Signalized Intersection Assessment [J]. *Journal of System Simulation*, 26(10): 2529–2534.
30. Wu, J. P., Brackstone, M., McDonald, M. (2000) Fuzzy Sets and Systems for a Motorway Microscopic Simulation Model [J]. *Fuzzy Sets and Systems*, 116(1): 65–76. [http://dx.doi.org/10.1016/S0165-0114\(99\)00038-X](http://dx.doi.org/10.1016/S0165-0114(99)00038-X)
31. Wu, J. P., Brackstone, M., McDonald, M. (2003) The Validation of a Microscopic Simulation Model: a Methodological Case Study [J]. *Transportation Research Part C*, 11(6): 463–479. <http://dx.doi.org/10.1016/j.trc.2003.05.001>
32. Li, T. Z., Zhu, Z. G., Tian, X. X. (2008) Environmental traffic capacity of link section of urban street [J]. *Journal of Southeast University (Natural Science Edition)*, 38(2): 309–313. (in Chinese) <http://dx.doi.org/10.1007/s11771-008-0058-z>
33. He, X. F., Jiang, W. M., Zhang, Y. Y. (2004) Research Of Atmospheric NO Diffusion Law and Controlling Method In Nanjing [J]. *Scientia Meteorologica Sinica*, 24(3): 269–276. (in Chinese)
34. Wang, W., Xiang, Q. J., Chang, Y. L., Li, T. Z., Li, X. G. (2002) *Method for analysis of energy consumption and environmental impact of city traffic system* [M]. Science Press. (in Chinese)

Health Risk Assessment of Heavy Metals and As in Vegetable and Soil System in Chongqing, Southwest of China

CHENG ZHANG^{1,2}, YONGMIN WANG¹, ZHENGLING ZHANG^{1,3}, DINGYONG WANG^{1,2,*},
CHENGZHONG LUO⁴ and FENG XU⁴

¹College of Resources and Environment, Southwest University, 400715, Chongqing, China

²Chongqing Key Laboratory of Agricultural Resources and Environment, Chongqing 400715, China

³Chongqing Environmental Protection Agency, Chongqing 401117, China

⁴Chongqing Solid Wastes Management Center, Chongqing 401117, China

ABSTRACT: A systematic survey of heavy metals and As concentrations in vegetables and soil in Chongqing was carried out to assess their potential health risks to local people. The results indicated that the Cr, Cd, Pb and As levels in some vegetables exceeded the Chinese safety standard of pollutants in food. The total carcinogenic risks of the heavy metals and As in 10 kinds of vegetables were all over the standard limits provided by USEPA and ICRP. Therefore, great attention should be paid to the issues of the heavy metals and As pollution in vegetables and the corresponding soil.

INTRODUCTION

WITH rapid development of industrialization and urbanization, the discharge amount of waste water, residue and gas containing heavy metals and As was greatly increased (Karim *et al.*, 2008; Bhuiyan *et al.*, 2011; Khillare *et al.*, 2012; Rahman *et al.*, 2014). Those heavy metals could deposit in soil and then accumulate in crops, which may possibly cause serious threat to human health (Chunilall *et al.*, 2005; Reynders *et al.*, 2008; Khan *et al.*, 2010; Bacigalupo *et al.*, 2012). Thus, it is important to figure out heavy metal pollution situations in soil and crops. Vegetables were one of the necessary foods in daily life so that many researchers have paid their attention to the heavy metal pollution in vegetable and soil system (Alam *et al.*, 2003; Sharma *et al.*, 2007; Noor-ul-Amin *et al.*, 2013; Mahmood and Malik, 2014; Kachenko and Singh, 2006; Sharma *et al.*, 2008; Mansour and Gad, 2010; Hu *et al.*, 2013). Numerous papers have previously reported that the heavy metal concentrations in vegetables in mine regions in Tongling, Anhui Province and Daye (Li *et al.*, 2013), Hubei Province (Sun *et al.*, 2013) were significantly higher than the background values. The target hazard quotients (THQ) of As and Pb were even up to 17.92 and 10.14, respectively. And the target cancer risk (TR) of As was 8.06×10^{-3} which was obviously

higher than the acceptable risk ($10^{-6} \sim 10^{-4}$) recommended by the United State Environmental Protection Agency (USEPA) and also higher than the maximum acceptable risk (5.0×10^{-5}) suggested by the International Commission on Radiation Protection (ICRP).

Chongqing, one of the oldest industrial cities in China and the largest-scale heavy metal industrial city in the upper reaches of Yangtze River, was also the main production base of foodstuffs and vegetable crops in the southwest region of China. In recent years, although the control and management of emission of heavy metal pollutants have been strengthened, environmental risks and some historically remaining issues still exist. Vegetables, as the main crops in Chongqing, are important food with a total production amount of 15.09 million tons (Chongqing municipal bureau of statistics, 2013), mainly distributed in Banan, Yubei, Bishan, and Jiangjin districts. In 2012, the cultivated areas of vegetables in Chongqing reached 65.27×10^4 hectares, accounting for about 18.8% of the total crop planting areas. Previous studies about the heavy metals and As pollution of soil and vegetables in Chongqing only focused on the market vegetables (Yang *et al.*, 2007; 2011), and limited data were obtained to systematically analyze the heavy metals in vegetable bases and corresponding soil (vegetable-planting soil) and assess the corresponding health risks caused by metal exposure.

Therefore, the objectives of this study were: (1) to investigate the heavy metals and As distribution fea-

*Author to whom correspondence should be addressed. Tel. +86-23-68251691;
E-mail address: dywang@swu.edu.cn

tures and the pollution status in vegetables and corresponding soil (major vegetable bases) in Chongqing; (2) to assess the health risks of heavy metals and As in vegetables in order to provide a basis for the risk warning and contamination control of heavy metals and As pollution in soil and vegetables in Chongqing.

MATERIALS AND METHODS

Study Area

Chongqing locates in the southwest of China and the upstream of the Yangtze River with a longitude range of $105^{\circ}11' - 110^{\circ}11'$ and a latitude range of $28^{\circ}10' - 32^{\circ}13'$. It has a total area of $82,400 \text{ km}^2$ with a population of over 31 million. Its topography is characterized by hills, valley and mountains, and has a typical subtropical humid monsoon climate with annual average temperature of 18°C and total annual sunshine time of 1,000 to 1,200 hours. The main soil in the study area is purple soil, paddy soil, yellow soil and yellow brown soil, and the main vegetables are pepper, eggplant, cucumber, cabbage, lettuce, etc.

Sample Collection and Analysis

According to the types and distribution of Chongq-

ing vegetable bases, five different types of vegetables including leafy (scallion, cabbage, amaranth, malabar spinach and lettuce), stem (romaine), solanaceous (pepper and eggplant), legume (kidney bean) and melon (cucumber) vegetables and their corresponding top soil (0~20 cm) were collected, obtaining a total of 183 vegetable samples and 183 soil samples. All these samples were mainly from vegetable bases in Banan, Yubei and Bishan districts (Figure 1) at the mature period (from March to May) of vegetables.

All the vegetable samples were firstly washed with regular water and then rinsed with deionized water repeatedly and kept in the oven for 30 min at 105°C followed by air drying in the laboratory. After that, the oven temperature was turned down to $60\sim 70^{\circ}\text{C}$ until to get the dry weight of vegetable samples which were then ground to powder. Meanwhile, the soil samples were also ground after air drying and then sieved by a 100-mesh sieve. All the treated samples were sealed in ziplock bags and stored in a dry environment. Cr, Cd, Pb and As in the vegetable and soil samples were analyzed after being digested by $\text{HNO}_3\text{-HClO}_4$ and $\text{HCl-HF-HNO}_3\text{-HClO}_4$, according to the methods described in the 'Analysis methods of heavy metals in soils' (China Environmental Monitoring Center, 1992) and 'The principle and application of agricultural environment monitoring' (Pi and Tang, 1998). As was measured by

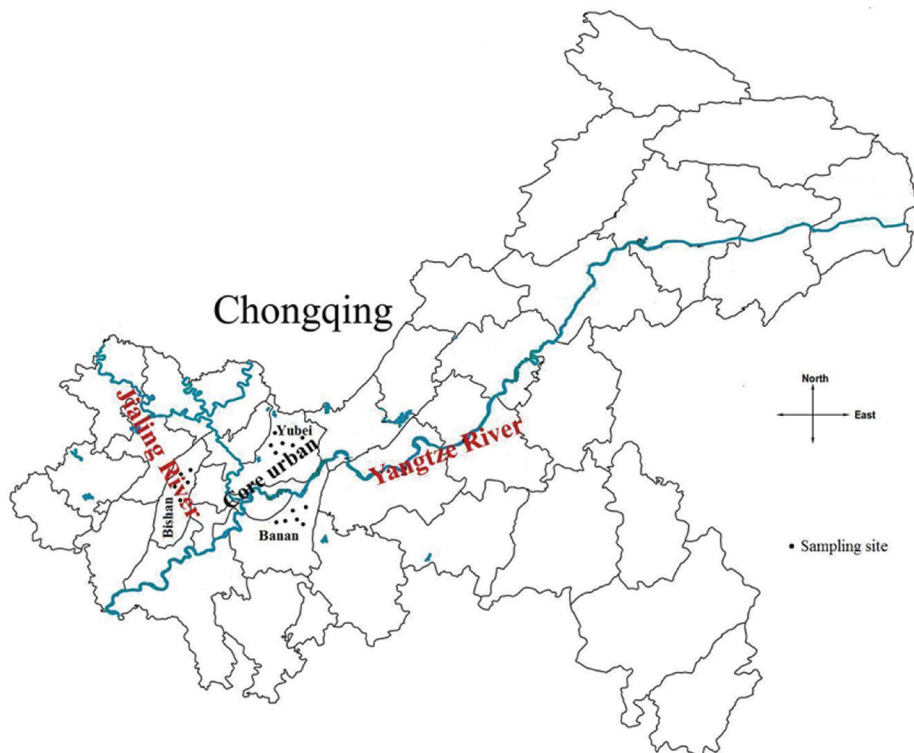


Figure 1. Sampling location of the study area.

a Visible Spectrophotometer (722 model, Shanghai) with the limit of detection (LOD) of 0.018 $\mu\text{g mL}^{-1}$ and the heavy metals were measured by an Atomic Absorption Spectrophotometer (TAS-990, Beijing) with the LODs of 0.057, 0.032 and 0.046 $\mu\text{g mL}^{-1}$ for Cr, Cd and Pb, respectively. The measured concentrations of heavy metals and As were in the dry weight of the vegetables which were then converted to those in the wet weight based on the water content. Thus, the present concentrations and calculated risk factors in this paper were all based on the wet weight. Quality control in this study included blanks, duplicates and matrix spikes included in the national standards GBW10015 (GSB-6 Spinacia) and GB W10021 (GSB-12 Beans). The matrix recovery ranged from 90% to 110%, and the relative standard deviation (RSD) was lower than 10%. Statistical analysis was performed using Origin 8.0 and SPSS 19.0.

Bio-concentration Factor (BCF) of Heavy Metals and As in Vegetables

BCF was used to characterize the ability of vegetable to accumulate heavy metals and As from soil. It can be calculated as follows (USEPA, 2000):

$$BCF = C_{veg}/C_{soil}$$

where C_{veg} and C_{soil} represent heavy metals and As concentrations in vegetables and corresponding soils, respectively.

Health Risk Assessment

The human health risks posed by single or multiple heavy metals and As exposure are usually characterized by the target hazard quotient (THQ) and target cancer risk (TR), which can be evaluated by the following formulas:

$$THQ = \frac{C_i \times FIR \times EF \times ED}{RfD_i \times BW \times AT_n} \times 10^{-3}$$

$$TR = \frac{C_i \times FIR \times EF \times ED \times CPS}{BW \times AT_c}$$

where, THQ is the average body intake dose, $\text{mg} \cdot \text{kg}^{-1} \cdot \text{d}^{-1}$; C_i is the metal concentrations in soil, mg kg^{-1} ; FIR is the vegetable ingestion rate, g d^{-1} (428 g d^{-1} per adult, 269 g d^{-1} per child) (Jiang *et al.*, 2007); EF is the exposure frequency (365d year^{-1}); ED is the ex-

posure duration (30 years for adults, 6 years for children, USEPA, 2000); RfD_i is the reference dose of heavy metals and As, $\text{mg kg}^{-1} \text{d}^{-1}$, and the RfD_i of Cr, Cd, Pb and As were 1.5, 1.0×10^{-3} , 4.0×10^{-3} and $3.0 \times 10^{-4} \text{mg kg}^{-1} \text{d}^{-1}$, respectively; BW is the average body weight, kg (60 kg for adults, 15 kg for children) (Wang *et al.*, 2009); AT_n is the average exposure time for non-carcinogens, d ($ED \times 365 \text{d}$) (USEPA, 2000); CPS is the carcinogenic concentration index, $\text{kg d}^{-1} \text{mg}^{-1}$, which is 0.5, 6.1 and 1.5 kg d mg^{-1} for Cr, Cd and As, respectively (USEPA, 2007; Ferré-Huguet *et al.*, 2008); AT_c is the duration of carcinogenic effect ($70 \times 365 \text{d}$).

The formulas for multi-metal health risk were as follows:

$$TTHQ = \sum_{i=1}^n THQ_i$$

$$TTR = \sum_{i=1}^n TR_i$$

where, THQ or $TTHQ < 1$ means the non-carcinogenic risk is minor or negligible, while THQ or $TTHQ > 1$ indicates that the exposure population is likely to experience adverse effects. TR can be used to estimate the carcinogenic level after consuming polluted vegetables, according to the acceptable risks (10^{-6} ~ 10^{-4} and 5.0×10^{-5}) recommended by USEPA and ICRP, respectively.

RESULTS AND DISCUSSION

Heavy Metals and As in Soil

The mean level of each element (Cr, Cd, Pb and As) in the vegetables and the corresponding soil was listed in Table 1. The average concentrations of Cr, Cd and Pb in soil were 51.68 ± 16.78 , 0.28 ± 0.10 and $36.53 \pm 11.62 \text{mg kg}^{-1}$, which were 1.06, 3.61, 1.65 times higher than the background values (Chen *et al.*, 1982), respectively. However, the mean level of As in soil ($6.40 \pm 3.89 \text{mg kg}^{-1}$) was lower than the background value.

Heavy metals and As concentrations in 10 different vegetable-planting soil were presented in Figure 2. According to the *Farmland environmental quality evaluation standards for edible agricultural products in China* (HJ/T 332-2006) (Ministry of Environmental Protection of China, 2007), the concentrations of Cd in the soil grown with scallion, amaranth, and cucumber slightly exceeded this standard, while the other metals

Table 1. Total Concentrations of Heavy Metals and As in Vegetables and Corresponding Soils.

	Vegetables (mg kg ⁻¹)				Corresponding Soils (mg kg ⁻¹)			
	Cr	Cd	Pb	As	Cr	Cd	Pb	As
Min	0.03	0.00	0.01	0.00	22.77	0.11	17.53	1.75
Max	0.93	0.30	0.67	0.10	163.35	0.76	120.96	23.65
Mean	0.15	0.03	0.11	0.02	51.68	0.28	36.53	6.40
SD	0.13	0.03	0.10	0.02	16.78	0.10	11.62	3.89
CV(%)	84.87	144.08	99.06	96.10	32.47	36.02	31.80	60.79
National Standard	0.5	0.2 ^a 0.05 ^d	0.3 ^a 0.2 ^c 0.1 ^e	0.5	200	0.30	50	25

Notes: ^aleafy vegetables, ^bstem and legume vegetables, ^clegume vegetables, ^dsolanaceous and melons vegetables, ^estem, solanaceous and melons vegetables.

in almost all the soil samples were within the limits. Sites with Cd and Pb exceeding the national standard accounted for 37.2% and 8.2% of the total sample sites, suggesting that the soil of planting base had been partly contaminated by Cd and Pb. Chongqing is one of the traditional industrial bases in the southwest region of China with the amount of industrial enterprises in urban area over 13,000. The discharge of industrial waste

gas from these enterprises even could reach up to 300 billion m³ year⁻¹. The two sampling regions of Ban-an and Yubei locate in the urban area of Chongqing, and another region (Bishan) is close to the urban area. Thus, the contaminants could be easily accumulated in the soil of these regions by atmospheric diffusion and deposition, resulting in high concentrations of metals in soil. In addition, the waste gas from transportation

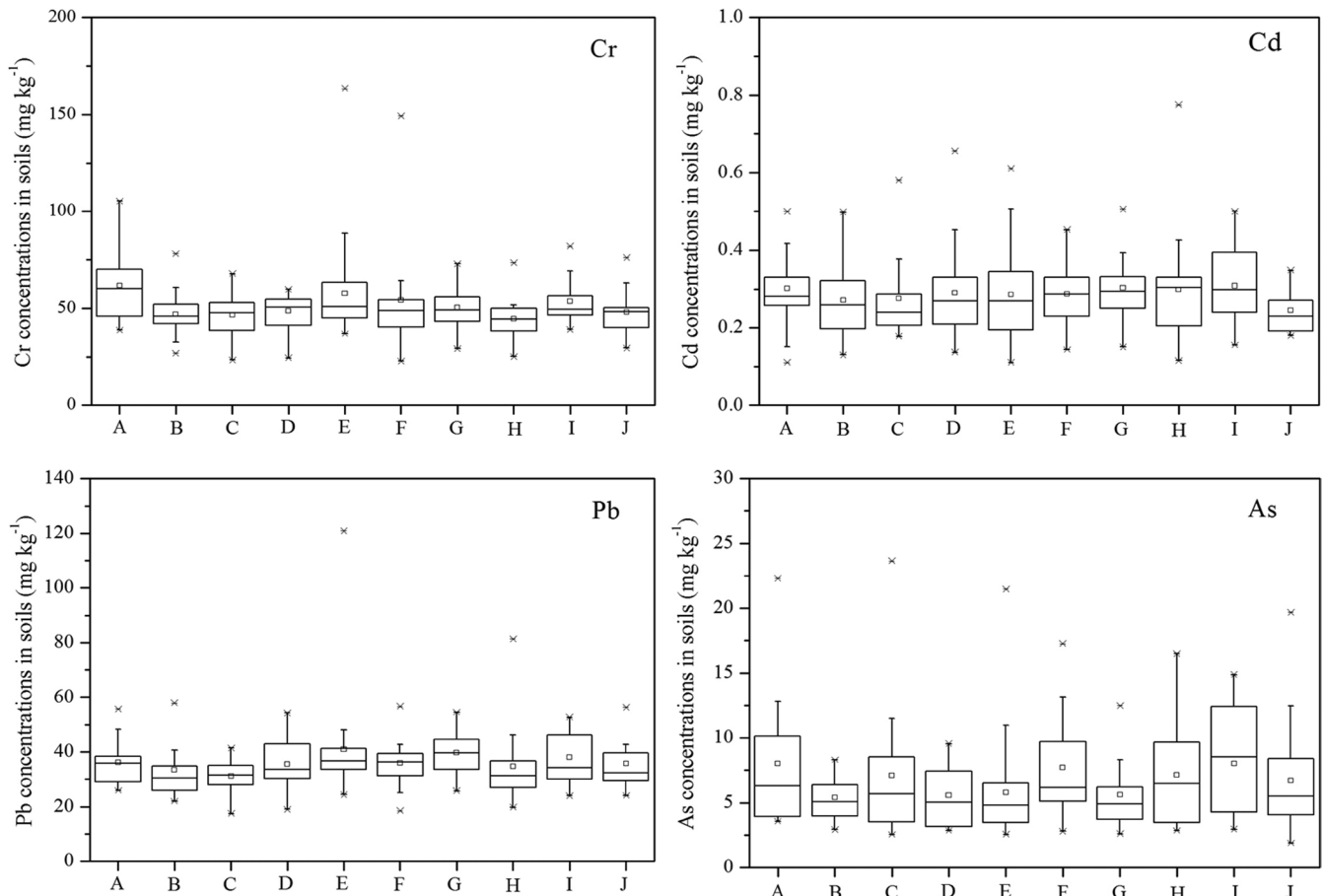


Figure 2. Heavy metals and As concentrations in vegetable-planting soils. Notes: A, B, C, D, E, F, G, H, I, J represent vegetable-planting soils of scallion, kidney bean, pepper, cabbage, lettuce, romaine, amaranth, eggplant, cucumber and malabar spinach, respectively.

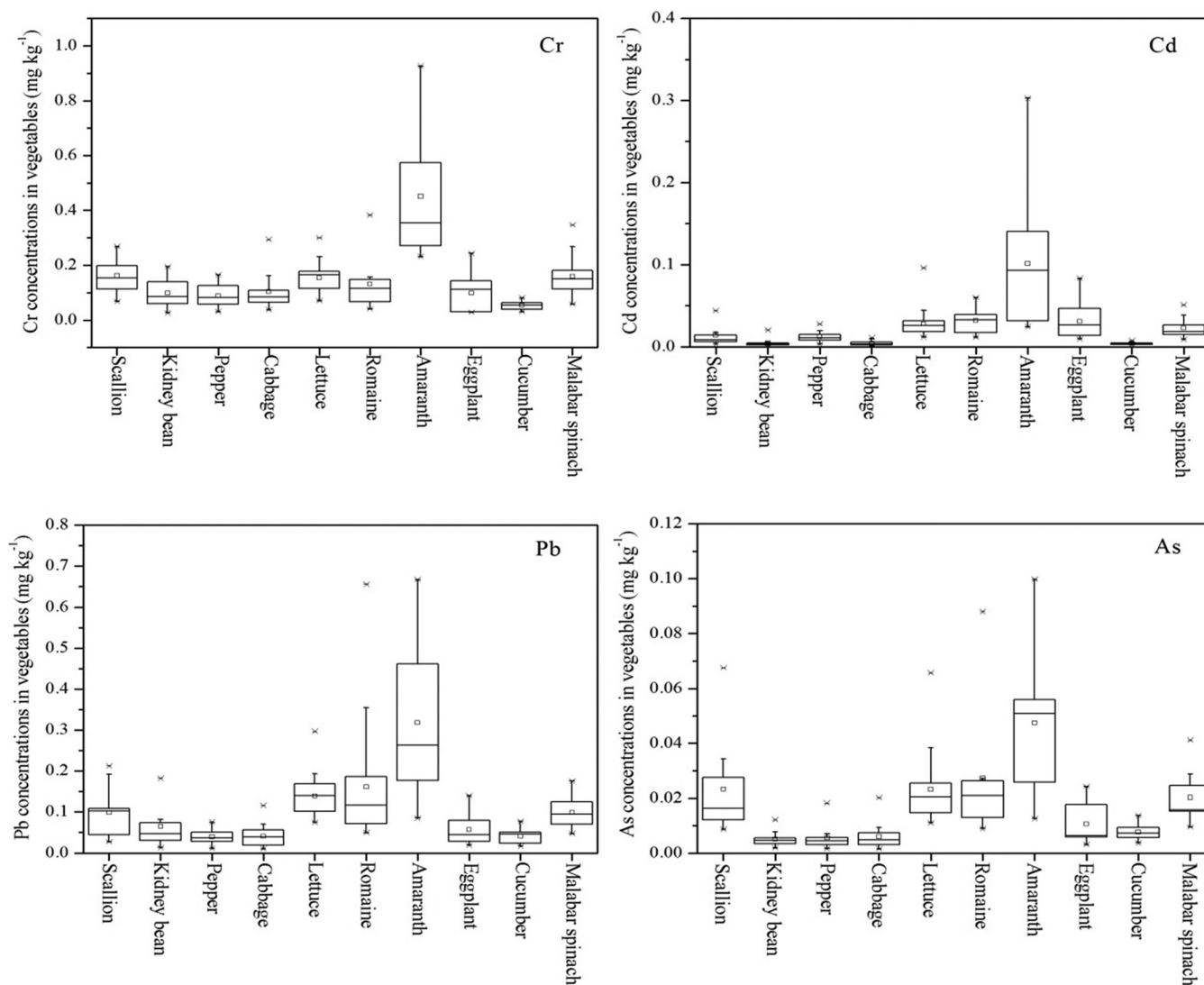


Figure 3. Heavy metals and As concentrations in different vegetables.

and fertilizers used in agricultural production, such as nitrogenous and organic fertilizer, were also potential factors causing high concentrations of heavy metals in soil.

Heavy Metals and As in Vegetables

Detection rates of all these four elements in the vegetable samples were up to 100%. However, significant differences for these four elements (Cr, Cd, Pb, and As) were found in various vegetables with coefficients of variation ranging from 84.87% to 144.08%. The average concentrations of Cr, Cd, Pb, and As in the ten different vegetables were 0.15 ± 0.13 , 0.03 ± 0.03 , 0.11 ± 0.10 and 0.02 ± 0.02 mg kg^{-1} , respectively. The highest levels of heavy metals and As were observed in the leafy vegetables, followed by the stem vegetables, and

lower values appeared in the solanaceous, legume, and melon vegetables (Table 1).

The distribution of heavy metals and As in the ten different vegetables was presented in Figure 3. The mean values of the four elements in the vegetables were within the Limit Standards of Pollutants in Food in China (GB2762-2012) (Ministry of Health of China, 2013). However, their concentrations in some individual vegetable samples still exceeded the standard, with over-limit ratios of 3.3% for Cr, 9.3% for Cd, 8.3% for Pb and 8.2% for As. The average concentrations of individual elements in amaranth were higher than those in the other vegetables, and the levels of Cd and Pb in amaranth were over the national standard. In addition, the average level of Pb in some other vegetables (romaine, malabar spinach and lettuce) also exceeded the standard.

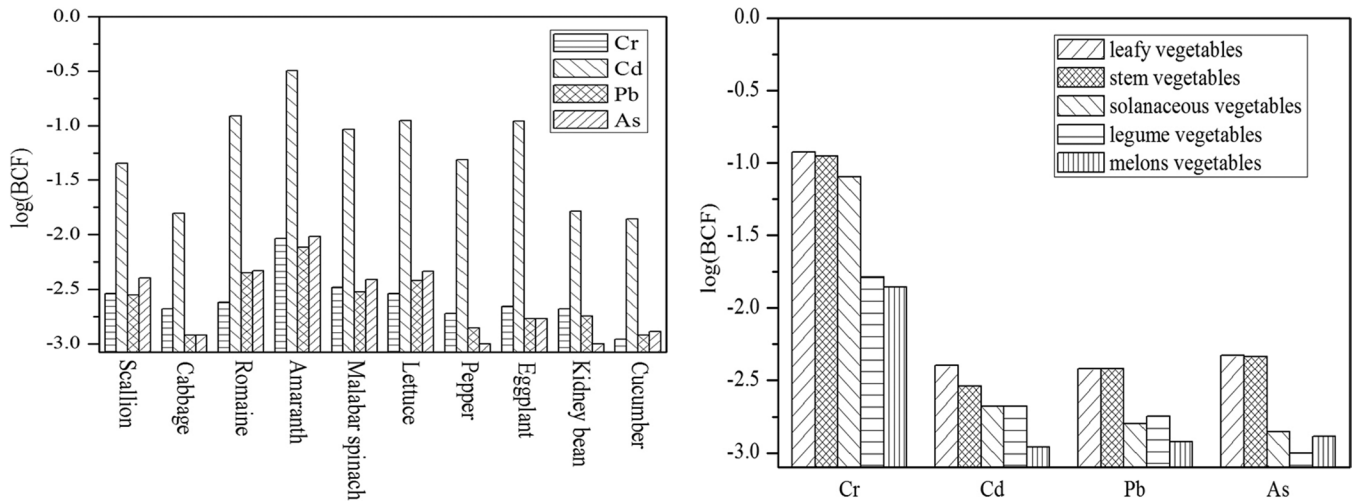


Figure 4. BCF of heavy metals and As in vegetables.

BCFs of Heavy Metals and As in Vegetables

Figure 4 displayed the BCFs of heavy metals and As accumulated from soils to vegetables. The BCF trends of metals in the vegetables was in the order of Cd > As > Pb > Cr. The BCF of Cd was the largest in all the selected vegetables, which was similar to the report by Chunilall *et al.* (2005). Meanwhile, the BCFs of Cr, Pb were lower than that in Lahore, Pakistan (Mahmood and Malik, 2014). Higher accumulation ability of amaranth for these four elements was observed, leading to higher concentrations of metals in amaranth than those in the other vegetables. In addition, previous studies also reported that amaranth was considered as a hyper accumulation plant for Cd with a BCF over 25 (Li *et al.*, 2012). Thus, it is necessary to pay attention to the amaranth contaminated by heavy metals and As. Mea-

sures should be taken to reduce the edible amaranth and control soil pollution by heavy metals.

The accumulation capability of metals varied with different vegetables. Generally, leafy vegetables had higher enrichment ability, followed by the stem, solanaceous, legume, and melon vegetables. Significant positive correlations of Cr, Cd and Pb concentrations between vegetables and the corresponding soil were observed ($R = 0.23^{**} - 0.26^{**}$, $P < 0.01$, $n = 183$), suggesting that the increase of metals in soil could influence their accumulation in vegetables (Figure 4). However, some other studies showed that heavy metals in vegetables had no significant relationship with soil metals (Liu *et al.*, 2013). These different results may be caused by the difference of regional environment, soil properties, farming methods and pollution conditions.

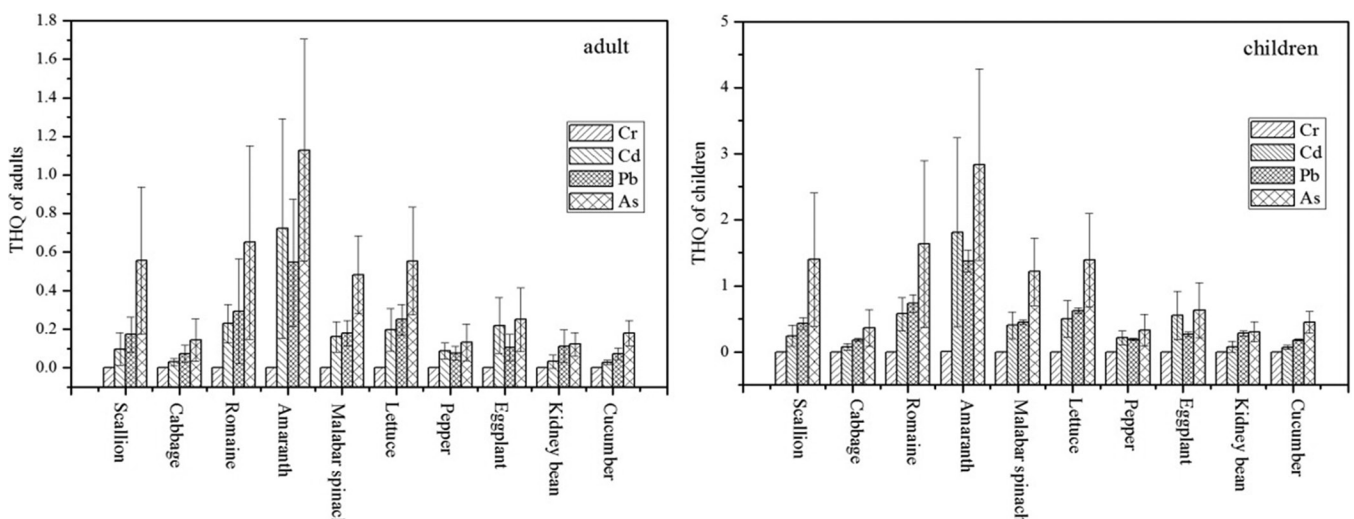


Figure 5. THQ of heavy metals and As.

Table 2. TTHQ for four metals.

	Scallion	Kidney Bean	Pepper	Cabbage	Lettuce	Romaine	Amaranth	Eggplant	Cucumber	Malabar Spinach
Children	2.08	0.67	0.74	0.62	2.52	2.95	6.02	1.45	0.71	2.07
Adults	0.83	0.27	0.29	0.25	1.01	1.17	2.40	0.58	0.28	0.82

Health Risks of Heavy Metals and As in Vegetables

Non-carcinogenic Risk

All these four investigated elements had non-carcinogenic risks. For children, the THQ of Cr, Cd, Pb and As were 0.001–0.005, 0.07–1.81, 0.18–1.37 and 0.31–2.84, respectively. The THQ of As in scallion, romaine, lettuce, amaranth and malabar spinach were all more than 1, demonstrating that a large daily intake of these vegetables was likely to cause non-carcinogenic risk by As. Also, daily intake of amaranth might cause health risk by Cd and Pb. The THQ of Cr, Cd, Pb and As for adults were 0.0003–0.0022, 0.03–0.72, 0.07–0.54 and 0.12–1.13, respectively. And THQs of these four elements were less than 1 except As in amaranth (Figure 5). From the calculated THQs, the non-carcinogenic risks of the four elements decreased in the order of As > Pb > Cd > Cr.

Non-carcinogenic risks of the four elements for children and adults were presented in Table 2. It showed that the TTHQ for children was in a range of 0.62–6.02 which was 2.5 folds higher than that for adults (0.25–2.40). Amaranth had the largest health risk for both children and adults with the TTHQs of 6.02 and 2.40, respectively. For children the TTHQs in romaine, let-

tuce, malabar spinach, scallion and eggplant were over 1, while the TTHQs in pepper, kidney bean, cabbage and cucumber were less than 1. For adults, besides amaranth, only lettuce and romaine had non-carcinogenic risks, the TTHQs of other vegetables were less than 1. As was the main non-carcinogenic element, which contributed 43.48–67.22% to the total non-carcinogenic risk, followed by Pb and Cd. The non-carcinogenic risk in vegetables decreased in the order of amaranth > romaine > lettuce > malabar spinach > scallion > eggplant > pepper > cucumber > kidney bean > cabbage for both adults and children. Therefore, it can be inferred that the largest non-carcinogenic risk in the vegetables was from amaranth due to its largest metal concentrations. In a word, the potential health risk in different vegetables decreased in the order of leafy vegetables > stem vegetables > solanaceous vegetables > legume vegetable > melons vegetables (Figure 6).

Cancer Risks

Cd, Cr and As were carcinogenic. The cancer risks of Cr, Cd and As for adults were in the ranges of 8.25×10^{-5} – 6.90×10^{-4} , 7.36×10^{-5} – 1.88×10^{-3} and 2.35×10^{-5} – 2.18×10^{-4} , respectively, which were almost double of those for children (4.15×10^{-5} – 3.47×10^{-4} ,

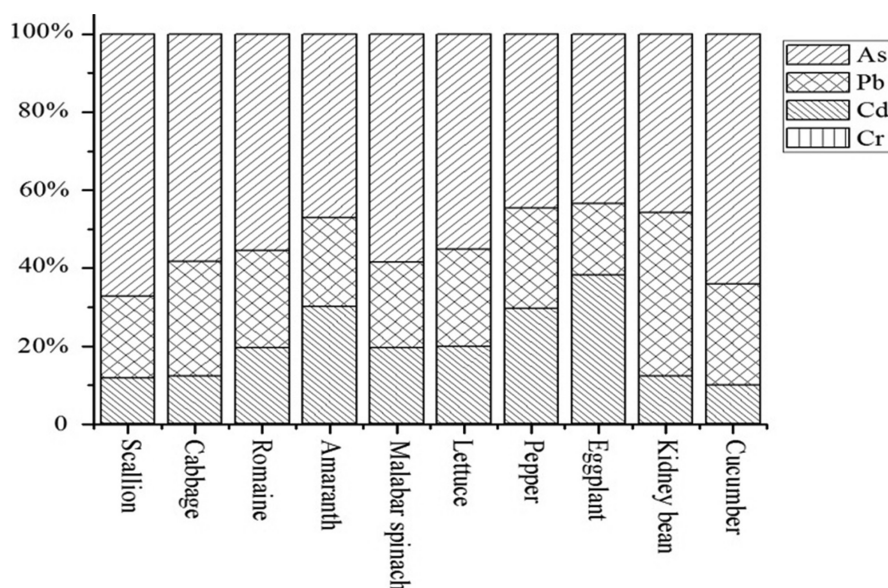


Figure 6. Contribution of each metal to non-cancer risk.

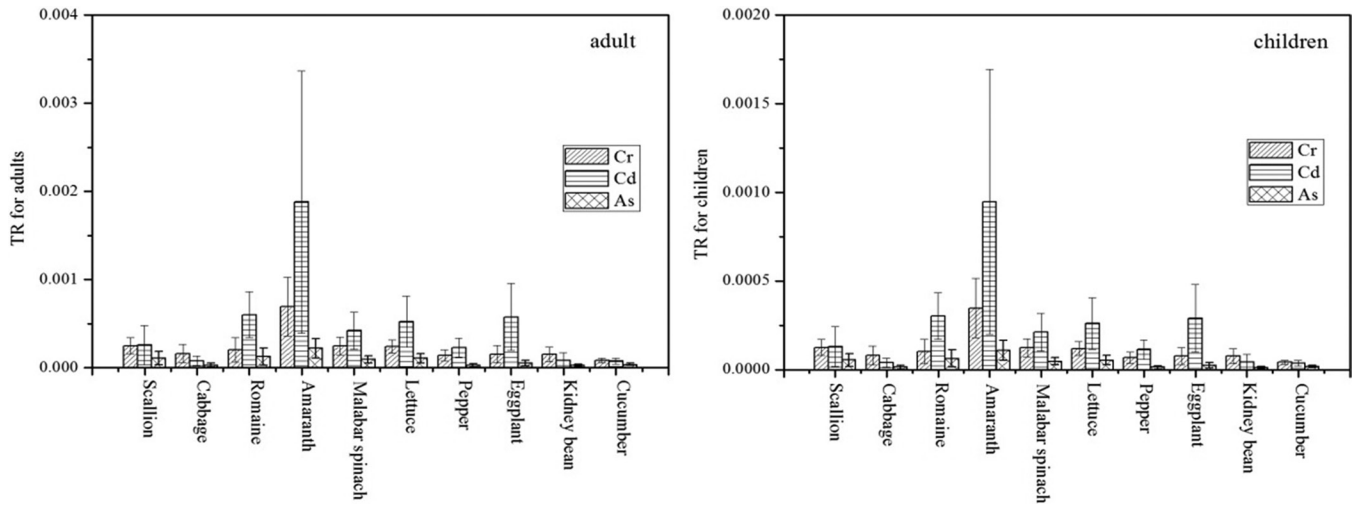


Figure 7. Cancer risk of main metals.

3.70×10^{-5} – 9.47×10^{-4} and 1.18×10^{-5} – 1.09×10^{-4}). Generally speaking, the cancer risks of these three elements showed the following order: Cd > Cr > As, and the TR of Cd was the highest in all other vegetables except the largest TR of Cr in kidney bean, cabbage and cucumber (Figure 7). Therefore, Cd appeared to be the main pollutant source of cancer risk among those elements. It was generally recognized that carcinogenic risk could be acceptable between 10^{-6} and 10^{-4} ; however, that less than 10^{-6} is the best as human may get exposure to other pollution sources.

A wide range of TTR was calculated, from 9.60×10^{-5} to 1.40×10^{-3} for children in the vegetables, and from 1.91×10^{-4} to 2.79×10^{-3} for adults, both of which slightly exceeded the acceptable range of 1×10^{-6} to 1×10^{-4} recommended by the USEPA and 5

$\times 10^{-5}$ recommended by the ICRP (Table 3). The main portion of cancer risks resulted from Cd, accounting for 29.55% to 74.10%, followed by Cr, occupying 19.54% to 59.85%. The TTR for adults and children decreased in the order of amaranth > romaine > lettuce > eggplant > Malabar spinach > scallion > pepper > cabbage > kidney bean > cucumber. Amaranth showed the largest carcinogenic risk which was consistent with the results of non-carcinogenic risk, as amaranth had a greater accumulation ability for these elements. Likewise, leafy vegetables had the highest cancer risk, followed by stem vegetables, solanaceous vegetables, legume vegetable, and melon vegetables (Figure 8). Therefore, measures should be adopted to control and avoid heavy metal and As pollution in vegetables and soils.

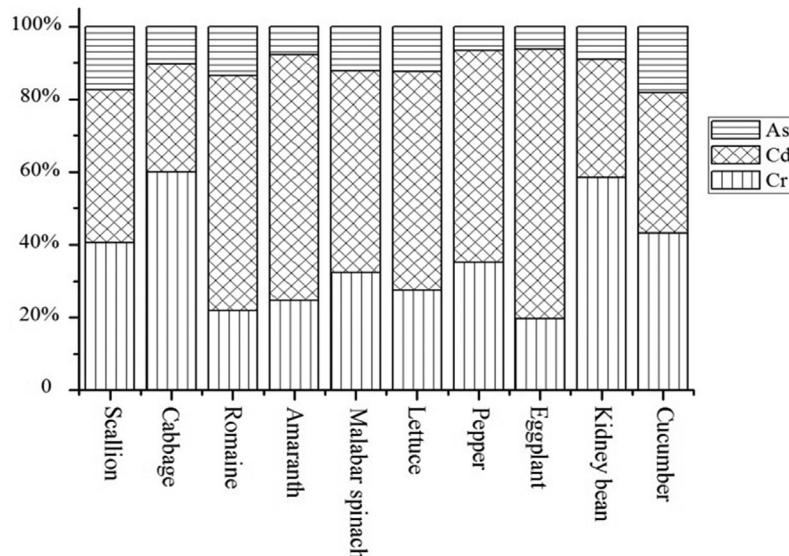


Figure 8. Contribution of each metal to cancer risk.

Table 3. TTR for Three Metals.

	Scallion	Kidney Bean	Pepper	Cabbage	Lettuce	Romaine	Amaranth	Eggplant	Cucumber	Malabar Spinach
Children	3.07E-04	1.31E-04	1.96E-04	1.34E-04	4.34E-04	4.66E-04	1.40E-03	3.90E-04	9.60E-05	3.80E-04
Adults	6.11E-04	2.61E-04	3.89E-04	2.66E-04	8.64E-04	9.27E-04	2.79E-03	7.75E-04	1.91E-04	7.57E-04

CONCLUSION

The average levels of heavy metals and As in 10 kinds of vegetables were within the Chinese national standard of pollutants in food, but the concentrations in some samples were over this standard. The highest levels of these elements were observed in leafy vegetables, followed by stem vegetables. The total carcinogenic risks of these four elements in the 10 kinds of vegetables all exceeded the standard limits of US EPA and ICRP. Meanwhile, amaranth, romaine and lettuce still had non-carcinogenic risks for human. As was the main element for non-carcinogenic risk, while Cd was the primary metal for carcinogenic risk. Amaranth had a greater accumulation ability for these elements (especially for Cd), resulting in larger carcinogenic and non-carcinogenic risks. Therefore, great attention should be paid to the heavy metal and As pollution issues in vegetables, and reducing the intake of amaranth and other leafy vegetables possibly could avoid the cancer risk effectively.

ACKNOWLEDGMENTS

This study was funded by the National Key Basic Research Program of China (2013CB430004), the National Natural Science Foundation of China (51208426), the Fundamental Research Funds for the Central Universities of China (XDJK2015B036), and Chongqing Environmental Protection Scientific Research Project of China (2014CF220).

REFERENCES

- Alam MG, Snow ET, Tanaka A (2003) Arsenic and heavy metal contamination of vegetables grown in Samta village, Bangladesh. *Sci Total Environ* 308: 83–96. [http://dx.doi.org/10.1016/S0048-9697\(02\)00651-4](http://dx.doi.org/10.1016/S0048-9697(02)00651-4)
- Bhuiyan MAH, Suruvi NI, Dampare SB, Islam MA, Quraishi SB, Ganyaglo S, Suzuki S (2011) Investigation of the possible sources of heavy metal contamination in lagoon and canal water in the tannery industrial area in Dhaka, Bangladesh. *Environ Monit Assess* 175: 633–649. <http://dx.doi.org/10.1007/s10661-010-1557-6>
- Bacigalupo C, Hale B (2012) Human health risks of Pb and As exposure via consumption of home garden vegetables and incidental soil and dust ingestion: a probabilistic screening tool. *Sci Total Environ* 423: 27–38. <http://dx.doi.org/10.1016/j.scitotenv.2012.01.057>
- Chen N, Lai W, Xu M, Zheng C (1982) Background values of 11 elements in soil of Chongqing in China. *Chongqing Environ Prot* 8: 38–51. (In Chinese)
- China environmental monitoring center (1992) *Analysis methods of heavy metals in soils*. Beijing: China Environmental Science Press. (In Chinese)
- Chongqing municipal bureau of statistics (2013) *Chongqing Statistics year-book 2012*, Beijing: China Statistics Press. (In Chinese)
- Chunilall V, Kindness A, Jonnalagadda SB (2005) Heavy metal uptake by two edible Amaranthus herbs grown on soils contaminated with lead, mercury, cadmium, and nickel. *J Environ Sci Heal* 40: 375–384. <http://dx.doi.org/10.1081/PFC-200045573>
- Ferré-Huguet N, Martí-Cid R, Schuhmacher M, Domingo JL (2008) Risk assessment of metals from consuming vegetables, fruits and rice grown on soils irrigated with waters of the Ebro river in Catalonia, Spain. *Biol Trace Elem Res* 123: 66–79. <http://dx.doi.org/10.1007/s12011-008-8113-z>
- Hu JL, Wu FY, Wu SC, Cao ZH, Lin XG, Wong MH (2013) Bioaccessibility, dietary exposure and human risk assessment of heavy metals from market vegetables in Hong Kong revealed with an in vitro gastrointestinal model. *Chemosphere* 91: 455–461. <http://dx.doi.org/10.1016/j.chemosphere.2012.11.066>
- Jiang DM, A LY, Wang DY, Wang XC (2007) Investigation on dietary patterns and intake level of heavy metals of inhabitants in Three Gorges Reservoir area. *Asian J Ecotox*. 2: 83–87. (In Chinese)
- Kachenko AG, Singh B (2006) Heavy metals contamination in vegetables grown in urban and metal smelter contaminated sites in Australia. *Water Air Soil Pollut* 169: 101–123. <http://dx.doi.org/10.1007/s11270-006-2027-1>
- Karim RA, Hossain SM, Miah MM, Nehar K, Mubin MS (2008) Arsenic and heavy metal concentrations in surface soils and vegetables of Feni district in Bangladesh. *Environ Monit Assess* 145: 417–425. <http://dx.doi.org/10.1007/s10661-007-0050-3>
- Khan S, Rehman S, Khan AZ, Khan MA, Shah MT (2010) Soil and vegetables enrichment with heavy metals from geological sources in Gilgit, northern Pakistan. *Ecotoxicol Environ Saf* 73: 1820–1827. <http://dx.doi.org/10.1016/j.ecoenv.2010.08.016>
- Khillare PS, Jyethi DS, Sarkar S (2012) Health risk assessment of polycyclic aromatic hydrocarbons and heavy metals via dietary intake of vegetables grown in the vicinity of thermal power plants. *Food Chem Toxicol* 50: 1642–1652. <http://dx.doi.org/10.1016/j.fct.2012.01.032>
- Li NY, Fu QL, Zhuang P, Guo B, Zou B, Li ZA (2012) Effect of fertilizers on Cd uptake of Amaranthus hypochondriacus, a high biomass, fast growing and easily cultivated potential Cd hyperaccumulator. *Int J Phytoremediat* 14: 162–173. <http://dx.doi.org/10.1080/15226514.2011.587479>
- Li RZ, Pan CR, Xu JJ, Chen J, Jiang YM (2013) Contamination and health risk for heavy metals via consumption of vegetables grown in fragmentary vegetable plots from a typical nonferrous metals mine city. *Environmental Science* 34: 1076–1085. (In Chinese)
- Liu XM, Song QJ, Tang Y, Li WL, Xu JM, Wu JJ, Wang F, Brookes PC (2013) Human health risk assessment of heavy metals in soil-vegetable system: A multi-medium analysis. *Sci Total Environ* 463–464: 530–540. <http://dx.doi.org/10.1016/j.scitotenv.2013.06.064>
- Mahmood A, Malik RN (2014) Human health risk assessment of heavy metals via consumption of contaminated vegetables collected from different irrigation sources in Lahore, Pakistan. *Arab J Chem* 7: 91–99. <http://dx.doi.org/10.1016/j.arabjc.2013.07.002>
- Mansour S A, Gad MF (2010) Risk assessment of pesticides and heavy metals contaminants in vegetables: A novel bioassay method using Daphnia magna Straus. *Food Chem Toxicol* 48: 377–389. <http://dx.doi.org/10.1016/j.fct.2009.10.026>
- Ministry of Environmental Protection of China (2007) Environmental quality evaluation standards for farmland of edible agricultural products (HJ/T332-2006). (In Chinese)

- Ministry of Health of China (2013) *Limits of Contaminants in food*, GB 2762-2012. (In Chinese)
- Noor-ul-Amin, Hussain A, Alamzeb S, Begum S (2013) Accumulation of heavy metals in edible parts of vegetables irrigated with waste water and their daily intake to adults and children, District Mardan, Pakista. *Food Chem* 136: 1515–1523. <http://dx.doi.org/10.1016/j.foodchem.2012.09.058>
- Pi GJ and Tang SY (1998) *The principle and application of agricultural environment monitoring*. Chengdu: Chengdu University of Science and Technology of China Science Press. (In Chinese)
- Rahman MA, Rahman MM, Reichman SM, Lim RP, Naidu R (2014) Heavy metals in Australian grown and imported rice and vegetables on sale in Australia: Health hazard. *Ecotox Environ Safe* 100: 53–60. <http://dx.doi.org/10.1016/j.ecoenv.2013.11.024>
- Reynders H, Bervoets L, Gelders M, De Coen WM, Blust R (2008) Accumulation and effects of metals in caged carp and resident roach along a metal pollution gradient. *Sci Total Environ* 391: 82–95. <http://dx.doi.org/10.1016/j.scitotenv.2007.10.056>
- Sharma RK, Agrawal M, Marshall F (2007) Heavy metal contamination of soil and vegetables in suburban areas of Varanasi, India. *Ecotoxicol Environ Saf* 66: 258–266. <http://dx.doi.org/10.1016/j.ecoenv.2005.11.007>
- Sharma RK, Agrawal M, Marshall FM (2008) Heavy metal (Cu, Zn, Cd and Pb) contamination of vegetables in urban India: A case study in Varanasi. *Environ Pollut* 154: 254–263. <http://dx.doi.org/10.1016/j.envpol.2007.10.010>
- Sjöström ÅE, Collins CD, Smith SR, Shaw G (2008) Degradation and plant uptake of nonylphenol (NP) and nonylphenol-12-ethoxylate (NP12EO) in four contrasting agricultural soils. *Environ Pollut*. 156: 1284–1289. <http://dx.doi.org/10.1016/j.envpol.2008.03.005>
- Sipter E, Rózsa E, Gruiz K, Tátrai E, Morvai V (2008) Site-specific risk assessment in contaminated vegetable gardens. *Chemosphere*. 71:1301–1307. <http://dx.doi.org/10.1016/j.chemosphere.2007.11.039>
- Sun QB, YiN CQ, Deng JF, Zhang DF (2013) Characteristics of soil-vegetable pollution of heavy metals and health risk assessment in Daye mining area. *Environmental Chemistry* 32:671–677 (In Chinese).
- US EPA (2000) *Handbook for non-cancer health effects evaluation*, Washington DC: US Environmental Protection Agency.
- US EPA (2007) *Guidance for evaluating the oral bioavailability of metals in soils for use in human health risk assessment*, Washington DC: US Environmental Protection Agency.
- Wang ZS, Duan XL, Liu P, Nie J, Huang N, Zhang JL (2009) Human exposure factors of Chinese people in environmental health risk assessment. *Res Environ Sci* 22: 1164–1170. (In Chinese)
- Yang QW, Xu Y, Liu SJ, He JF, Long FY (2011) Concentration and potential health risk of heavy metals in market vegetables in Chongqing, China. *Ecotox Environ Safe* 74: 1664–1669.
- Yang QW, Li H, Long FY (2007) Heavy Metals of Vegetables and Soils of Vegetable Bases in Chongqing, Southwest China. *Environ Monit Assess* 130: 271–279. <http://dx.doi.org/10.1007/s10661-006-9395-2>

Root Nitrogen Uptake in Wastewater-Irrigated Pepper Fields

XIAOHUI LU*, PEIFANG WANG, YANJIE ZHANG and DOU ZHI

Ministry of Education Key Laboratory of Integrated Regulation and Resource Development on Shallow Lakes,
Hohai University, Nanjing, Jiangsu, 210098, China

ABSTRACT: Given the shortage of fresh water in semi-arid and arid zones, wastewater is becoming an increasingly important source of irrigation. This study analyzes the principles of root water/nitrogen uptake dynamics in wastewater-irrigated pepper fields. Comparison of pepper root uptake rates of nitrogen show that the root uptake rate of $\text{NO}_3\text{-N}$ is an order of magnitude higher than that of $\text{NH}_4\text{-N}$. When the original $\text{NO}_3\text{-N}$ content in the soil is high, additional wastewater irrigation will not increase the root uptake of $\text{NO}_3\text{-N}$. The pepper root water uptake rates gradually increase with increasing light intensity and air temperature.

INTRODUCTION

AGGRAVATED shortages in water resources and water pollution have led to the increasing use of treated or untreated wastewater for farmland irrigation in arid and semi-arid regions. Wastewater primarily represents a source of water and nutritive elements, such as nitrogen, phosphorous and potassium, which contribute to the growth of many crops [1]. However, the excessive input of wastewater into the soil may lead to adverse effects on the soil and groundwater by causing nitrogen leaching below the root zone [2–4], destroying crops and causing economic losses to farmers [5]. Furthermore, pollutants in wastewater, particularly heavy metals and organic matter, can potentially threaten the environment and human health [6].

The nitrogen contained in wastewater functions not only as one of the most valuable plant nutrients but also as a soil and water contaminant [7,8]. Nitrogen in the soil mainly exists in four forms: organic nitrogen, ammonia nitrogen, nitrate nitrogen and gaseous nitrogen. Nitrate nitrogen is the predominant pollutant in groundwater [9]. By polluting drinking water sources, nitrate nitrogen can significantly harm humans by causing diseases such as arteriosclerosis and cancer. Therefore, studies on the principles and influential factors of nitrogen transport and transformation are becoming increasingly significant.

Pepper is one of the most popular vegetables in large

planting areas, and is in abundant supply in China. The pepper root, which is an important organ that adsorbs nutrients and moisture and assimilates, transforms and synthesizes many substances, plays a dominant role in root-zone soil water and solute dynamics. Therefore, the growth and vitality of the pepper root directly affects the growth, nutrition and yield levels of pepper. Although many studies have been conducted on the morphogenesis of the pepper root, root system distribution in the soil, root physiological activity in the development process and morphological structure of the root system, few studies have investigated the function of its growth and a water uptake model of the root system. Furthermore, because studies on pepper root under wastewater irrigation are almost nonexistent, the influence of the root system distribution and the water uptake pattern on nitrogen migration need to be studied comprehensively and their interaction mechanism under wastewater irrigation analyzed.

The objective of the work reported in this paper was to analyze the principle of nitrogen transport and the influence of the distribution and density of the pepper root on nitrogen transport in the vadose zone. To achieve this objective, field experiments, indoor tests and numerical simulations were conducted on the nitrogen migration of a wastewater-irrigated pepper field. Based on a one-dimensional (1D) water flow model, observed soil water content and temperature were used to calibrate the performance of the modified HYDRUS-1D code. Thereafter, the modified HYDRUS-1D code was used to produce the transformation of nitrogen in the unsaturated zone of the study area.

*Author to whom correspondence should be addressed. Tel.: +86 13770750595;
E-mail address: luxiaohui945@hhu.edu.cn.

MATERIALS AND METHODS

Experimental Site and Measurements

A wastewater irrigation experiment was conducted at the water environment test site of the Department of Irrigation and Drainage Engineering of Wu Han University (30° 55' N, 114° 36' E), Hubei Province, China. The mean annual temperature at the site was 16.7–17.0°C. The average annual rainfall and evaporation were in the ranges 1140–1265 mm and 1437–1573 mm, respectively. The annual average wind speed was 2.7 m/s.

Air temperature, relative humidity, radiation, wind speed and daily weather conditions (e.g., rainfall) were collected from the meteorological station of Wu Han University and then transmitted using WeatherLink equipment and software. Drying density measurements, grain-size analysis experiments and double-ring infiltration experiments were performed in the proving ground test pit to measure the physical properties of the soil.

Lysimeters with pressure gauge probes, time-domain reflectometer (TDR) probes to measure soil moisture and temperature probes were installed at different locations on the study site. Some pepper plants were cultivated in the lysimeters for the experiments. The TDR and temperature probes were used for the hourly determination of volume moisture content and soil temperature, respectively, at depths of 10, 25, 40, 55 and 70 cm. A negative pressure meter probe was applied to monitor the soil matric potential, which was calculated using the equation

$$h = 12.6h_{\text{Hg}} + h_x + (h_0 - h_z) \quad (1)$$

where h is the matrix potential (cm), h_{Hg} is the height of the mercury column (cm), h_x is the revised capillary height of the capillary tube (set at 7.4 cm), h_0 is the height from the ground to the mercury surface (cm) and h_z is the burial depth of the ceramic head (cm).

The wastewater was raw domestic sewage, it was

slightly alkaline (pH 8.4), marginally sodic and its salinity hazard was considered to be medium to high. The soil was Arenosol (silicious sand, Typic Udipsamment). Apart from some residual roots within a depth of 20 cm, there was no visible heterogeneity in the sandy soil. The natural groundwater table was deeper than 5 m. After photographing dye stained patterns of soil layers, undisturbed soil samples of 100 cm³ were collected at depths of 0–10, 10–20, 20–50 and 50–100 cm. The samples were used to measure soil properties, including soil texture, bulk density, porosity and saturated soil hydraulic conductivity.

According to the watering requirements of pepper, two irrigations were conducted (on July 9 and 17, 2013) during the whole observation period (July 8 to 27, 2013). The total irrigation quantity was 480 L, which was divided equally into two irrigations lasting for 3 h each. For each wastewater irrigation process, the concentrations of ammonium nitrogen (NH₄-N) and nitrate nitrogen (NO₃-N) in the applied wastewater were determined using a dual channel continuous-flow colorimetric analyzer (ChemLab Instruments Ltd.) and subsequently converted into the nitrogen amount added to the model (Table 1). The concentrations of NH₄-N and NO₃-N in the soil and soil water were tested at depths of 10, 25, 40 and 55 cm.

Pepper Root Distribution Characteristics Data

The pepper root distribution characteristics data were studied by measuring the root depth, total root surface area, root volume and root average diameter at different pepper growth stages using a WinRHIZO Pro 2008 root scanner (Germany). The scanned images were analyzed using WinRHIZO software (shown in Table 2).

Numerical Modeling of the Experiment

The HYDRUS-1D model was developed by Šimůnek *et al.* [10] for the simulation of water, heat and solutes in 1D variably saturated porous media.

Table 1. Application of Nitrogen Content during Irrigation Regime.

Date	Irrigation Amount (L)	Item	Concentration (mg/L)	Total Amount of Nitrogen Applied (mg total)	Amount of Nitrogen Applied per Unit Soil (mg/cm ²)
July 9	240	NH ₄ -N	18.05	4332	1.08 × 10 ⁻¹
		NO ₃ -N	0.27	64.8	1.60 × 10 ⁻³
July 17	240	NH ₄ -N	24.19	5805.6	1.45 × 10 ⁻¹
		NO ₃ -N	0.26	62.4	1.60 × 10 ⁻³

Table 2. Pepper Root Distribution Characteristic Data.

Number of Days	Number of Hours	Root Area (cm ²)	Root Width (cm)	Root Depth (cm)	Root Length (cm)	Total Root Surface Area (cm ²)	Total Root Projection Area (cm ²)	Total Root Volume (cm ³)	Root Average Diameter
70	1680	28.121	3.567	7.885	105.154	18.988	6.044	0.273	0.575
90	2160	77.362	12.869	6.011	134.725	21.56	6.863	0.275	0.509
110	2640	165.499	15.716	10.53	320.913	65.326	20.794	1.058	0.648
130	3120	343.225	18.098	18.968	266.332	69.027	21.972	1.424	0.825
160	3840	604.213	20.879	28.939	1174.717	229.18	72.95	3.558	0.621
190	4560	602.396	20.796	28.967	642.43	126.393	40.232	1.979	0.626

This model was applied in the present study to simulate heat and water movement and nitrogen transport while considering the water uptake of the pepper root.

Pepper plant growth was measured during the wastewater irrigation experiment, and pepper root water and nitrogen uptake were taken into account in the simulation model. The root system growth model and root water and nitrogen uptake model were thus developed.

Initial and Boundary Conditions

For 1D unsaturated soil water transport in this experiment, the upper and lower boundaries denote the flow boundary and variable pressure head boundary, respectively, as given in the following equations:

$$h(z, 0) = h_0(z) \quad (2)$$

$$-K(\theta) \left(\frac{\partial h}{\partial z} + 1 \right) \Big|_{z=0} = q_0(t) \quad (3)$$

where θ is the volumetric water content [-], h is the pressure head [L], z is the vertical coordinate [L] (assumed to be zero at the soil surface and directed upward), t is the time [T], K is the unsaturated hydraulic conductivity [L T⁻¹], $h_0(z)$ is the initial condition and $q_0(t)$ is the fluid flux across the soil surface boundary [L T⁻¹].

In the soil heat transport module, the temperature boundary conditions were chosen as the upper and lower temperature boundaries. Moreover, the measured values of the soil temperature and soil volume water content at 00:00 on July 8 (i.e., the starting point of the simulation period) were entered into the model as the initial conditions for the soil heat and water transport.

For solute transport in this model, the concentration flux boundary condition was selected according to the wastewater irrigation experiment conditions. The fertilizer application amount was reflected in the product

of the nitrogen concentration and water flux through the upper boundary determined by the differences between the rainfall, evaporation and irrigation supplies. The zero gradient condition was used as the lower boundary. Given the complication of the nitrogen transport and transformation processes, the mineralization of the organic nitrogen in the soil and the soil particle uptake of NO₃-N were ignored in the model development. The nitrification of NH₄-N and the denitrification of NO₃-N were aligned with the first-order kinetics reaction [11]. According to the chemical analysis results before the simulation period, the initial values of the NO₃-N and NH₄-N concentrations were obtained using a linear interpolation method for each node of the soil profile.

Model Parameters

Evapotranspiration rate, soil hydraulic and thermal properties, and solute transport parameters are required to solve the above mathematical model.

Evapotranspiration

In this study, the evapotranspiration rate, ET₀ (mm/d), was calculated using the Penman–Monteith combination equation [11]:

$$ET_0 = \frac{0.408 \cdot \Delta \cdot (R_n - G) + \frac{900}{T + 273} \cdot \gamma \cdot u_2 \cdot (e_a - e_d)}{\Delta + \gamma \cdot (1 + 0.34u_2)} \quad (4)$$

where R_n is the net solar radiation (J/m²/d), G is the soil heat flux (J/m²/d), e_a is the saturation water vapor pressure at the mean air temperature (kPa), e_d is the mean actual vapor pressure (kPa), T is the temperature (°C), Δ is the slope of the saturation vapor pressure (kPa/°C), γ is the psychrometric constant (kPa/°C) and u_2 is the wind speed at a height of 2 m (m/s).

Table 3. Soil Characteristics Data.

Depth (cm)	θ_r	θ_s	α	n	K_s	l
0–10	0.0956	0.4679	0.0117	1.3863	0.242083	0.5
10–50	0.0934	0.4496	0.0117	1.3802	0.17625	0.5
50–230	0.09	0.4238	0.0117	1.3536	0.108333	0.5

θ is the volumetric water content (–), θ_r and θ_s are the residual and saturated water contents (–), respectively, and α and n are empirical parameters determined by soil properties.

Soil Characteristics Data

Soil water characteristic curves represent the relationship between the soil matric potential and soil water content. In the present study, indoor measurements and field calibration values were combined to obtain soil water characteristic curves. In the field, a negative pressure meter probe and a TDR probe were used to monitor the soil matric potential and soil volumetric water content, respectively. Indoors, the measured results were fitted to the characteristic curve empirical equation with the RETC software [11]. The empirical equation can be expressed as:

$$\theta(h) = \begin{cases} \theta_r + \frac{\theta_s - \theta_r}{[1 + |\alpha h|^n]^m} & h > 0 \\ \theta_s & h \geq 0 \end{cases} \quad (5)$$

where θ is the volumetric water content (–), θ_r and θ_s are the residual and saturated water contents (–), respectively, h is the soil water pressure head (cm), and α , m and n are empirical parameters determined by the soil properties, with $m = 1 - 1/n$.

The good fit of the results indicates that the van Genuchten equation can adequately describe the measured soil water characteristic curve. The corresponding soil hydraulic properties of the soil profile are presented in Table 3.

RESULTS AND DISCUSSION

The numerically modeled water flow plays an important role in evaluating the physical processes that govern soil water and root nitrogen uptake transport between the soil and the atmosphere, because water movement is often an important part of the total flux since it controls the partitioning of the available energy into latent and sensible heat fluxes into the atmosphere. In addition, biological processes such as soil microbial activity and plant growth depend on the moisture and temperature status in the vadose zone, which are main-

ly influenced by the water movement. The HYDRUS-1D code was used to produce hourly profiles of the isothermal and non-isothermal liquid water fluxes, water vapor fluxes and soil temperatures from July 8 to 27, 2013.

Simulation Results

In this section, the measured water contents, soil temperature data and nitrogen concentrations during the simulation period (July 8 to 27, 2013) are compared with those calculated using the modified HYDRUS-1D code, which refers to the coupled liquid water, water vapor and heat transport in the soil. Moreover, an inverse solution was performed for the soil profile. A fitting analysis of the simulated and measured values was performed by modifying the soil hydraulic and thermal parameters. When the error (E) reached the standard value, we assumed that the current parameters can reasonably represent the parameters of the simulated soil layers. The objective function of the fitting can be expressed as follows:

$$E = \sum_{i=1}^m \sum_{j=1}^n W_j (\theta_{ij}^e - \theta_{ij}^0)^2,$$

where m is the total number of hours, n is the total number of observation holes, W_j is the weight coefficient, and θ_{ij}^e and θ_{ij}^0 denote the calculated and measured soil water content, temperature and nitrogen concentration of the observed point j at time i , respectively.

To evaluate the calibration and validation, we used the following performance criteria:

$$\text{RMSE} = \sqrt{\frac{1}{N} \sum_{i=1}^N (s_i - o_i)^2},$$

where RMSE represents the root mean square error, N is the number of observations, and s_i and o_i are the estimated and measured values, respectively.

The RMSEs of the temperature at depths of 10, 25, 40, 55 and 70 cm were 0.01, 0.012, 0.019, 0.012 and 0.075, respectively. The simulated and measured temperatures generally agreed at all five depths and both showed typical sinusoidal diurnal variation, with a maximum absolute deviation of 5.794°C at a 25 cm depth.

There is a discrepancy between the observed and simulated water contents. The RMSEs of the water content at depths of 10, 25, 40, 55 and 70 cm were 0.001, 0.0081, 0.0083, 0.0011 and 0.0098, respective-

ly. At 10 cm depth, the simulated water content follows the general trend of observation, while at 25 cm depth, the simulation shows a decreasing trend instead of the variation that the measurement has. However, apart from the poor fit of the simulation to the trend in the water content variation at 25 cm depth, the mean of the simulated water content is close to that of the measurements.

Root Water Uptake Rule of Pepper

A solute transport module was added to the water-heat coupling model to study the pepper root nitrogen uptake. A numerical simulation was conducted by using the established model, and the analysis results can be concluded as follows.

A comparison of the results of the pepper root uptake rate of $\text{NH}_4\text{-N}$ and $\text{NO}_3\text{-N}$ (Figure 1) shows that the uptake rate of $\text{NO}_3\text{-N}$ is an order of magnitude higher than that of $\text{NH}_4\text{-N}$, suggesting that the pepper root absorbs more $\text{NO}_3\text{-N}$ than $\text{NH}_4\text{-N}$. The performances of the pepper root uptakes of $\text{NH}_4\text{-N}$ and $\text{NO}_3\text{-N}$ in the soil conform to those of most plants [11]. Furthermore, a comparison of the two curves in Figure 1 shows that the changes of the pepper root uptake of water and nitrogen (referred to as $\text{NO}_3\text{-N}$) are similar during the whole simulation period.

Figure 1 shows that the root uptake rate of $\text{NO}_3\text{-N}$ on July 8 was high (approximately 1.86×10^{-4} $\text{mg}/\text{cm}^2\text{h}$). However, given that the first wastewater irrigation was applied on July 9, the maximum value of the root $\text{NO}_3\text{-N}$ uptake rate was only 1.19×10^{-4} $\text{mg}/(\text{cm}^2\cdot\text{h})$. After the second wastewater irrigation was applied on July 17, the root uptake rate of

$\text{NO}_3\text{-N}$ further decreased. This finding shows that when the original $\text{NO}_3\text{-N}$ content in the soil is relatively high, additional wastewater irrigation will not increase the root uptake of $\text{NO}_3\text{-N}$, while a decrease in the root uptake of $\text{NO}_3\text{-N}$ will probably cause groundwater nitrogen contamination through wastewater irrigation because of the $\text{NO}_3\text{-N}$ leaching effect. During the first irrigation (containing nitrate), the plants took up excess nitrate, which is known as “luxury nitrate uptake” [12]. Such luxury nitrate would have been stored in the vacuole and used if and when necessary. As the endogenous nitrate was high, there was little need for the plants to take up more at the second irrigation, particularly as the nitrate uptake requires active transporters.

Therefore, determining the nitrogen content in the soil on a regular basis, the biomass and the total nitrogen of the plant for calculation of the nitrogen use efficiency of the crop and formulating scientific and reasonable wastewater irrigation schemes are important.

Figure 1 shows that the variation regularities of the root uptake rates of $\text{NH}_4\text{-N}$ and $\text{NO}_3\text{-N}$ are similar. However, the absorption rate of $\text{NO}_3\text{-N}$ is an order of magnitude higher than that of $\text{NH}_4\text{-N}$, and the present results revealed that pepper roots had a much greater uptake of $\text{NO}_3\text{-N}$ than of $\text{NH}_4\text{-N}$. The uptake of $\text{NO}_3\text{-N}$ was dominant, as reported elsewhere for ryegrass on a daily basis [13], and oscillated diurnally with a greater amplitude than that for $\text{NH}_4\text{-N}$, although both ions showed progressive increases in uptake rate during the light period, and were approximately synchronous with respect to the timing of the maximum and minimum rates of uptake. It has been indicated that $\text{NH}_4\text{-N}$ is inhibited in the presence of $\text{NO}_3\text{-N}$, but $\text{NO}_3\text{-N}$ is stimulated by $\text{NH}_4\text{-N}$ [13]. This may be ex-

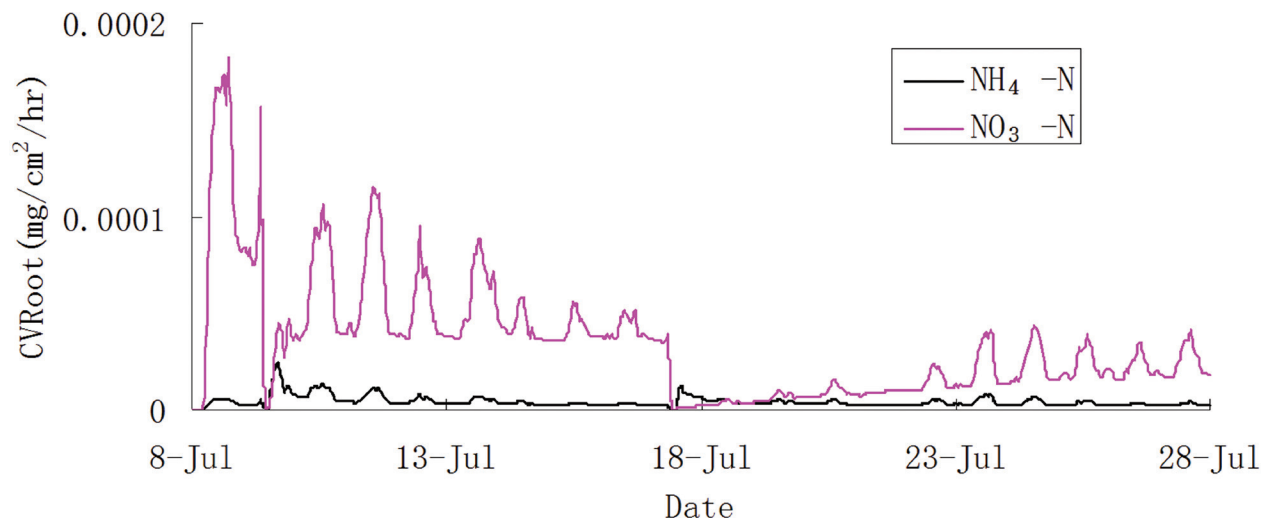


Figure 1. Comparison of pepper root uptake rates of $\text{NH}_4\text{-N}$ and $\text{NO}_3\text{-N}$.

plained in terms of allosteric regulation by cytoplasmic concentrations of $\text{NH}_4^+\text{-N}$, given that the obligate assimilation of $\text{NH}_4^+\text{-N}$ in the roots may have become limited by the availability of carbohydrates, although this requires experimental verification.

The pepper root nitrogen uptake rate curve only has peaks without any obvious troughs. The nitrogen uptake rates exhibit low levels each day before 07:00. Thereafter, the pepper root water uptake rates gradually increase with increasing light intensity and air temperature. The root nitrogen uptake rate reaches a maximum between the times of 12:00 and 15:00. The root nitrogen uptake rate then gradually decreases to the same level as that before 07:00. The root nitrogen uptake rate then remains at a low level during the whole nighttime period. The diurnal variation of the root nitrogen uptake rate therefore appears as a single-peak curve.

The proposed subsurface modeling approach substantially improves the scenario testing for soil–plant systems by including plant uptake mechanisms, such as the pepper root uptake rate of nitrogen and the diurnal variation regularity of the root nutrient uptake. The results show that the pepper root water uptake rates gradually increase with increasing light intensity and air temperature. An alternative hypothesis is that diurnal changes in $\text{NH}_4\text{-N}$ and $\text{NO}_3\text{-N}$ uptakes are primarily dependent upon varying the 'sink-strength' for nitrogen caused by diurnal fluctuations in growth rate, specifically in leaf expansion. Leaf elongation rates exhibit marked diurnal rhythms, depending on the temperature and light conditions, amongst other factors, although there is wide variation between species. It is generally accepted that $\text{NO}_3\text{-N}$ and $\text{NH}_4\text{-N}$ uptakes are higher in light than in darkness [14].

CONCLUSION

In conclusion, the pepper root adsorbed more $\text{NO}_3\text{-N}$ than $\text{NH}_4\text{-N}$. During the first exposure to irrigation (containing nitrate), the plants took up excess nitrate, which would have been stored in the vacuole and used if and when necessary. As the endogenous nitrate was high, there was little need for the plants to take up more at the second irrigation, particularly as nitrate uptake requires active transporters. The root nitrogen uptake rate reached a maximum between the times of 12:00 and 15:00. The root nitrogen uptake rate then gradually decreased to the same level as that before 07:00. The root nitrogen uptake rate then remained at a low level during the whole nighttime period. The pep-

per root water uptake rates gradually increased with increasing light intensity and air temperature. The diurnal variation of the root nitrogen uptake rates was therefore a single-peak curve. This study indicates that measuring the biomass and total nitrogen of the plant for calculation of the nitrogen use efficiency of the crop should be future work.

ACKNOWLEDGEMENTS

The study was financially supported by the Open Research Fund Program of the Ministry of Education Key Laboratory of Integrated Regulation and Resource Development on Shallow Lakes, Open Research Fund Program of State Key Laboratory of Water Resources and Hydropower Engineering Science(2011B081) and "The National Natural Science Funds" (41202172). We gratefully acknowledge the reviewers (Professor M. Paula Watt and two anonymous reviewers) for their constructive comments and suggestions for the article.

REFERENCES

1. Jun, Y., Keqiang, Z., Qingheng, M., Zhiping, H. and Feng, W., Advances in research on nitrogen transportation regularity and models in sewage irrigation (in Chinese), *Chinese Agricultural Sci. Bull.*, Vol. 24, No. 3, 2008, pp. 374–378.
2. Butt, M. S., Sharif, K., Bajwa, B. E. and Aziz, A., Hazardous effect of sewage water on the environment: irrigated with wastewater, *Plant Soil*, Vol. 261, No. 1, 2005, pp. 189–196.
3. Gheysari, M., Mirlatifi, S. M., Homae, M., Asadi, M. S. and Hoogenboom, G., Nitrate leaching in a silage maize field under different irrigation and nitrogen fertilizer rates, *Agricultural Water Management*, Vol. 96, 2009, pp. 946–954. <http://dx.doi.org/10.1016/j.agwat.2009.01.005>
4. Wang, H., Ju, X., Wei, Y., Li, B., Zhao, L. and Hu, K., Simulation of bromide and nitrate leaching under heavy rainfall and high-intensity irrigation rates in North China Plain, *Agricultural Water Management*, Vol. 97, 2010, pp. 1646–1654. <http://dx.doi.org/10.1016/j.agwat.2010.05.022>
5. Tafteh, A. and Sepaskhah, A. R., Application of HYDRUS-1D model for simulating water and nitrate leaching from continuous and alternate furrow irrigated rapeseed and maize fields, *Agricultural Water Management*, Vol. 113, 2012, pp. 19–29. <http://dx.doi.org/10.1016/j.agwat.2012.06.011>
6. Blumenthal, U. J. and Peasey, A. 2002. Critical Review of Epidemiological Evidence of the Health Effects of Wastewater and Excreta Use in Agriculture. World Health Organization.
7. Chen, Z. J., and Zhou, J., Application of treated wastewater on agriculture in Israel (in Chinese), *Agro-environmental Protection*, Vol. 20, No. 6, 2001, pp. 462–464.
8. Xuebin, Q., Juju, Q. and Xiangyang, F., Wastewater irrigation research status and progress at home and abroad, *China Rural Water Hydropower*, Vol. 1, 2006, pp. 13–15.
9. Ping, L., Hongbin, P. and Xuebin, Q., Effect of sewage irrigation on nitrogen of soil and groundwater in different groundwater depth (in Chinese), *J. Irrigation Drainage*, Vol. 6, 2007, pp. 1–5.
10. Šimůnek, J., Sejna, M., Saito, H., Sakai, M. and van Genuchten, M. T. 2008. The HYDRUS-1D Software Package for Simulating the One-dimensional Movement of Water, Heat, and Multiple Solutes in Variable-saturated Media. Department of Environmental Sciences, University of California Riverside.

11. Liu, S., Yang, J. Y., Zhang, X. Y., Druryb, C. F., Reynoldsb, W. D. and Hoogenboomd, G., Modeling crop yield, soil water content and soil temperature for a soybean–maize rotation under conventional and conservation tillage systems in Northeast China, *Agricultural Water Management*, Vol. 123, 2013, pp. 32–44. <http://dx.doi.org/10.1016/j.agwat.2013.03.001>
12. Ruffel, S., Gojon, A. and Lejay, L., Signal interactions in the regulation of root nitrate uptake, *J. Experimental Botany*, Vol. 65, No. 19, 2014, pp. 5509–5517. <http://dx.doi.org/10.1093/jxb/eru321>
13. Clarkson, D. T., Hopper, M. J. and Jones, L. H. P., The effect of root temperature on the uptake of nitrogen and the relative size of the root system in *Lolium perenne*. I. Solutions containing both NH_4^+ and NO_3^- , *Plant, Cell and Environment*, Vol. 9, 1986, pp. 535–545.
14. Kupper, P., Rohula, G., Saksing, L., Sellin, A., Löhmus, K., Ostonen, I., Helmisaari, H. -S. and Söber, A., Does soil nutrient availability influence night-time water flux of aspen saplings?, *Environmental and Experimental Botany*, Vol. 82, 2012, pp. 37–42. <http://dx.doi.org/10.1016/j.envexpbot.2012.03.013>

The Research of Corrected First Order Kinetics on Hydrolysis and Biogas Generation in Batch Anaerobic Digestion

LEI FENG, HONGLI KOU, XUDONG ZHANG and RUNDONG LI*

Liaoning Province Clean Energy Key Laboratory, Shenyang Aerospace University, Shenyang Daoyi street No.37, 110136 Shenyang, China

ABSTRACT: Research on sequencing batch anaerobic digestion was performed for kitchen waste and its components at 37°C. Biogas production models of flat, cylindrical spherical particulates were proposed and analyzed for single component. It is shown that the hydrolysis of starches, celluloses, fats and proteins prefers to follow the model of cylindrical, spherical and flat particulates, respectively. Moreover, biogas production models of flat, cylindrical, spherical, and mixed particulates were proposed and analyzed for multi-component (kitchen waste). Biogas production models of flat and mixed particulates most closely match the actual situation before and after the 24th day, respectively.

INTRODUCTION

In the current economic and environmental context of sustainable management, anaerobic digestion is a significant process to manage wastes and produce energy. This process is all the more interesting that it can be applied to many different types of wastes. Which-ever the inputs, anaerobic digestion is a fermentation process divided into four main biochemical steps resulting from different specific microorganisms [1,2]. It is generally admitted that the limiting reaction is the hydrolysis, the kinetic being the slowest [2]. Anaerobic digestion (AD) is a biochemical process that produces energy in the form of biogas [3]. Biogas comprises of methane (CH₄) and carbon dioxide (CO₂), which is renewable and the replacement of fossil fuels [4].

Studies on mathematic model of anaerobic digestion producing CH₄ have been performed for a long time by scholars in many countries [5–7]. There are several models to assess the kinetics of anaerobic digestion of organic waste. The first-order model is the modest, which can compare the performance of AD under practical conditions [8]. On the contrary, Anaerobic Digestion Model No. 1 (ADM1) is the multifaceted model, which represents great complexity and includes an excessive number of parameters [9]. Such a complexity increases the precision of the model, but conversely produces practical complications as all the required data is not often collected [10].

Following the presence of model, some researches on complement and correction for it have been carried out successively [11–12]. Valentini and Borja et al argued that Monod equation is suitable for describing the hydrolysis of soluble organics but not for insoluble organics [13,14], and Contois model could not explain the effect of temperature on hydrolysis rate [15–17]. Particulate breakup model suggested that the particulates should be broken into smaller ones due to the hydrolysis, leading to the increasing specific surface area of particulates [18]. Some authors have made prediction of biogas production potential using modified Gompertz model [19–21]. Wu, Zhang and Yang [22] proposed segmented hydrolysis kinetics model. In this model, the first segment corresponds to the diffusion of organic particulates with large size, and the second segment corresponds to the reaction rate when the size of organic particulates becomes small enough. It is believed that the hydrolysis is basically unrestricted from diffusion for kitchen waste with a size of 10 mm. Vavilin proposed hydrolysis rate equation for particulates with different shapes [23]. This equation is consistent with corrected first order model proposed by Liu [24].

In this work, corrected first order model including models of flat particulates, cylindrical particulates and spherical particulates was used to simulate sequencing batch anaerobic digestion for single component and mixed kitchen waste without considering diffusion and mass transfer, and the kinetics model of kitchen waste was studied on the basis of fitting hydrolysis and biogas generation.

*Author to whom correspondence should be addressed.
Email: fl_iceee@163.com

Table 1. The Hydrolysis Conclusions of Flat Particulates, Cylindrical Particulates and Spherical Particulates.

Flat Particulates Model	Cylindrical Particulates Model	Spherical Particulates Model
$c = c_0 e^{-kt}$	$c = c_0 \left(\frac{1}{2} kt + 1 \right)^{-2}$	$c = c_0 \left(\frac{2}{3} kt + 1 \right)^{-3/2}$
$\frac{dc}{dt} = -kc$	$\frac{dc}{dt} = -k \frac{c^{3/2}}{c_0^{1/2}}$	$\frac{dc}{dt} = -k \frac{c^{5/3}}{c_0^{2/3}}$

ESTABLISHMENT OF MODEL

Establishment of Biogas Production Kinetics Model for Single Component

For deducing the model, the following assumptions are made [24]:

1. The solid particulates could be simplified to soluble organics and insoluble solid skeleton, and the volume of soluble organics decreases with hydrolysis.
2. The organics in solid particulates are dispersed uniformly, and the dissolution of particulate organics carries out gradually from outside to inside during hydrolysis. And the lysates of water and particulate organics could penetrate freely the hydrolysed solid skeleton outside, i.e. ignoring the mass transfer resistance of hydrolyses from solid skeleton.
3. The organic particulates would not be broken during hydrolysis, and the surface area increase coefficient ψ between organic particulates and water is constant.
4. The shapes remain during hydrolysis, and undissolved organics per unit volume are dispersed uniformly with a concentration density of ρ .

For the hydrolysis of flat particulates, cylindrical particulates and spherical particulates, conclusions are obtained as following in Table 1.

In this paper, we reference first order hydrolysis model to express hydrolysis degree of substrate with accumulated biogas production. Some researches showed that biogas production rate of biological waste anaerobic digestion is proportional to degradation rate of organics. For sequencing batch anaerobic digestion, G_0 (initial accumulated biogas production) for the initial reaction is zero, so

$$G = \alpha(c_0 - c) \quad (1)$$

The α value is 395.22, 229.26, 465.77 and 354.46 for single component starches, celluloses, fats, and proteins, respectively.

The hydrolysis conclusions of flat particulates, cylindrical particulates and spherical particulates were introduced into Equation (1). Thus, corresponding biogas production models are expressed as following:

$$G = \alpha c_0 (1 - e^{-kt}) \quad (2)$$

$$G = \alpha c_0 \left[1 - \left(\frac{1}{2} kt + 1 \right)^{-2} \right] \quad (3)$$

$$G = \alpha c_0 \left[1 - \left(\frac{2}{3} kt + 1 \right)^{-3/2} \right] \quad (4)$$

Where

- G = accumulated biogas production at t time with the unit of mL
- c = concentration of volatile solid, g VS
- c_0 = initial concentration of volatile solid, g VS
- α = biogas conversion of volatiles with the unit of mL·g⁻¹VS
- k = hydrolysis rate constant, d⁻¹

Equation (2), (3), and (4) is the biogas production model of single component flat particulates, cylindrical particulates and spherical particulates, respectively.

Establishment of Biogas Production Kinetics Model for Mixed Kitchen Waste

To well study digestive characteristics of starches, celluloses, fats, and proteins in mixed system, the mixed kitchen waste was divided carefully according to initial VS content and biogas potential of the components, thus establishing multicomponent biogas production model for flat particulates, cylindrical particulates and spherical particulates. The models are expressed as following:

$$G = \sum_{i=1}^4 a_i \alpha_i c_{0i} (1 - e^{-k_i t}) \quad (5)$$

$$G = \sum_{i=1}^4 a_i \alpha_i c_{0i} \left[1 - \left(\frac{1}{2} k_i t + 1 \right)^{-2} \right] \quad (6)$$

$$G = \sum_{i=1}^4 a_i \alpha_i c_{0i} \left[1 - \left(\frac{2}{3} k_i t + 1 \right)^{-3/2} \right] \quad (7)$$

In the above equations, a_i is the actual proportion of starches, celluloses, fats, and proteins, respectively, α_i is biogas conversion with the unit of $\text{mL} \cdot \text{g}^{-1} \text{VS}$, c_{0i} is initial concentration of volatile solid with the unit of g VS , k_i is hydrolysis constant with the unit of d^{-1} , and $i = 1, 2, 3, 4$ is the parameters of starches, celluloses, fats, and proteins, respectively.

Equation (5), (6), and (7) is the biogas production model of multicomponent flat particulates, cylindrical particulates and spherical particulates, respectively.

RAW MATERIALS AND METHOD

Raw Materials and Their Properties

50 g of rice, lettuce, fats filling, and egg whites was selected as fermentation material for starches, celluloses, fats, and proteins, respectively, in the single component digestion test.

The life waste from Northern Hospital community in Shenyang was selected as mixed kitchen waste. The separated kitchen waste was composed of proteins (20 wt%), starches (19.3 wt%), celluloses (31.9 wt%) and fats (28.8 wt%). The kitchen waste was cut into particulates with a diameter of 10 mm by a cutter. The mid-temperature domesticated inoculation sludge was obtained from waste water treatment plant in north Shenyang. The parameters of single component waste materials were listed in Table 2.

Experimental Apparatus

The experimental apparatus contained self-designed anaerobic fermentation reactor was acted as the reactor. Two wild-mouth bottles (1L) were acted as gas collecting bottle and water collecting bottle, respectively, whose bottlenecks were sealed with rubber stopper and sealants. The bottles were connected with glass tubes

and anti-aging treated emulsion pipe. This apparatus must have good airtightness and anaerobic environment. The thermostat water bath was use to heat digestion tank.

Experimental Method and Devices

For single component experiment, the mixture of 50 g dried fermentation material and 300 ml sludge was mixed with 50 g of rice, lettuce, fats filling, and egg whites, respectively. The mixed kitchen waste was cut into particulates with a diameter of 10 mm by a cutter. 15 parallel samples were set in every test, and every fermentation cylinder was added 50 g dried kitchen waste and 300 ml sludge.

The fermentation cylinder was metered volume to 1 L, and was cultured at 37°C for 30 days in thermostat water bath. The fermentation parameters were tested once a day initially and once every 2 days after 4 days, biogas production was recorded at the same time interval. Since first order kinetics have no lag phase time, accumulated biogas production was fitted for mixed kitchen waste after the 10th experiment day when the biogas production has been recovered, while the data of whole experimental period was given to illustrate the single component hydrolysis process in the round.

Drying method at 103–105°C and 600°C was used to determine TS and VS, respectively. The pH was determined by pH meter, and the biogas was collected by drainage.

KINETICS FITTING OF ACCUMULATED BIOGAS PRODUCTION FOR SINGLE COMPONENT

The single component accumulated biogas production was fitted by biogas production model of single component flat particulates, cylindrical particulates and spherical particulates, respectively. The fitting on accumulated biogas production was shown in Figure 1, and its parameters were listed in Table 3. The constant k shows that proteins and starches have a higher hydrolysis rate; celluloses have a low hydrolysis rate, while fats have a lowest hydrolysis rate. The fitting coefficients of starches and celluloses are over 0.90, suggesting good correlation. Only fats and proteins show poor correlation. The hydrolysis of starches, celluloses, fats and proteins prefers to follow the model of cylindrical particulates, spherical particulates, and flat particulates, respectively.

Table 2. The Characteristic Parameters of Test Materials

Single Component	TS/g	VS/g
Starch	18.9	6.73
Cellulose	12.1	5.63
Fat	47.38	29.78
Protein	40.83	16.23

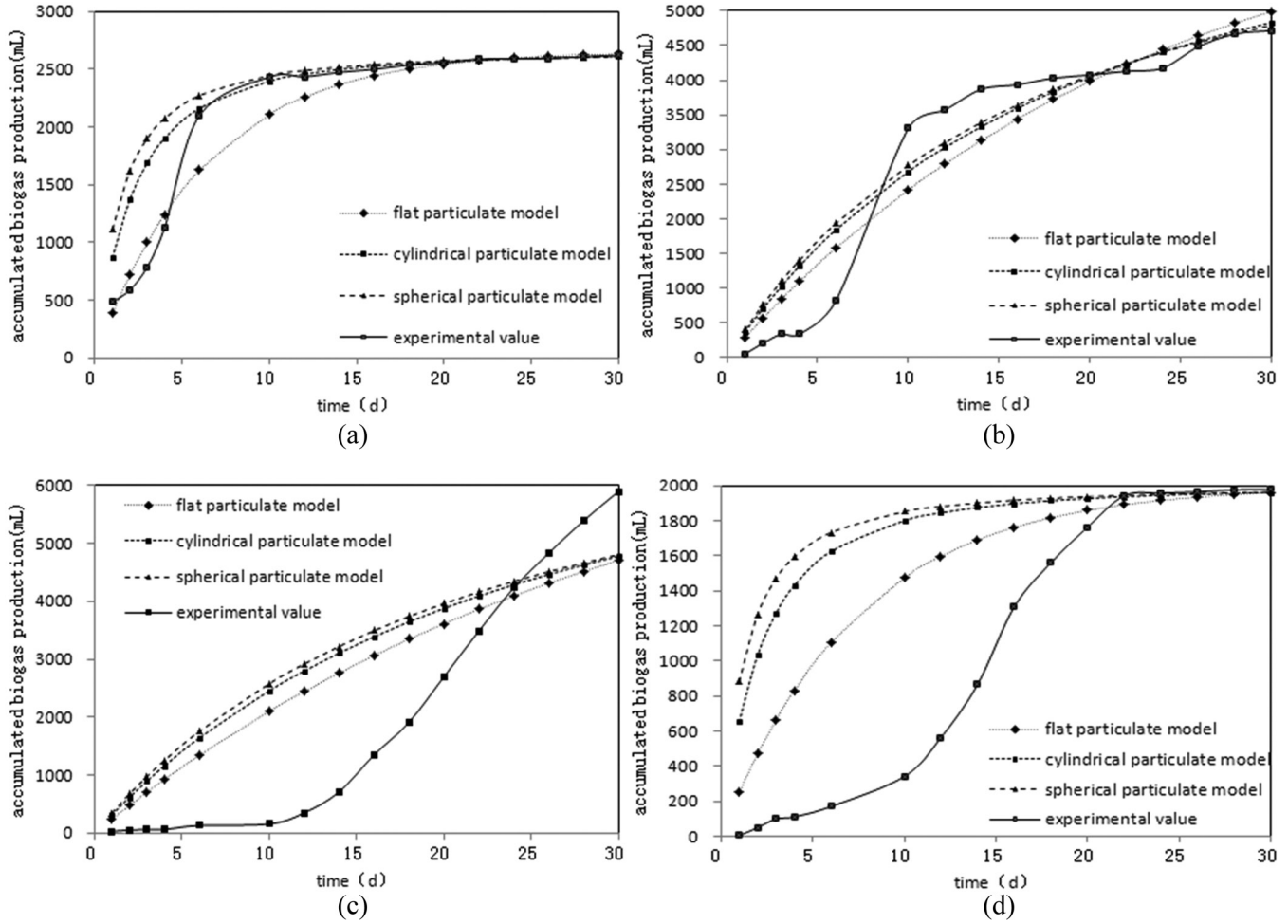


Figure 1. The comparison between actual biogas production and theoretical accumulated production under different model for various organics anaerobic digestion. (a) starch; (b) cellulose; (c) fat; and (d) protein.

KINETICS FITTING OF ACCUMULATED BIOGAS PRODUCTION FOR MIXED KITCHEN WASTE

As the above 4 kind of organics follow different models, biogas production model of multicomponent mixed particulates was established as following:

$$G = \left[\begin{aligned} & a_1\alpha_1c_{01} \left[1 - \left(\frac{1}{2}k_1 + 1 \right)^{-2} \right] \\ & + a_2\alpha_2c_{02} \left[1 - \left(\frac{2}{3}k_2 + 1 \right)^{-3/2} \right] \\ & + a_3\alpha_3c_{03}(1 - e^{-k_3t}) + a_4\alpha_4c_{04}(1 - e^{-k_4t}) \end{aligned} \right]$$

In this part, biogas production model of multicom-

ponent flat particulates, cylindrical particulates, spherical particulates and mixed particulates can be reduced to flat particulates model, cylindrical particulates model, spherical particulates model and mixed particulates model, respectively.

Table 2. The Fitting Parameters of Single Component Accumulated Biogas Production.

Model		Flat Particulates Model	Cylindrical Particulates Model	Spherical Particulates Model
Starch	R ²	0.9153	0.9742	0.9429
	k(1/d)	0.1575	0.4374	0.6549
Cellulose	R ²	0.9057	0.9340	0.9412
	k(1/d)	0.0438	0.0567	0.0621
Fat	R ²	0.7125	0.6495	0.6268
	k(1/d)	0.0325	0.0433	0.0480
Protein	R ²	0.7981	0.6575	0.6137
	k(1/d)	0.1341	0.4382	0.7123

The value fitted by the flat particulates model, cylindrical particulates model, spherical particulates model and mixed particulates model was compared with actual biogas production from sequencing batch mixed kitchen waste. As shown in Figure 2(a), the simulated biogas production is higher than the actual production for all models. Figure 2(a) and Figure 2(b) showed that the simulated production from flat particulates model closes to actual production between from the 10th day to the 22nd day, the simulated production from mixed particulates model closes to actual production from the 24th day to the 30th day. We could observe the exceeded percentages between the simulated biogas production from different models and actual production during anaerobic digestion [Figure 2(c)]. It can be seen that the exceeded percentages generally decrease and then increase, and reach their minimums of 5%, 8%, 8% and 5%, respectively, on the 20th day and 22nd

day. The maximum exceeded percentage is 37% on the 10th day from spherical particulates model and 19% on the 30th day from flat particulates model, respectively. The minimum exceeded percentage is 15% on the 10th day from flat particulates model and 17% on the 30th day from mixed particulates model and spherical particulates model, respectively. The cylindrical particulates model exhibited an exceeded percentage of 18% on the 30th day. And the two models exhibited almost the same exceeded percentage since the 20th day. Based on the above analysis, we could conclude that flat particulates model and mixed particulates model most closely match the actual situation before and after the 24th day, respectively. This is not consistent with corrected first order cylindrical particulates model proposed by Liu [24], probably owing to the higher content of proteins and fats in our experiment.

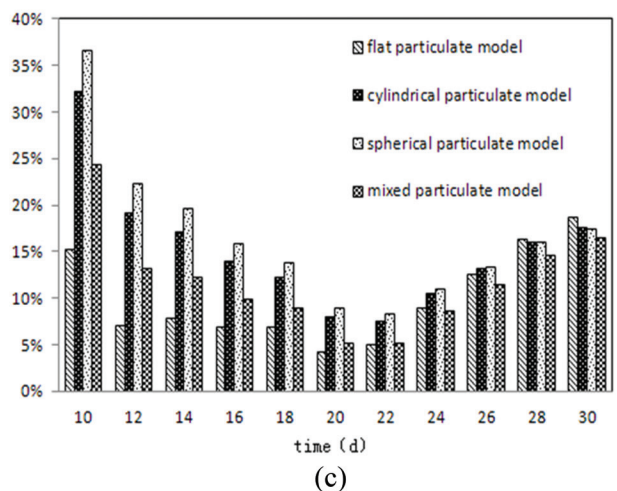
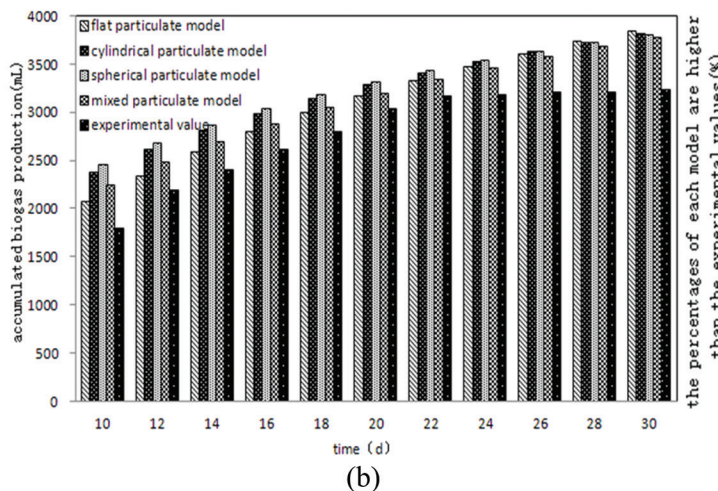
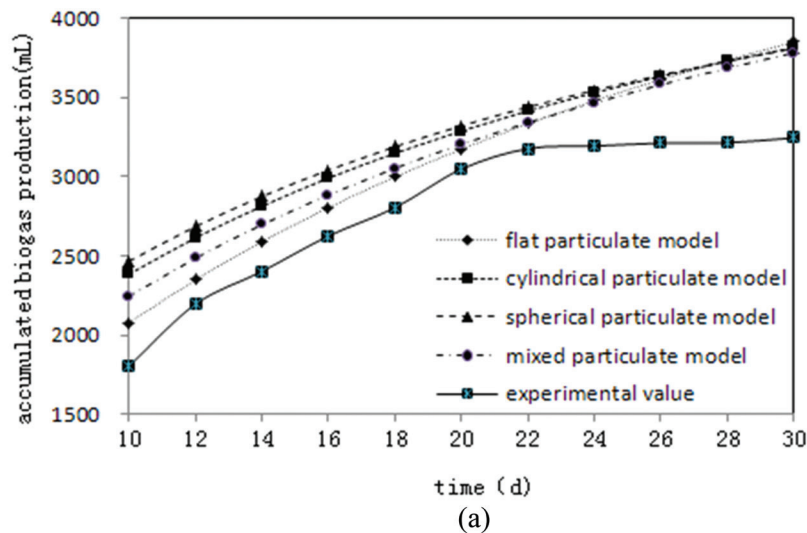


Figure 2. The comparison between accumulated biogas production under different models and actual production for anaerobic digestion from kitchen waste.

CONCLUSIONS

1. For hydrolysis and biogas production for single component, proteins and starches exhibit higher rate, celluloses exhibit low rate, and fats exhibit lowest rate. The actual biogas production of starches is close to simulated one of cylindrical particulates model and spherical particulates model, while is closer to the former with a R^2 of 0.9742 and a k of 0.4374 d^{-1} . The actual biogas production of celluloses is close to simulated one of cylindrical particulates model and spherical particulates model, while is closer to the latter with a R^2 of 0.9412 and a k of 0.0621 d^{-1} . The actual biogas production of fats and proteins is close to simulated one of first order kinetics model with a R^2 of 0.7125 and a k of 0.0325 d^{-1} for fats and a R^2 of 0.7981 and a k of 0.1341 d^{-1} for proteins.
2. Biogas production model of single component flat particulates, cylindrical particulates and spherical particulates are expressed as following:

$$G = \alpha c_0 (1 - e^{-kt})$$

$$G = \alpha c_0 \left[1 - \left(\frac{1}{2} kt + 1 \right)^{-2} \right]$$

$$G = \alpha c_0 \left[1 - \left(\frac{2}{3} kt + 1 \right)^{-3/2} \right]$$

Biogas production model of multicomponent flat particulates, cylindrical particulates, spherical particulates and mixed particulates are expressed as following:

$$G = \sum_{i=1}^4 a_i \alpha_i c_{0i} (1 - e^{-k_i t})$$

$$G = \sum_{i=1}^4 a_i \alpha_i c_{0i} \left[1 - \left(\frac{1}{2} k_i t + 1 \right)^{-2} \right]$$

$$G = \sum_{i=1}^4 a_i \alpha_i c_{0i} \left[1 - \left(\frac{2}{3} k_i t + 1 \right)^{-3/2} \right]$$

$$G = \left[\begin{array}{l} a_1 \alpha_1 c_{01} \left[1 - \left(\frac{1}{2} k_1 + 1 \right)^{-2} \right] \\ + a_2 \alpha_2 c_{02} \left[1 - \left(\frac{2}{3} k_2 + 1 \right)^{-3/2} \right] \\ + a_3 \alpha_3 c_{03} (1 - e^{-k_3 t}) + a_4 \alpha_4 c_{04} (1 - e^{-k_4 t}) \end{array} \right]$$

3. For the whole biogas production process of mixed kitchen waste, biogas production model of flat particulates and mixed particulates most closely match the actual situation before and after the 24th day, respectively. However, the simulated biogas production from the four models is over the actual one.

ACKNOWLEDGEMENTS

This work was supported by the National science and technology support. (No. 2012BAC25B07)

REFERENCES

1. Pavlostathis, S.G., Giraldo-Gomez, E., "Kinetics of anaerobic treatment", *Water Science Technology*, Vol. 24, No. 8, 1991, pp. 35–59.
2. Frédéric, S., Lugardon, A., "Méthanisation des effluents liquides", *Techniques de l'Ingénieur*, 2007, pp. 3943.
3. Romano, R. T., R. Zhang, "Co-digestion of onion juice and wastewater sludge using anaerobic mixed biofilm reactor", *Bioresour. Technol.*, Vol. 99, 2008, pp. 631–637. <http://dx.doi.org/10.1016/j.biortech.2006.12.043>
4. Chynoweth, D.P., J.M., Owens, R. Legrand, "Renewable methane from anaerobic digestion of biomass", *Renewable Energy*, Vol. 22, 2011, pp. 1–8. [http://dx.doi.org/10.1016/S0960-1481\(00\)00019-7](http://dx.doi.org/10.1016/S0960-1481(00)00019-7)
5. Christensen T. H. 1996. *Landfill of waste: biogas*, London: E and FN-Spon.
6. Schumacher M. M. 1983. *Landfill methane recovery*, USA: New Jersey.
7. El-fadel M., Findikakis A. N., "A numerical model for methane production in managed sanitary landfills", *Waste Management and Research*, Vol. 7, No. 1, 1989, pp. 31–42. <http://dx.doi.org/10.1177/0734242X8900700105>
8. Rao, M. S. and S. P. Singh, "Bioenergy conversion studies of organic fraction of MSW: kinetic studies and gas yield-organic loading relationships for process optimization", *Bioresour. Technol.*, Vol. 95, pp. 173–185. <http://dx.doi.org/10.1016/j.biortech.2004.02.013>
9. Batstone, D. J., J. Keller, I. Angelidaki, S.V. Kalyuzhnyi, S.G. Pavlostathis, A. Rozzi, W.T.M. Sanders, H. Siegrist and V.A. Vavilin, 2002, *Anaerobic Digestion Model No.1 (ADM1)*, London, IWA Publishing.
10. Golkowska, K., N. Sibisi-Beierlein and M. Greger, "Kinetic Considerations on Thermophilic Digestion of Maize Silage at Different Feeding Modes", *Chemie Ingenieur Technik*, Vol. 84, No. 9, 2012, pp. 1551–1555. <http://dx.doi.org/10.1002/cite.201100242>
11. Fedorovich V., Lens P., Kalyuzhnyi S., et al. "Extension of anaerobic digestion model No.1 with processes of sulfate reduction", *Applied Biochemistry and Biotechnology*, Vol. 109, No. 1-3, 2003, pp. 33–45. <http://dx.doi.org/10.1385/ABAB:109:1-3:33>
12. Parker W. J., Wu G. H., "Modifying ADM1 to include formation and emission of odourants" [J]. *Water Science and Technology*, Vol. 54, No. 4, 2006, pp. 111–117. <http://dx.doi.org/10.2166/wst.2006.532>

13. Borja R., Martin A., Sanchez E., *et al.* "Kinetic modelling of the hydrolysis, acidogenic and methanogenic steps in the anaerobic digestion of two-phase olive pomace", *Process Biochemistry*, Vol. 40, 2005, pp. 1841–1847. <http://dx.doi.org/10.1016/j.procbio.2004.06.026>
14. Valentini A., Garuti G., Rozzi A., *et al.* "Anaerobic degradation kinetics of particulate organic matter: A new approach", *Water Science and Technology*, Vol. 36, No. 6-7, 1997, pp. 239–246. [http://dx.doi.org/10.1016/S0273-1223\(97\)00528-3](http://dx.doi.org/10.1016/S0273-1223(97)00528-3)
15. Fang H. H. P., Yu H., "Mesophilic acidification of gelatinaceous wastewater", *Journal of Biotechnology*, Vol. 93, No. 2, 2002, pp. 99–108. [http://dx.doi.org/10.1016/S0168-1656\(01\)00397-2](http://dx.doi.org/10.1016/S0168-1656(01)00397-2)
16. Yu H. Q., Fang H. H. P., "Acidogenic of gelatine-rich wastewater in an up flow anaerobic reactor: influence of pH and temperature", *Water Research*, Vol. 37, No. 1, 2003, pp. 55–66. [http://dx.doi.org/10.1016/S0043-1354\(02\)00256-7](http://dx.doi.org/10.1016/S0043-1354(02)00256-7)
17. Song Y. C., Kwon S. J., Woo J. H., "Mesophilic and thermophilic temperature co-phase anaerobic digestion compared with single-stage mesophilic-and thermophilic digestion of sewage sludge", *Water Research*, Vol. 38, 2004, pp. 1653–1662. <http://dx.doi.org/10.1016/j.watres.2003.12.019>
18. Dimock R., Morgenroth E., "The Influence of Particle Size on Microbial Hydrolysis of Protein Particles in Activated Sludge", *Water Res.*, Vol. 40, 2006, pp. 2064–2074. <http://dx.doi.org/10.1016/j.watres.2006.03.011>
19. Budiyo, I.N., J. Widiasta and S. Sunarso, "The kinetic of biogas production rate from cattle manure in batch mode". *Int. J. Chem. Biol. Eng.*, Vol. 3, No. 1, 2010, pp. 39–44.
20. Adiga, S., R. Ramya, B.B. Shankar, J.H. Patil and C.R. Geetha, "Kinetics of anaerobic digestion of water hyacinth, poultry litter, cow manure and primary sludge: A comparative study", *Proceeding of the 2nd International Conference on Biotechnology and Environment Management*, Vol. 14, 2012, pp. 73–78.
21. Patil, J.H., M.A. Raj, P.L. Muralidhara, S.M. Desai and G.K.M. Raju, "Kinetics of anaerobic digestion of water hyacinth using poultry litter as inoculum". *Int. J. Environ. Sci. Dev.*, Vol. 3, No. 2, 2012, pp. 94–98. <http://dx.doi.org/10.7763/IJESD.2012.V3.195>
22. Wu Y., Zhang D. J., Yang G., "The mechanism and kinetics of hydrolysis in the anaerobic digestion of kitchen wastes", *Acta Scientiae Circumstantiae*, Vol. 30, No. 1, 2010, pp. 142–147.
23. Vavilin V. A., Rytov S. V., Lokshina L. Y. "A description of hydrolysis kinetics in an aerobic degradation of particulate organic matter", *Bioresource Technol.*, Vol. 56, 1996, pp. 229–237. [http://dx.doi.org/10.1016/0960-8524\(96\)00034-X](http://dx.doi.org/10.1016/0960-8524(96)00034-X)
24. Liu G. T., Peng X. Y., Long T. R., *et al.*, "Improved hydrolysis kinetic model for batch anaerobic digestion of organic solid waste", *Acta Scientiae Circumstantiae*, Vol. 27, No. 7, 2007, pp. 1227–1232.

GUIDE TO AUTHORS

1. Manuscripts shall be sent electronically to the Editor-in-Chief, Dr. P. Brent Duncan at pduncan@unt.edu using Microsoft Word in an IBM/PC format. If electronic submission is not possible, three paper copies of double-spaced manuscripts may be sent to Dr. P. Brent Duncan, (Editor of the *Journal of Residuals Science & Technology*, University of North Texas, Biology Building, Rm 210, 1510 Chestnut St., Denton, TX 76203-5017) (Tel: 940-565-4350). Manuscripts should normally be limited to the space equivalent of 6,000 words. The editor may waive this requirement in special occasions. As a guideline, each page of a double-spaced manuscript contains about 300 words. Include on the title page the names, affiliations, and addresses of all the authors, and identify one author as the corresponding author. Because communication between the editor and the authors will be electronic, the email address of the corresponding author is required. Papers under review, accepted for publication, or published elsewhere in journals are normally not accepted for publication in the *Journal of Residuals Science & Technology*. Papers published as proceedings of conferences are welcomed.
2. Article titles should be brief, followed by the author's name(s), affiliation, address, country, and postal code (zip) of author(s). Indicate to whom correspondence and proofs should be sent, including telephone and fax numbers and e-mail address.
3. Include a 100-word or less abstract and at least six keywords.
4. If electronic art files are not supplied, submit three copies of camera-ready drawings and glossy photographs. Drawings should be uniformly sized, if possible, planned for 50% reduction. Art that is sent electronically should be saved in either a .tif or .JPEG files for superior reproduction. All illustrations of any kind must be numbered and mentioned in the text. Captions for illustrations should all be typed on a separate sheet(s) and should be understandable without reference to the text.
5. DEStech uses a numbered reference system consisting of two elements: a numbered list of all references and (in the text itself) numbers in brackets that correspond to the list. At the end of your article, please supply a numbered list of all references (books, journals, web sites etc.). References on the list should be in the form given below. In the text write the number in brackets corresponding to the reference on the list. Place the number in brackets inside the final period of the sentence cited by the reference. Here is an example [2].
Journal: 1. Halpin, J. C., "article title", *J. Cellular Plastics*, Vol. 3, No. 2, 1997, pp. 432–435.
Book: 2. Kececioglu, D. B. and F.-B. Sun. 2002. *Burn-In Testing: Its Quantification and Optimization*, Lancaster, PA: DEStech Publications, Inc.
6. Tables. Number consecutively and insert closest to where first mentioned in text or type on a numbered, separate page. Please use Arabic numerals and supply a heading. Column headings should be explanatory and carry units. (See example at right.)
7. Units & Abbreviations. Metric units are preferred. English units or other equivalents should appear in parentheses if necessary.
8. Symbols. A list of symbols used and their meanings should be included.
9. Page proofs. Authors will receive page proofs by E-mail. Proof pages will be in a .PDF file, which can be read by Acrobat Reader. Corrections on proof pages should be limited to the correction of errors. Authors should print out pages that require corrections and mark the corrections on the printed pages. Pages with corrections should be returned by FAX (717-509-6100) or mail to the publisher (DEStech Publications, Inc., 439 North Duke Street, Lancaster, PA 17602, USA). If authors cannot handle proofs in a .PDF file format, please notify the Editor, Dr. P. Brent Duncan at pduncan@unt.edu.
10. Index terms. With proof pages authors will receive a form for listing key words that will appear in the index. Please fill out this form with index terms and return it.
11. Copyright Information. All original journal articles are copyrighted in the name of DEStech Publications, Inc. All original articles accepted for publication must be accompanied by a signed copyright transfer agreement available from the journal editor. Previously copyrighted material used in an article can be published with the *written* permission of the copyright holder (see #14 below).
12. Headings. Your article should be structured with unnumbered headings. Normally two headings are used as follows:
Main Subhead: DESIGN OF A MICROWAVE INSTALLATION
Secondary Subhead: Principle of the Design Method
If further subordination is required, please limit to no more than one (*Third Subhead*).
13. Equations. Number equations with Arabic numbers enclosed in parentheses at the right-hand margin. Type superscripts and subscripts clearly above or below the baseline, or mark them with a caret. Be sure that all symbols, letters, and numbers are distinguishable (e.g., "oh" or zero, one or lowercase "el," "vee" or Greek nu).
14. Permissions. The author of a paper is responsible for obtaining releases for the use of copyrighted figures, tables, or excerpts longer than 200 words used in his/her paper. Copyright releases are permissions to reprint previously copyrighted material. Releases must be obtained from the copyright holder, which is usually a publisher. Forms for copyright release will be sent by the editor to authors on request.

Table 5. Comparison of state-of-the-art matrix resins with VPSP/BMI copolymers.

Resin System	Core Temp. (DSC peak)	T _E	Char Yield, %
Epoxy (MY720)	235	250	30
Bismaleimide (H795)	282	>400	48
VPSP/Bismaleimide copolymer			
C379: H795 = 1.9	245	>400	50
C379: H795 = 1.4	285	>400	53

General: The *Journal of Residuals Science & Technology* and DEStech Publications, Inc. are not responsible for the views expressed by individual contributors in articles published in the journal.